

## General Disclaimer

### One or more of the Following Statements may affect this Document

- This document has been reproduced from the best copy furnished by the organizational source. It is being released in the interest of making available as much information as possible.
- This document may contain data, which exceeds the sheet parameters. It was furnished in this condition by the organizational source and is the best copy available.
- This document may contain tone-on-tone or color graphs, charts and/or pictures, which have been reproduced in black and white.
- This document is paginated as submitted by the original source.
- Portions of this document are not fully legible due to the historical nature of some of the material. However, it is the best reproduction available from the original submission.

FLOW EFFECTS WITH CROSS-BLOWN LIFTING JETS OF V/STOL AIRCRAFT AND  
THEIR REACTIONS ON AERODYNAMICAL FORCES AND  
MOMENTS OF THE AIRFRAME

GÜNTER VIEHWEGER

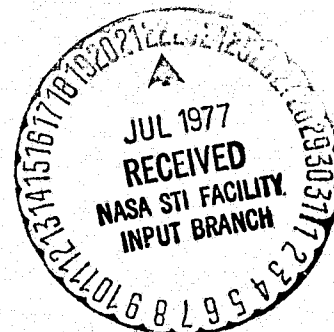
(NASA-TM-75143) FLOW EFFECTS WITH  
CROSS-BLOWN LIFTING JETS OF V/STOL AIRCRAFT  
AND THEIR REACTIONS ON AERODYNAMICAL FORCES  
AND MOMENTS OF THE AIRFRAME (Kanner (Leo)  
Associates) 141 p HC A07/MF A01

N77-27070

Unclas  
36777

CSCL 01A G3/02

Translation of "Strömungsvorgänge bei angeströmten Hubstrahlen  
von Kurz- und Senkrechtstartern und ihre Rückwirkungen auf die  
Luftkräfte und Momente der Zelle," Deutsche Luft- und Raumfahrt  
Forschungsbericht [German Aerospace Research Report] DLR-FB 76-  
34, Braunschweig, Deutsche Forschungs- und Versuchsanstalt für  
Luft Raumfahrt 1976, 113 pages



1. Report No. NASA TM-75143		2. Government Accession No.		3. Recipient's Catalog No.	
4. Title and Subtitle FLOW EFFECTS WITH CROSS-BLOWN LIFTING JETS OF V/STOL AIRCRAFT AND THEIR REACTIONS ON AERODYNAMICAL FORCES AND MOMENTS OF THE AIRFRAME				5. Report Date July 1977	
				6. Performing Organization Code	
7. Author(s)  Günter Viehweger, German Aerospace Research and Test Facility				8. Performing Organization Report No.	
				10. Work Unit No.	
				11. Contract or Grant No. NASw-2790	
9. Performing Organization Name and Address Leo Kanner Associates Redwood City, California 94036				13. Type of Report and Period Covered  Translation	
				14. Sponsoring Agency Code	
12. Sponsoring Agency Name and Address National Aeronautics and Space Administration, Washington, D.C. 20546					
15. Supplementary Notes This is a translation of "Strömungsvorgänge bei angeströmten Hubstrahlen von Kurz- und Senkrechtstartern und ihre Rückwirkungen auf die Luftkräfte und Momente der Zelle," Deutsche Luft- und Raumfahrt, Forschungsbericht [German Aerospace Research Report], DLR-FB 76-34, Braunschweig, Deutsche Forschungs- und Versuchsanstalt für Luft Raumfahrt 1976, 113 pages.					
16. Abstract Systematical basic studies on the close and distant effects of cross blown single and twin lifting jets are performed with the aid of a principle model. The different effects will be described in detail. The number of the experimental parameters is reduced to the most essential ones: The angle of attack, the flight and the jet velocities as well as the jet diameter, the distance between the twin jets, the location of the wing relative to the jets and the fuselage, and the ground distance. The emphasis of this report is put on the results of systematic pressure distribution measurements on the fuselage surface, especially in the close vicinity of the jet exits. From these results functions on the influence of the parameters are deduced.					
17. Key Words (Selected by Author(s))  Jet lift, Airframe-jet interference, pressure distribution measurements			18. Distribution Statement  Unclassified-Unlimited		
19. Security Classif. (of this report) Unclassified		20. Security Classif. (of this page) Unclassified		21. No. of Pages	22. Price

Table of Contents

	page
Notation.....	iii
1. Introduction.....	1
2. Lift Jet Reactions on the Airframe.....	2
3. Review of Studies on Free Jets in a Cross Flow.....	4
4. Purpose of the Present Work.....	8
5. Test Setup and Procedure.....	9
5.1 Low Speed Wind Tunnel.....	9
5.2 Fuselage Model.....	9
5.3 Jet Air Supply Line.....	11
5.4 Velocity and Flow Direction Measurements.....	12
5.5 Visualization of the Outer Field of the Jets.....	13
5.5.1 Flow Observation with an Oil Mist.....	13
5.5.2 Visualization of the Jets using Water Injection.....	15
5.6 Aerodynamic Parameters.....	15
5.7 Evaluation.....	16
6. Jet Expansion Effects.....	17
6.1 General Considerations.....	17
6.2 Experimental Determination of Jet Drift for Single and Double Jets.....	21
6.3 Flow Effects in Flow Around a Jet.....	24
7. Studies on the Interaction of the Injector Effect and Displacement Effect for a Free Jet in a Cross Wind.....	28
8. Fuselage with a Single Jet.....	36
9. 8.1 Influence of the Relative Jet Intensity $\phi$ .....	37
8.2 Influence of the Jet Diameter.....	38
8.3 Influence of the Angle of Attack.....	40
8.4 An Approach to an Analytical Determination of Changes in Perpendicular Force Along the Fuselage Body.....	41
9. Fuselage with Double Jet.....	47
10. Fuselage with Wing.....	52



	page
11. Effect of the Ground.....	58
12. Summary.....	60
13. References.....	63
14. Figures.....	66

Notation

17

Geometrical Quantities

$D = 0.15$	[m]	Fuselage diameter
$d_j$	[m]	Jet orifice diameter
$b$	[m]	Jet width
$d_j/D$		Dimensionless jet diameter
$F_A = \frac{\pi}{4} \cdot d_j^2$	[m <sup>2</sup> ]	Jet cross-section at the jet orifice
$F_E/F_A$		Jet nozzle reduction ratio
$L_j$	[m]	Distance between the two jet axes
$L$	[m]	Fuselage length (cylindrical portion)
$x, y, z$	[m]	Cartesian coordinates (fixed)
$x/d_j = \xi$		dimensionless x-coordinate
$y/d_j = \eta$		dimensionless y-coordinate
$z/d_j = \zeta$		dimensionless z-coordinate
$z_p/d_j$		dimensionless potential core length
$\xi_o$		dimensionless x-coordinate of the line sink
$\Delta\xi$		coordinate shift in the jet wake
$\varphi$	[degree]	Azimuth angle of the pressure holes in a fuselage bulkhead
$l_F = 2D$	[m]	Chord length
$x_V$	[m]	Horizontal position of the wing with respect to the forward jet

$z_0$	[m]	Vertical position of the wing with respect to the fuselage axis
$Q_0$	[m <sup>3</sup> /s]	Initial jet volume
$\Delta Q$	[m <sup>3</sup> /s]	Increase in volume

### Aerodynamic Quantities

$v_\infty$	[m/s]	Velocity of the undisturbed oncoming flow
$\rho_\infty$	[kp·s <sup>2</sup> /m <sup>4</sup> ]	Density of the undisturbed oncoming flow
$q_\infty = \frac{\rho_\infty}{2} \cdot v_\infty^2$	[kp/m <sup>2</sup> ]	Dynamic pressure of the undisturbed oncoming flow
$v_j$	[m/s]	Jet velocity at the nozzle orifice <span style="float: right;">/8</span>
$\rho_j$	[kp·s <sup>2</sup> /m <sup>4</sup> ]	Density of the jet
$q_j = \frac{\rho_j}{2} \cdot v_j^2$	[kp/m <sup>2</sup> ]	Dynamic pressure of the jet
$\lambda = v_j/v_\infty$		Velocity ratio (cross wind No.)
$\phi = \frac{q_j}{q_\infty}$		Relative jet intensity
$\psi$	[m <sup>2</sup> /s]	Flow function
$\phi_D$	[m <sup>2</sup> /s]	Potential of the displacement effect of the jet
$\phi_J$	[m <sup>2</sup> /s]	Potential of the injector effect of the jet.
$m$	[m <sup>3</sup> /s]	Line dipole moment
$q$	[m <sup>2</sup> /s]	Line sink intensity
$M_j$		Mach number in the jet orifice
$p_\infty$	[kp/m <sup>2</sup> ]	Static ambient pressure
$p_n$	[kp/m <sup>2</sup> ]	Static pressure on a measuring point

$$\frac{P_n - P_\infty}{q_\infty}$$

Pressure ratio on a measuring point (simplified in the isobar diagrams as  $\Delta p/q_\infty$ )

$$c_{p\infty} = \int_0^{2\pi} \left( \frac{P_n - P_\infty}{q_\infty} \right) \cdot \frac{\cos \varphi}{2\pi} \cdot d\varphi$$

Dimensionless pressure coefficient of a circular section, determined experimentally

$$\Delta p_N = c_{p\infty} \cdot q_\infty \quad [\text{kp/m}^2]$$

Pressure component of a fuselage bulkhead in the z-direction

$$c_N = \frac{\pi \cdot d}{D} \int_{\xi_1}^{\xi_2} \int_0^{2\pi} \left( \frac{P_n - P_\infty}{q_\infty} \right) \cdot \frac{\cos \varphi}{2\pi} \cdot d\varphi \cdot d\xi$$

Perpendicular force coefficients of the cylindrical portion of the fuselage determined experimentally

$$c_M = \frac{\pi \cdot d}{D} \int_{\xi_1}^{\xi_2} \int_0^{2\pi} \xi_S \left( \frac{P_n - P_\infty}{q_\infty} \right) \cdot \frac{\cos \varphi}{2\pi} \cdot d\varphi \cdot d\xi$$

Pitching moment coefficient of 1/9 the cylindrical portion of the fuselage determined experimentally

$$\alpha \quad [\text{degree}]$$

Angle of attack of the fuselage body

$$\theta = \alpha + 90^\circ \quad [\text{degree}]$$

Jet inclination angle

### Subscripts

- j Jet
- $\infty$  Undisturbed oncoming flow
- F Wing
- S Reference point
- B Ground
- $\alpha$  Angle of attack

FLOW EFFECTS WITH CROSS-BLOWN JIFTING JETS OF V/STON AIRCRAFT AND  
THEIR REACTIONS ON AERODYNAMICAL FORCES AND  
MOMENTS OF THE AIRFRAME<sup>1</sup>

Günter Viehweger  
German Aerospace Research and Test Facility

1. Introduction

/11\*

With V/Stol aircraft the effect of jets on the shape of the flow field in the region of the aircraft is very great. The jets enter at high velocity into a quiescent or moving medium and thereby produce additional flows which can extensively modify the behavior of the aircraft in terms of forces and moments.

These effects, which are comprised by the term free jet interference, are on the order of magnitude of normal aerodynamic loads [1] especially in the case of small forward velocities. It is thus very important to understand and control these effects on the airframe. The more precise our knowledge of the physical processes taking place in the interaction between the airframe, jets and surrounding medium, the more likely it is to obtain a reliable estimate of these interference effects.

Up to now detailed studies in this area have been done primarily on specific aircraft configurations. But in many cases the results of these studies cannot be translated to other configurations, since even a small change in the position of the jets can strongly modify the flow field in the vicinity of the airframe. But above all these studies for the most part are limited to force measurements which tell us nothing about local

---

1. This work is appearing simultaneously as a dissertation accepted by the faculty for Machinery Technology of the Rhein-Westphalian Technical College, Aachen, in fulfillment of the Ph. D. degree in Engineering.

\*Numbers in the margin indicate pagination in the foreign test.

relationships and give only integral data.

The present paper reports on systematic studies of the author on the close and distant effects of individual and multiple jets which issue perpendicularly from a cylindrical fuselage placed longitudinally or obliquely to the flow. An airfoil wing can be attached to this fuselage. In order to study the close effect the pressure distribution on the surface of the body was measured. In addition, the outer field of the flow was sampled with direction probes.

Flow photographs of the jets and of the outer field provided valuable information for interpreting individual physical processes.

## 2. Lift Jet Reactions on the Airframe

The forces and moments close to an aircraft created by the /12 effect of jets depend in large degree on the velocity of the aircraft. Hence it seems expedient to divide the flight up into three different phases:

- 1) In the hovering phase the suction of the downward blowing jet causes intake flows to the jet which induce low pressure fields and thus negative aerodynamic forces on the underside of the airframe. Since the central point of a depression produced by a particular individual jet of the aircraft naturally more or less coincides with the jet axis and since the jets are set partially in front of or behind the center of gravity of the aircraft, along with the change in buoyancy under certain circumstances a considerable change in the pitching moment develops. If the aircraft comes close to the ground then this effect is amplified by the increasing reduction in intake area for secondary

air between the airframe components and the ground. Below a certain distance above the ground, depending on the arrangement of the jet nozzles, it happens that between the jets an impulse is directed from the ground towards the airframe, thus forming a fountain so that a portion of the jet impulse also strikes the airframe and there in particular causes an increase in buoyancy [1,2]. It should also be mentioned that under certain circumstances there could also be very adverse and dangerous thermal stress on the airframe due to rising jet exhausts.

2) In the transition phase from hover flight close to the ground to aerodynamic flight the influence of the ground has already died out. At this point due to the increase in cross flow of the jets there develops a complicated three dimensional combination of events between two flows which differ sharply in direction and magnitude. Secondary flows develop in the immediate vicinity of the aircraft. These cause changes in the local dynamic pressure and direction of the flow on all components of the airframe with a corresponding change in local forces. Yet another parameter which emerges in this phase is the pivot angle of the jet nozzles. This strongly affects the pitching moment over time mainly in the pivot range of  $45^\circ \leq \sigma \leq 90^\circ$ . Of particular importance here is the arrangement of the jet nozzles, in particular their position with respect to the wings and elevator. Detailed information on this point is contained in [1] and [2]. Reference [1] is only a summary of very comprehensive jet studies which were performed with a model of the VAK 191 B of VFW-Fokker.

3) In flight conditions with dominating airfoil lift /13 (high-speed flight) the jet effects are of small importance. Essentially they involve a modification in the oncoming flow of the elevator due to the jet nozzles which are now pivoted towards the back. This can be compensated for by trimming.

In order to give an impression of the magnitude of the interference effects a few quantitative results using a typical V/STOL aircraft are presented. Fig. 1 shows that the losses in lift with the power unit setting chosen here (the jets are blowing downward) depend only slightly on the angle of attack but are strongly dependent on the arrangement of the power units. The independent lift effect of the lift jets issuing from the underside of the fuselage (Config. II) is only about half as large as that of the cruise engine. This naturally due to the special mounting location of this engine directly beneath the root of the wing. However the total depression is not the sum of the individual depressions, but it is "accidentally" only as large as the depression of the cruise engine jets. Quantitative agreement is determined by the geometry of this design.

This example alone clearly reveals the complexity of jet interference and shows that only systematic fundamental studies on initially simple models can lead to an estimation of these effects.

### 3. Review of Studies on Free Jets in a Cross Flow

A large number of theoretical and experimental studies exist on the behavior of a free jet in a cross flow, its reaction on the outer flow and thus on the surrounding pressure field.

The most important case of a round jet in a cross flow was



treated theoretically for the first time by Chang [11]. With a potential theory formula, which assumes uniform static pressure on the discontinuity surface, it was proved that the cross-section of the jet is deformed into a horseshoe shape as a result of being deflected by the flow. It was also shown that the tail of the jet rolls up into two counter rotating vortices. This result has been confirmed in numerous experimental studies by field measurements and by visualization [4,5,6]. Williams and Wood [6] assumed that the decisive interference effect of the jet stemmed from the action of this pair of vortices, and on this assumption they based their semi-empirical vortex-sheet theory. To be sure, their theory assumes that the jet direction and flow direction are identical at the edge of the jet, thus restricting its application to the distant region of the jet. This formula is important for the parts of the airframe not in the immediate vicinity of the jet orifice, i.e. the control surfaces. The subject of the distant effects of jets has been dealt with in the work by Seidel [7].

Wooler, Burghart and Gallagher [8] as well as Schmidt [9] have recently developed theoretical models of the flow field which develops when a jet in a cross flow spreads out during the transition phase of flight. Wooler et. al. described the jet in terms of its axis, its geometry (oblique ellipse) and its velocity averaged over the cross-sectional area. Empirical formulas are set up for the geometry of the jet cross-section. The coefficients for these formulas are taken from experimental studies by Jordinson [4] and Keffer and Baines [10]. The interaction between jet and cross flow is considered in terms of the force which the outer flow exerts on the jet and in terms of the mass sucked in by the jet from the surroundings. For the variable distribution of the intake amount over the contour of the jet the coefficients were determined on the basis of results from [10] and [4]. The thus obtained sink distribution

fulfills the limit conditions of Ricou and Spalding [12] for the cross flow  $v_{\infty} = 0$ . By means of a sink-dipole distribution substituted for the jet it is possible to calculate the path of the jet and the jet-induced velocity and pressure fields. Comparisons of results obtained by this method with pressure distribution measurements on a smooth plate longitudinal to the flow and from which a jet is issuing normally are in quite good agreement up to a certain distance on both sides of the jet. But in front of and in particularly behind the jet the differences are quite considerable. So whereas this theory does not predict any depressions in the wake of the jet, such depressions do exist in reality.

Schmidt [9] relies heavily on the theoretical model of Wooler, Burghart and Gallagher [8], but uses new formulas for the amount of air sucked in and the cross-sectional area of the jet in order to get balance equations for jet mass and jet impulse which form a complete equation system which was not given in the work cited above. The independent parameters of mass intake, of the cross-sectional area of the jet and of the core length are determined by fitting the theoretical curves to measured values.

In the work of Schulz [13] the attempt is made for the first time to theoretically calculate the pressure distribution on a fuselage body with a lift jet. The injector effect, the displacement of the jet and of the fuselage are represented by singularities such as sources, sinks and dipoles. The interaction between the jet and fuselage is expressed by correction singularities. The results of his method for the portion of the fuselage in front of the jet and on both sides of the jet orifice show qualitative agreement with comparison measurements, but quantitatively there is considerable difference, since the combined events are not properly understood. Moreover, the events in the wake space of the jet cannot be determined with this

potential theory formula.

Fundamental experimental studies deal exhaustively with the formation of the jet after leaving the jet engine orifice by determining the pressure and velocity distribution [4,5,18] in the jet and in its immediate vicinity. In some of these works pressure distribution measurements were done on simple body shapes such as smooth plates held longitudinal to the flow. Single and multiple jets issued perpendicularly from these plates [3,6,14,15,17].

Measurements on these two-dimensional bodies have already shown how extraordinarily complex the interaction of jet and cross flow is, involving a number of parameters, in the presence of a smooth plate. An important flow parameter here for example is the initial turbulence of the jet, as is quite obvious from the different shape of the two isobar fields shown in Fig. 2. The velocity ratio for jet and flow in both experiments was  $v_j/v_\infty = 3.3$  ( $\phi \approx 11$ ). The jets differ only in their core length, which without any cross flow ( $v_\infty = 0$ ) were 0.5 and 5 jet nozzle diameters respectively. The jet with the shorter core length, i.e. with the larger initial turbulence, induces larger depression fields on the plate. This is because the jet mixes thoroughly with the cross flow whereby the intake mass transfers its impulse to the jet. By contrast, the flow around the jet with the small amount of turbulence is stronger, similar to a rigid cylinder, and thus has a depression area extending further behind it. For the behavior of moments over time it is important that the center of gravity of the induced negative aerodynamic force with the turbulent jet -- which can be regarded as practical for the large-scale version -- is located close to the jet axis with this velocity ratio.

Up to now, systematic pressure distribution measurements on

cylindrical bodies with a lift jet have been available from Ousterhout [16]. However the practical applicability of his results is limited, since on the one hand the diameter ratio of the jet to the body of the model ( $d_j/D$ ) is less than 0.1. In /16 the immediate vicinity of the jet this causes flow conditions which are similar to those on a flat plate. On the other hand, the maximum jet exit velocity ( $v_j$ ) is only 90 m/s. In addition, he does not study the influence of the angle of incidence, which is especially important for the behavior of moments with respect to time.

Finally we should mention the comprehensive studies of Vogler [19, 20]. By means of force measurements he deals with the effect of different shaped jets, for example round and slit-shaped, for different jet engine arrangements on the force and moment behavior of a certain aircraft model.

#### 4. Purpose of the Present Work

The present studies are mainly concerned with a closer treatment of the interference effects of different geometric and aerodynamic parameters on the aerodynamic forces and moment of a fuselage body with lift jets exhausting normally towards the ground. A theoretical explanation of these effects is possible only to a limited extent since we still do not have sufficient knowledge of the turbulent interaction effects close to the airframe. Accordingly, systematic measurements will supply the required data. These studies include pressure distribution measurements on the surface of the fuselage and direction measurements in the outer field. The actual purpose was to develop reliable methods for estimating the close interference on the fuselage body, a point which is of interest to the project engineers.

In keeping with the character of a basic study the large number of test parameters was reduced to the most important ones.

## 5. Test Setup and Procedure

### 5.1. Low Speed Wind Tunnel

The tests were performed in the test section of a low-speed wind tunnel of the DFVLR [German Aerospace Research and Test Facility] in Porz-Wahn.

This is a wind tunnel with a closed air circuit and an open test section. The cross-sectional area of the test section measures about  $7 \text{ m}^2$  and the wind velocity can be adjusted over a range from 10 to 85 m/s. The maximum deviation in dynamic pressure and the degree of turbulence of the test jet are but small (0.1% and 0.3%) because of the 1:10 reduction in jet engine size. A brief description and cross-section sketch of the /17 wind tunnel are given [21].

By connecting the wind tunnel to the powerful compressed air storage facility of the Institute for Applied Gas Dynamics it is particularly suited for the production of jets with a high Mach number.

### 5.2. Fuselage Model

For studying the close effect of the jets the basic model used was a cylindrical fuselage body ( $D = 150 \text{ mm}$ ). From the underside of this fuselage individual or multiple jets can discharge normally to the model axis. The nose of the fuselage is in the shape of a half spheroid. The model is built in monocoque construction using the mechanical assembly technique, thereby permitting rapid and extensive changes in the most

important geometric parameters. Along with the jet orifice diameter these parameters include the distance between the jets when more than one jet is present. Moreover, this type of construction guarantees that full advantage is taken of the volume of the fuselage, which is required for the following purposes:

- a) Housing the compressed air delivery lines, the guide vein inserts and the jet engines;
- b) Guiding and laying the numerous pressure measuring hoses;
- c) Mounting the Scanivalve blocks for switching the pressure measurement points.

Fig. 3 shows a sketch of the model drawn to scale.

By means of appropriate spacers which can be inserted between the two jet nozzles the distance between the jets can be set from 1.5 to 4 fuselage diameters.

The model also allows the attachment of airfoil wings whose position can be varied with respect to the location of the jet (Fig. 4). Of course the surfaces are not fitted with measuring devices, rather they only create the required flow environment. The wing chord corresponds to two fuselage diameters. For pressure distribution measurements the cylindrical portion of the fuselage has a maximum of 288 holes 0.6 mm in diameter. Because of the symmetrical position of the jet nozzles and the limited capacity of the measuring apparatus these are located on only one-half shell. Because of the expected steep pressure gradients in the vicinity of the jet nozzles the surface density of the holes is especially high in this area (Fig. 6). Pressure hoses lead from the individual test points to a total of 6 scanivalves which are housed in the nose of the fuselage (Fig. 5). The electrical /18 signals of the pressure cells are carried to amplifiers by junction lines and further to an integrating digital voltmeter by means of which they are read successively and recorded on perforated tape.

Since there is a large variation in surface pressures especially in the vicinity of the jet orifice the pressure cells signals were averaged before being recorded. A time of two seconds turned out to be sufficient for this.

The pressure pick-ups used (manufactured by Statham) had a working range of  $\pm 2.5$  psi (corresponding to  $\pm 1700$  mm WS). The resolution of the measuring apparatus including pressure pick-ups, amplifiers and recording instruments was around 0.4 mm WS.

### 5.3. Jet Air Supply Line

The lift jets are represented by means of cold compressed air which is delivered to the model through a pipe which is divided longitudinally from the tail forward. At the same time the pipe acts as a support for the model. The jet nozzles are supplied separately by the two lines and the strength of the jet emitted from the nozzles is controlled by regulating valves and diversion valves connected in series. A solidly installed aperture and temperature measuring apparatus determines the flow rate with an error of less than  $\pm 1\%$ . Fig. 7 shows a simplified diagram of the compressed air system including the regulating and diversion valve system.

A total of 3 jet orifice diameters are studied (Fig. 8). In keeping with the usual data used in aircraft construction the diameters are graded as follows with respect to the fuselage diameter D:

$$\begin{aligned}d_{j1} &= 0.2 \cdot D = 30 \text{ mm} \\d_{j2} &= 0.25 \cdot D = 37.5 \text{ mm} \\d_{j3} &= 0.3 \cdot D = 45 \text{ mm}\end{aligned}$$

By selecting different jet orifice diameters its was possible to study also those interference effects which are induced when the total impulse remains the same but the specific impulse varies, i.e. by varying the jet cross-section and the jet velocity.

All of the jet nozzles have the same initial diameter of 72 mm and thus reduction ratios of

$$F_A/F_E = 5.75; 3.69 \text{ and } 2.56.$$

The interior contour was so chosen so as to produce the greatest uniform velocity distribution in the outlet plane. An /19 equation given in [8] was used to determine the coordinates.

The jet nozzles together with the twin chamber pipe were studied in perliminary experiments to find out their jet characteristics [22]. Fig. 9 shows the total pressure profile measured 3 mm downstream from the jet orifice in the axis of symmetry in case of nozzle 1 ( $d_j = 30$  mm) in the core the total pressure  $P_{tj}$  is nearly constant. The small irregularities are due to the wake effect of the guide veins. The boundary layer at the edge, which was formed inside the nozzle and is determined by the walls and the pressure gradients in the flow direction, is relatively narrow.

#### 5.4. Velocity and Flow Direction Measurements

For measuring the direction of the flow in the jet and in particular in the outer field a probe is required with excellent direction characteristics. Moreover, it should interfere with the flow as little as possible during velocity distribution measurements in the jet. For these measurements small 5-hole probes were used. Electric pressure pick-ups were connected to



their test holes.

The outer field was measured in a total of 8 horizontal sections at different distances parallel to the plane of the jet orifice. The surface density of the test points in the planes was suited to the expected velocity gradients. The required position changes of the probes were accomplished with the probe moving device shown in Fig. 10. It has 3 translational and 2 rotational degrees of freedom. The probe support can be turned around the horizontal probe axis by means of a remote controlled motor by an angle of  $\alpha = \pm 180^\circ$ . The angle of rotation of the probe in each case was also recorded on perforated tape like the 3 position coordinates together with the output signals of the pressure pick-ups. Together with the calibration curves of the direction probes for the x,y plane and the x,z plane this perforated tape was fed into a Hewlett-Packard 2116C computer which calculated the velocity vector for each test point.

### 5.5. Visualization of the Outer Field of the Jets

Visualization of the flow events produces valuable information for clarifying the very complex 3-dimensional interactions of the outer flow and free jets in a cross flow and it contributes considerably to the understanding of these combined events.

#### 5. 5.5.1. Flow Observation with an Oil Mist

/20

In order to obtain information on the flow line pattern of the outer field the outer flow was made visible by means of threads of oil mist. For this purpose a light, residue free mineral oil was atomized by a pressurized stream of  $\text{CO}_2$  gas and then vaporized in a thermostatically controlled heater. Afterwards the gas was released in a nozzle, thus creating a nearly dry,

highly concentrated white oil mist. By feeding in cold compressed air the oil mist was cooled down. The amount of mist being discharged at 1-second intervals could be set over a continuous range by controlling the addition of compressed air.<sup>1</sup>

In order to visualize the flow lines of the outer field the oil mist was blown out of a probe rack fitted with 30 thin-walled tubes (inside diameter  $d_r = 3\text{mm}$ ) spaced 30 mm apart. The tubes were sharpened to form a pointed outlet. The velocity of the outcoming mist was set somewhat below the velocity of the outer field in order to prevent the threads from breaking after leaving the capillary tubes and thus quickly mixing with the surrounding air. Thus the mist thread can still be used 2.5-3 m down stream.

In order to obtain good contrast between the mist threads and their surroundings the test model from which the jets issued was covered with a black film, and in addition a dark film curtain was used as a background. The field was illuminated with back lighting by means of light boxes with a laterally limited light band. The light sources for the photographs were 1,000 watt photography lamps. The test setup is shown in Fig. 11.

Since 3-dimensional events are involved when free jets in a cross flow combine with the outer flow, the mist filaments were photographed with vertically and horizontally arranged probe racks. In the vertical arrangement the probe rack was located in the plane of the jet axis ( $\eta = 0$ ) or was shifted to the side by 1 or 3 jet nozzle diameters. A similar procedure was followed with the horizontal arrangement.

---

1. The oil mist producer was developed by the Vereinigte Flugtechnische Werke-Fokker of Bremen.

### 5.5.2. Visualization of the Jets Using Water Injection

/21

The path of the jets was made visible by injecting water. The special interest here pertained to the shape of the rear jet lying in the wind shadow in the test arrangements with multiple jets. Because of its smaller flow velocity it has a weaker wind and after traversing several jet nozzle diameters (depending on the test conditions) it passes through the equally strong forward jet which in the meantime has become completely turbulent (Fig. 18).

The water was injected into the jet engine air far enough upstream so that both mediums could mix together before reaching the jet orifice (Fig. 7). Because of the large density difference between air and water the amount of water added was very carefully measured so as not to falsify the original jet pattern. The maximum water/air ratio ( $Q_W/Q_A$ ) was about  $9 \cdot 10^{-5}$ .

### 5.6. Aerodynamic Parameters

The most important aerodynamic parameters of the test program were the relative jet intensity  $\phi = q_j/q_\infty$  (dynamic pressure of the jet over the aerodynamic pressure) and the angle of attack of the model body. In order to restrict the number of test parameters only events with symmetric oncoming flow ( $\beta = 0^\circ$ ) were treated.

The angle of attack was initially changed in large intervals in the range  $-6^\circ \leq \alpha \leq 15^\circ$ . Due to intermediate plottings which were produced by large changes in the normal force and pitching moment patterns in the range between  $6^\circ$  and  $15^\circ$  the intervals in this range were decreased.

The relative jet intensity was varied within wide limits

between  $\phi = 290$  and  $\phi = 16$ , thus taking in the velocity spectrum from start and landing to the transition phase of V/STOL aircraft. The influence of the ground was taken into consideration for a few test setups.

$q_{\infty}$ [mm WS]	$q_j$ [mm WS]	$\phi$	
25	7250	290	
25	4640	186	
25	3225	129	
100	7250	72	
200	7250	36	
200	3225	16	(only in outer field)

/22

### 5.7. Evaluation

The results of the pressure distribution measurements were evaluated from two points of view:

- 1) In order to evaluate the local events the pressure distribution on the surface of the model was illustrated by means of isobar diagrams on the cylindrical middle section of the fuselage projected onto a plane.
- 2) To evaluate the totality of events the pressure, normal force and pitching moment coefficients were calculated by integrating the pressure distribution. The reference surface area used was  $D^2$  ( $D =$  fuselage diameter). The moment reference point in the setups with the individual jet is the point of intersection between the axis of the model and the jet axis. In the double jet setups the reference point is the point of intersection between the axis of the model and the axis of the forward jet. The reference length is  $D$ .

The results of the measurement of the outer field were represented in the form of flow line images and isocline diagrams.

## 6. Jet Expansion Effects

### 6.1. General Considerations

For the following considerations of close interference on the fuselage body it is important to know what interaction there is between a free jet and the outer flow. First of all it is important to know what shape the jet takes and what parameters its injector effect, i.e. its exchange of momentum with the surrounding air, depends on. The simple case of a free jet entering into a quiescent environment ( $v_\infty = 0$ ) has been dealt with in several theoretical [23, 24, 27] and experimental [12, 25, 26, 28] studies. According to these studies the spreading out of the jet and the intensity of its drag effect depend on the geometry of the jet nozzle in the broadest sense, i.e. the shape of the orifice cross-section, the reduction ratio, and the intake conditions. They /23 also depend on the Mach number of the jet and to a large extent on the initial turbulence in the jet orifice. The latter is also largely determined by the geometry of the jet nozzle.

In the fuselage model the jet air, which is fed in through the tail, flows through a 90° deflection grid immediately in front of the jet nozzle (Fig. 3). The grid divides the jet up into several individual jets of varying velocity which then again mix with one another before entering the nozzle. Complete mixing is accomplished only after the air has left the orifice at some distance from it. By means of this process the jet takes on a very high initial turbulence and therefore has only a relative core length of  $z_p/d_j = 0.5$ . With a jet width of

$$b = 0.075 \cdot z \quad (1)$$

The spreading out of the jet is more pronounced than in the case of a jet which is not very turbulent, i.e. with a constant velocity

over the orifice cross-section, for which Reichardt [25] has determined that

$$b = 0.067 \cdot z \quad (2)$$

The increase in volume of the jet over its length at a jet Mach number of  $M_j = 1$  and a nozzle reduction ratio of  $F_E/F_A = 2.56$ , which realates to the jet nozzle with  $d_j = 45$  mm ( $d_j/D = 0.3$ ), can be described by the following equation:

$$\frac{\Delta Q}{Q_0} = 0.18 \cdot \zeta \quad (3)$$

Since at greater distances from the orifice the increase in air volume no longer occurs linearly, the range to which this equation can be applied is restricted to the following:

$$0 \leq \zeta \leq 3$$

With a homogenous jet, assuming the same jet nozzle reduction ratio and the same jet Mach number, the increase in volume is about  $0.159 \cdot \zeta$  [25]. The relavent jet in practice is the turbulent jet.

If the jet issues into a medium with a cross flow the mixing process is considerable different in comparison with a jet which issues into a quiescent medium. Since the particles of the fundamental flow already have a mometum in the x-direction prior to mixing, the mixing process of the horizontal component of the oncoming flow with the jet now overlaps the rotation symmetrical turbulence pattern of the round free jet in the quiescent medium. In addition to this there is also the displacement effect of the jet including the wake space caused by the cross wind. The first interaction effect between the jet and cross wind arises because the jet, as a result of the tur- /24

bulent mixing of these flows which differ in magnitude and direction, picks up a certain amount from the cross flow. As a result of this process the structure of the two flows changes simultaneously [34]. The mixing which takes place directly behind the jet orifice occurs primarily only in the edge regions of the jet, but with increasing distance from the orifice the particles in the interior of the jet are also included in this process. In this mixing process the portions sucked in from the cross flow transmit their momentum acting in the x-direction to the jet and thereby alter the direction and magnitude of the jet momentum. Because of the increased intake of particles from the cross flow the increase in volume along the path of the jet is then greater than in the case of a jet in a quiescent medium. However, as a result of this the velocity on the axis of the jet along its path decreases more sharply. Mehmel [29] showed in his free jet studies that the decrease in velocity increases with the angle of inclination  $\theta$ . His studies were concerned with the range  $0^\circ \leq \theta \leq 90^\circ$ .

The other effect of the interaction between jet and cross flow is the displacement effect of the jet. The portions of the cross flow which are not taken in by the jet flow around the jet similar to a rigid cylinder and thereby exert a force on the jet. Because of the pressure differences between the windward side and lee side, i.e. the wake space, and because of the frictional forces thus created -- which in any case are smaller than with a cylinder because of the fluid transition from the cross flow into the jet -- the jet is deflected from its initial axis direction into the x-direction (Fig. 12). With a rigid cylinder the outer flow separates from the cylinder wall if the boundary layer, which has lost energy, can no longer overcome the pressure drag. It is well known that the separation takes place at subcritical Re numbers in front of the greatest thickness of the cylinder, whereas at super critical Re numbers it takes place

behind the greatest thickness. In the first case the wake space becomes greater than the cylinder diameter and in the second case it becomes smaller. This phenomenon cannot occur with round free jets in a cross flow, since a clear wall boundary layer cannot form on the fluid outer contour of the jet. In any event, on the basis of test results the flow around a free jet seems to be so similar to flow around a cylinder that a wake space forms behind the free jet and only its changes in width follow laws other than which prevail in the case of a rigid cylinder. Obviously the wake space never exceeds the jet diameter. Moreover, with large relative jet intensities the injector effect insures that the outer flow behind the jet flows strongly back together due to the suction of the wake medium. Thus the flow around the jet /25 simulates even more the frictionless flow around a cylinder.

Furthermore, with the  $\phi$  values studied here the mixing between the jet and outer flow always results in turbulent flow conditions in the vicinity of the jet. Since these turbulent mixing events are clearly not a function of a Reynolds number, it can confidently be assumed that these events also apply to the full scale version. The shearing forces between the jet and cross flow are greatest in the lateral border regions of the jet due to the excess velocity as a result of the displacement effect. Because of this these portions of the jet are the most strongly deflected. With increasing distance from the orifice the varied deflection of the jet along its circumference results in the well known phenomenon of a counter rotating pair of helical vortices on both sides of the jet axis. This pair of vortices deforms the initial round cross section into a horseshoe shaped cross section.



## 6.2. Experimental Determination of Jet Drift for Single and Double Jets

The jet emerges perpendicular to the underside of the fuselage. Its subsequent deflection by the cross flow in the x-direction was determined in detail point by point by means of field measurements using a 5-hole Pitot probe and by means of water injection. Figs. 13 and 14 show the path of the axis of a single jet with increasing distance from the orifice for several relative jet intensities of  $\phi = 290$  to  $\phi = 16$ . The path curves shown in Fig. 13 which spread out in a fan shape can quite easily be brought together in a single curve (Fig. 14) if the term  $\zeta \cdot \frac{1}{\sqrt{\phi}}$  is used for the path coordinate in the z-direction. The following general equation is valid in good approximation for the path of the jet axis:

$$\xi = 1.727 \left( \zeta \cdot \frac{1}{\sqrt{\phi}} \right)^{2.65} . \quad (4)$$

It is applicable for the entire range of  $16 \leq \phi \leq 290$ . Small discrepancies between the measured path curves and the coordinates calculated in this way show up only with large relative jet intensities. The equation is valid for the angle of inclination  $\theta = 90^\circ$  with respect to the oncoming flow and for a turbulent jet with an undisturbed core length of 0.5 jet orifice diameters. Another influence on the path of the jet is the fuselage body above the jet which affects the intake conditions for the air which is sucked in. Fig. 13 shows that for the same jet Mach number the drift of the jet increases quadratically with the velocity of the oncoming flow. This means that the mixing of the jet (injector effect) and the deformation of the jet (displacement) increases with the velocity of the oncoming flow. The familiar equation of Iwanow [30]

$$\xi = (\zeta)^3 \cdot \frac{1}{\phi^{1/3}} + \zeta \cdot \cot \theta \quad (5)$$

for  $\phi = 129$  gives path coordinates which are close to the measured values, however for  $\phi = 36$  it gives a considerably stronger drift. The shape of the path curve  $\xi = f(\zeta)$  is determined not only by the relative jet intensity  $\phi$  but also by the initial inclination  $\theta$ . In Fig. 15 the path curves of jets with different angles of inclination are represented in a fixed coordinate system. If the jet is directed against the oncoming flow ( $\theta > 90^\circ$ ), then its drift at first increases very rapidly over a small angle range of  $\theta = 90^\circ$  to  $99^\circ$ , and changes only slightly up to  $\theta = 105^\circ$  hence does not follow the second term of the Iwanow equation. It is to be assumed that the mixing of the jet at first increases with  $\theta$ . But at the same time this effect is overlapped by another. The fuselage body above the jet, which is now in a cross flow directed from below, obviously causes increased aeration of the rear wake due to the damming effect of the fuselage. This could not occur with a free jet without a body. This decreases the depression on the lee side of the jet immediately after it leaves the orifice, hence in the immediate vicinity of the fuselage. The thus altered initial conditions of the jet with respect to the angle of inclination  $\theta = 90^\circ$  influence the further shape of the jet with increasing distance from the orifice in the direction shown. In the later treatment of the close effect of jets on the pressure distribution close to the fuselage body this process is confirmed by the formation of high pressure fields on the underside of the fuselage behind the jet orifice for positive angles of attack of the model, hence for jet inclination angles of  $\theta > 90^\circ$  with respect to the flight direction.

In the important practical case of two tandem jets the conditions for the jet and cross flow become considerably more complex due to the interaction of the two jets. This particularly applies to the rear jet lying in the wind shadow when the distance separating the two jets is small. In this case the rear jet

experiences a smaller oncoming flow velocity than the forward jet similar to a cylindrical flow wake. Moreover, the velocity varies locally. The configuration oblique to the flow direction depends here on the configuration of the jet wake which is determined by  $\phi$  and the distance from the jet axis. Fig. 16 shows the velocity distribution in the jet wake in a horizontal plane /27 at a distance of 1 jet orifice diameter beneath the jet outlet. The curves look like Gaussian bell-shaped curves. In the x-direction the effect of the jet wake extends very far and has still not died away even after 15 jet orifice diameters. If now a second jet is set up in this wake region the drift will be less than for the forward jet due to the reduction in velocity of the oncoming flow. The effective relative jet intensity has become greater:

$$\phi_{\text{eff}} = \frac{q_j}{q_{\infty \text{ eff}}} \quad (6)$$

In Fig. 17 both jets are made visible by water injection. The photographs clearly show that the drift for the two jets is very different and that the rear jet in the wind shadow is struck from above by the more strongly blown forward jet which in the meantime has become completely turbulent. Only then is the rear jet more strongly deflected downstream (Fig. 18). In the case of a strongly blown jet with  $\phi = 36$  the point where the forward jet strikes the rear jet is about six jet orifice diameters from the orifice for an initial angle of inclination  $\theta = 90^\circ$  ( $\alpha = 0^\circ$ ). Fig. 19a shows the wind shadow effect on the rear jet as a function of the relative jet intensity. The data for this example was taken in part from Fig. 18. The distance between the two jets is small in this case, being only six jet orifice diameters. The curve shows that the shadowing is greatest at  $\phi = 36$ , hence for larger oncoming flow velocities. As  $\phi$  increases the shadowing effect becomes smaller. From this it can be concluded that the configuration of the jet wake, in

particular its spreading out, changes sharply with the velocity of the oncoming flow. We can expect the actual explanation of this effect to be given by the more detailed study of flow around a jet discussed in the next section.

With the aid of equation (4) applied to the single jet and the double jet it is possible to determine the effective relative jet intensity  $\phi_{\text{eff}}$  of the rear jet. After slight transformations we get the following equation for this:

$$\frac{\phi_{\text{eff}}}{\phi} = \left(\frac{x_E}{x_H}\right)^{0.75} = \frac{q_H}{q_E} \quad (7)$$

In this equation  $x_E$  and  $x_H$  stand respectively for the single jet and the rear jet in the double jet configuration for the same  $\zeta$ , and  $q_H$  and  $q_E$  are the corresponding local dynamic pressures of the oncoming flow.

With the values from Fig. 19a it is possible to represent /28  
the wind shadow factor  $\phi_{\text{eff}}/\phi$  in diagram form as a function of the relative jet intensity for a distance between the jets of  $L_j/d_j = 6$  (Fig. 19b). These results are in quite good agreement with the values given by the curves for the local velocity distribution in the jet wake in Fig. 16. The photographs in Fig. 17 do not give enough information on how strongly the shape of the forward jet and its outer field is affected by the rear jet. This can be determined in detail later on by means of vapor photographs and can be thoroughly analyzed with the aid of pressure distribution measurements on the fuselage body.

### 6.3. Flow Effects in Flow Around a Jet

Figs. 20 through 27 give an idea of the configuration of the outer flow through which a jet is blowing normally. This configuration is standard for the expansion and intensity of pressure

fields in the vicinity of the jet orifice and thus for the pressure distribution on the adjacent parts of the airframe.

In Figs. 20 through 23 the flow line path of the outer flow was made visible by means of vapor filaments in several planes beneath the jet orifice perpendicular to the z-axis for the single and double jet. For these photographs the camera was positioned below or obliquely above the model. The penetration point of the jets is revealed on the dark background by means of the white vapor filaments. In the arrangement with  $\phi = 290$ , in which the jet exists from the nozzle at the speed of sound and the velocity of the oncoming flow of  $v_\infty = 20$  m/s is small in comparison to this, it is possible to observe locally different phenomena. In the forefield of the jet up to the edge of the jet the vapor filaments run nearly parallel to each other, quite in contrast to flow around a cylinder. In spite of the proximity of the jet the outer flow here continues to behave as if no displacement body were present. This happens because of the dominating influence of the injector effect, for the greater the amount which is deflected from the cross flow ( $v_\infty$ ) into the jet, the less the amount which can flow around the jet. The oncoming flow is only first slowed down immediately in front of the jet due to the displacement effect of the jet and the vapor filaments indicate a flow around the jet by moving slightly to the side. As they enter into the mixing region of the high-energy jet the vapor filaments are no longer visible. Here the cross flow is very quickly deflected by the jet and accelerated in the direction of its path. In so doing the vapor filaments, after mixing with the air of the jet, become practically invisible due to a high degree of attenuation. Actual lateral flow around the jet, such as in the case of a rigid /29  
body like a cylinder, can hardly be detected.

Particularly striking is the behavior of the outer flow

further downstream. This region is characterized by a strong inward movement towards the back side of the jet. For this to occur it is essential that the oncoming flow conditions for the injector air in this region are less favorable than on the forward side of the jet, since the outer flow and the injector flow move in opposite directions. Here also by its efforts to take in as much air as possible from the surrounding medium the jet influences the direction field of the outer flow. Thus the inward movement is caused by the strong intake effect of the jet. This reduces the wake of the jet and to some extent almost prevents it. The vapor photographs show that behind the jet in the plane of symmetry there is a flat depression in place of the wake.

Figs. 22 and 23 ( $M_j = 1$ ,  $v_\infty = 20$  or  $40$  m/s) show the effect of oncoming flow velocity on the flow around the jet. By doubling the velocity of the oncoming flow more air particles are ultimately added to the jet per unit area on its forward side than it is capable of taking up. The particles which are not taken in by the jet -- as in the case of a rigid body -- flow laterally past the jet. But since the border between the jet and the oncoming flow is not rigid but fluid, more particles of the outer flow are taken up by the jet during flow around the jet. This process is revealed in Fig. 23 ( $v_\infty = 40$  m/s) by the fact that the width of the vapor filaments in the vicinity of the jet decreases downstream during flow around the jet. Due to the flow around the jet stronger and stronger depressions appear on the lateral boundary regions which affect the jet. It can be assumed that this is the cause of the increasing pulling apart of the jet laterally [34]. The deformation of the original circular cross-section into the familiar horseshoe shape, whereby the jet simultaneously spreads out, thus occurs all the closer to the jet orifice, the greater the ratio of the oncoming flow velocity to the velocity of the jet. Figs. 22 and 23 of the

double jet arrangement show in addition that the inward movement behind the forward jet is less with higher oncoming flow velocities, i.e. at a relative jet intensity of  $\phi = 72$  less air in the surrounding medium flows into the lee region of the jet than when  $\phi = 290$ . This was to be expected because of the variations in flow around the jet, since in the vicinity of the jet orifice the displacement effect of the jets indeed increases almost proportionally with the dynamic pressure of the oncoming flow, whereas the injector effect of the jets does not. For the rear jet this means a smaller average oncoming flow velocity and thus a greater wind shadow effect from the forward jet. This trend could already be seen in Fig. 19 which was discussed /30 in connection with jet drift under heading 6.2.

The configuration of the flow around the jet shown in the vapor photographs and its dependence on the relative jet intensity is confirmed and quantitatively verified by the flow line diagrams in Fig. 24. They were calculated using data from field measurements. Because the flow lines are shown closer together the diagrams give considerably more detailed information, especially in the jet wake, than the vapor photographs can give. As  $\phi$  becomes smaller, the jet and its mixing region expands more strongly both laterally and downstream. In the jet wake itself the flow lines run together in this region (surface sink) due to the downward component of the outer flow. The isocline diagrams in Figs. 25 and 26 show how large this downward component is and how far downstream it is still effective. In Fig. 25, with  $\phi = 290$  (strong jet), the flow field in front of the jet displays a small upward movement of the oncoming flow. Its maximum is at  $\zeta = 8$ . In back of the jet, due to the injector effect of the jet, a spatially limited region is formed with smaller back flow towards the jet. This has already been observed by Jordinson [4]. Here the maximum value of the upward movement in front of the jet is about the

same as the maximum back flow in the region of the wake. Thus one can assume that the two phenomena are related to each other. If we go to  $\phi = 36$  as in Fig. 26 then the intensity of the upward movement in front of the steam increases and shifts its maximum closer to the jet orifice. At the same time the range of the back flow behind the jet also moves towards the orifice. In comparison with  $\phi = 290$  the jet is now more strongly dissipation from behind, whereby a portion of the rear mixing region of the jet flows off into the wake.

The upward movement of the oncoming flow in front of the jet is also made visible in Fig. 27 by means of vapor filaments with probes positioned vertically. Shifting the probe rack laterally out of the plane of the jet axis ( $\eta = 0$ ) to  $\eta = 1$  illustrates this movement in three dimensions. The pictures also show that the flow field experiences a clear upward component above and beside the model due to the injector effect of the jets. As expected, this is especially strong with a weak oncoming flow ( $\phi = 290$ ). At the site of the rear jet this component is increased even more, especially on both sides of the model, while above the fuselage body it remains nearly unchanged because of the equally acting effect of the fuselage. Because of this effect the model has an effectively negative angle of attack with respect to the oncoming flow in spite of the 0 setting, and this increases even more along its axis. /31

#### 7. Studies on the Interaction of the Injector Effect and Displacement Effect for a Free Jet in a Cross Wind

Normally it is not possible to separately examine or measure the two individual effects of displacement activity and injector activity which occur next to a free jet in a cross wind since the two effects interact. In particular, the injector effect varies a great deal as a result of the wind in front of,



next to and behind the jet. A good theory for these events must be capable of indicating the two effects separately and in common. In what follows an attempt is made to mathematically determine the flow around a jet by overlapping the individual effects. By comparing these findings with the flow line diagrams in Fig. 24 it will be tested to what extent it is permissible and reasonable to separate the two effects.

As a rule it can be assumed that the velocity of the lift jets is always much greater than that of the aircraft when the aircraft is taking off and landing. The quantity  $\phi$  is very large and therefore the drift is but very slight. As a result the jets first behave like rigid bodies in a flow. But with increasing distance from the jet orifice the jets are blown in the direction of the flow and at the same time their cross-section is modified. Since at lower oncoming flow velocities (hence small drift) only the jet close to the fuselage has a considerable influence on the pressure distribution on the fuselage, the lift jets can as a first approximation be considered as semi-infinite long rigid cylinders perpendicular to the oncoming flow. The displacement effect of such a jet can then be simply represented by a line-dipole and its sink effect can be represented by a line sink.

At some distance from the orifice the jets can be considered as infinitely long cylinders (instead of semi-infinitely long), since the effect of the example is no longer present. Likewise the correction singularities according to [10], which are required directly next to the fuselage with regard to its contour, are not applicable.

With these assumptions the flow function of a jet in a cross flow can be written as follows:

$$\psi = \psi_{\infty} + \psi_D + \psi_J ,$$

(8)

where  $\psi_\infty$  stands for the parallel flow,  $\psi_D$  for the line-dipole and  $\psi_j$  for the line sink. /32

If we set it up so that the line-dipole is located in the  $x = y = 0$  and the line sink in the example point  $x = x_0$  or  $y = 0$ , whereby  $x_0$  is a quantity which still has to be determined, we obtain

$$\psi = v_\infty \cdot y - \frac{m}{2\pi} \cdot \frac{y}{x^2 + y^2} + \frac{q}{2\pi} \cdot \left[ \operatorname{arctg} \left( \frac{y}{x - x_0} \right) + K \right] \quad (9)$$

with  $K = 0$  for  $\arctan \left( \frac{y}{x - x_0} \right) \geq 0$  and  $K = \pi$  for  $\arctan \left( \frac{y}{x - x_0} \right) < 0$ .

If  $m = 2\pi \cdot r_j^2 \cdot v_\infty$  is put into equation (9) for the dipole moment and  $q = k \cdot \pi \cdot r_j \cdot v_j$  for the sink intensity, whereby  $k$  is an experimental constant, then the flow function reads as follows:

$$\psi = v_\infty \cdot y - r_j^2 \cdot v_\infty \cdot \left( \frac{y}{x^2 + y^2} \right) + \frac{k}{2} \cdot r_j \cdot v_j \cdot \left[ \operatorname{arctg} \left( \frac{y}{x - x_0} \right) + K \right] \quad (10)$$

With the dimensionless coordinates  $\eta = y/d_j$  and  $\xi = x/d_j$ , and after putting in the velocity ratio  $\lambda = v_j/v$  we finally obtain

$$\psi = \frac{v_\infty \cdot d_j}{4} \cdot \left\{ \eta \cdot \left( 1 - \frac{1}{(\xi^2 + \eta^2)} \right) + k \cdot \lambda \cdot \left[ \operatorname{arctg} \left( \frac{\eta}{\xi - \xi_0} \right) + K \right] \right\} \quad (11)$$

The flow line diagrams for the flow around the jet calculated using this equation for the relative jet intensities  $\phi = 290$  ( $v_j = 330$  m/s,  $v_\infty = 20$  m/s) and  $\phi = 32.2$  ( $v_j = 220$  m/s,  $v_\infty = 40$  m/s) are shown in Figs. 28 and 29. By appropriately varying the location of the sink ( $\xi_0$ ) and the sink intensity ( $k$ ) quite good agreement with the measured values was obtained

with  $\phi = 290$  for the boundary flow line which surrounds the quantity of air taken in by the jet. By contrast, even with an additional increase in the effective diameter of the jet good agreement with the measured values could not be obtained with the lower jet intensity, since the formula does not take into consideration the deformation of the jet which is already quite strong at  $\phi = 36$ . Behind the jet the measured flow line diagrams differ considerably from the mathematically determined diagrams, since only the two-dimensional case of an infinitely long line sink was considered in the calculation. Better agreement could be obtained here by means of an additional surface sink in the x, z-plane.

The comparison shows that in order to separate the two effects mathematically -- in so far as such a separation is at all possible -- we must have more knowledge about the mixing effects between the jet and the cross flow.

The attempt was therefore made to achieve this separation experimentally for effects in the vicinity of the fuselage. To do this the pressure distribution on the fuselage body is measured for the following arrangements: /33

- a) jet without cross flow
- b) jet with cross flow
- c) cylinder in place of jet with cross flow.

Figs. 30 and 31 show the isobar fields on the cylindrical portion of the fuselage projected on a plane for the injector effect (a) and the displacement effect (c). The configuration of the fields differs considerably so in the case without any cross flow (Fig. 30) low pressure fields are induced on the underside of the fuselage by the air taken in which streams into the jet from all sides and partially from the regions above the fuselage. These fields surround the jet orifice in a ring-like

manner. Their exact shape is determined by the geometry of the fuselage body and by the diameter ratio of the fuselage and jet. The isobars would be circular if the jet emerged perpendicularly from a circular smooth plate, in which case the influx of injector air from all sides would take place uniformly. The pressure on the fuselage body decreases more and more as the jet gets closer. This results in a downward pressure on the fuselage which decreases the net lifting force of the jet.

In estimating the pressure distribution of the arrangement with the cross blown rigid cylinder (Fig. 31) it must be noted that the flow around the cylinder in the vicinity of the point of attachment with the fuselage has a three-dimensional character. Here it is possible for the flow medium to move laterally over the contour of the fuselage, whereby the configuration of the lateral and rear positive pressure regions in particular changes in comparison with the two-dimensional case. For this reason, in the case of the subcritical flow around a cylinder being studied here, the depressions on the shell of the fuselage close to the cylinder are less than the familiar values for the two-dimensional case for less than those for a jet emerging from an infinite plate. Thus for example with an inscribed angle of the cylinder of  $90^\circ$  only values of  $\Delta p/q = -0.4$  were reached as opposed to values  $-0.7$  in the two-dimensional case. Thus the two pressure distribution fields in Fig. 30 and 31 differ in that only the injector effect is operative in Fig. 30. Flow around the jet does not occur in this case. By contrast, in Fig. 31 "flow around the jet," i.e. displacement and wake formation, takes place without the injector effect.

The two special arrangements are now compared in Figs. 32 and 33 with experiments with free jets in a pure cross flow. In both cases the Mach number at the orifice is  $M_j = 1$  only the

velocity of the oncoming flow was varied. In Fig. 32 the force of the oncoming wind is stronger. At first glance both isobar fields show a certain similarity with that for a cylinder in a flow. There is a weak high pressure in front of the jet and low pressures next to the jet and a wake behind the jet. The injector effect, however, considerably modifies the pressure field with increasing jet intensity. In the immediate vicinity of the jet the pressure drops and the lateral positive pressure regions become more pronounced. The high pressure region in front of the jet extends further forward in front of the jet and thereby becomes smaller and weaker. The wake space behind the jet becomes strongly "sucked in" and smaller due to the injector effect.

On the rear side of the jet the isobars are moved close together by the strong inward movement of the outer flow which amply supplies this region with secondary air. This is also confirmed by the vapor flow line photographs (see above). The differences in the configuration of the positive pressure regions of the two arrangements in this region -- whereby with  $\phi = 36$  the isobars spread out more both towards the back and towards the sides -- are due to the different degrees of mixing of the jet with the outer flow immediately behind the jet orifice. On the whole the center of gravity of the depression in these two arrangements moves towards the jet axis in comparison with the depression for the cross blown cylinder. Figs. 34 and 35 show the curve of the integral pressure component  $\Delta p_N$  in the z-direction along the fuselage for the three arrangements. The pressure component  $\Delta p_N$  was obtained by partial integration of the pressure distribution over the circumference of the fuselage. This dimensionalized plotting was chosen to illustrate the depression portion of the undisturbed jet, since comparison in another form between the three different arrangements is otherwise not possible. The

space in the upper portion of the diagrams indicates the location and diameter of the jet or cylinder. In the arrangements with the jet the Mach number at the orifice is  $M_j = 1$  in each case and in the two figures only the oncoming flow velocity is different.

Comparison of the two diagrams clearly show that the interference effect of the unblown jet on the fuselage is quite large in comparison with the jet in a cross wind with  $v_\infty = 20$  m/s. However this effect is only small when compared with that for an oncoming flow velocity of  $v_\infty = 56$  m/s. On the other hand, the interference portion of the cylinder increases proportionally with  $q_\infty$  as expected. Fig. 36 shows the changes in perpendicular force along the fuselage for the arrangements with a rigid /34 cylinder in a cross flow and a pure jet in a cross flow. The graphs for perpendicular force were likewise obtained by partial integration of the pressure distributions along the circumference of the fuselage. In the arrangements with the jet the Mach number at the orifice is  $M_j = 1$  in each case; only the oncoming flow velocity was varied. Here the rigid cylinder, the curve for which is represented by a solid line, behaves in a way which is unsuitable for representing the jet:

- a) It does not spread out. This is typical of only a single jet with a relative jet intensity of  $\phi = q_j/q_\infty = \infty$ .
- b) It has no injector effect. This is typical of only a single jet with vanishing jet velocity, hence at  $\phi = 0$ .

Since we are here not considering the distant field ( where deformation and drift dominate) but rather the pressure

distribution on the fuselage, hence the close field, deformation and drift do not yet play any noticeable role. Thus any behavior such as with  $\phi = \infty$  is not expected to occur. Rather the  $c_p$  curve for the rigid cylinder would have to fall into line with the  $\phi$  variables for the jets as if it were a jet with  $\phi \approx 0$ . This actually occurs: the dissipation positive pressure region in front of the jet by the injector effect can clearly be seen if we consider the cylinder or "zero jet" as the starting point. It is interesting that  $\phi = 36$  there is only a small positive  $c_p$  component in front of the jet because the influence of the injector effect is already so dominating. Also very evident is the drop in low pressure in or of the wake itself. Without the injector effect the usual strong low pressure ( $0.5 < x/d_j < 4$ ) prevails behind the cylinder. With the injector effect ( $\phi = 36$  to 290) the wake is practically sucked away and therefore the lateral low pressure also sharply increases. Thus flow around a jet with the injector effect more closely approximates the theoretical frictionless flow around a cylinder than the flow around an actual cylinder with a viscosity effect. The maximum lateral low pressure coefficients are reached with a  $\phi$  value as low as 36 and with further increases in the coefficients again decrease. The above mentioned variation in jet mixing is responsible for this.

Even experimentally it is not possible to fully separate the injector effect from the displacement effect. However the comparative measurements dealt with here contribute considerably to our understanding of these complicated events.

Fig. 37 shows the perpendicular force coefficients on the 37 fuselage for the following model configurations:

- a) fuselage alone

- b) fuselage with a solid body substituted for the jet
- c) fuselage with a lift jet of  $\phi = 290$  or  $\phi = 36$ .

The graph shows that the rigid cylinder, with its displacement effect on the fuselage, induces only small negative perpendicular forces. Initially they do not increase with the angle of attack. At angles of attack greater than  $\alpha = 12^\circ$  the lift component of the cross blown fuselage becomes clearly recognizable. In contrast, with actual lift jets in a cross flow considerably greater negative perpendicular forces develop on the fuselage due to the interaction of the injector effect and displacement. These negative perpendicular forces are clearly dependent on  $\phi$ , as has already been shown in the graph of cross-wind forces in Fig. 36. The dependence on  $\phi$  is due mainly to the monotonic decrease with  $\phi$  of the positive pressure region in front of the jet, i.e. depression.

This finding shows that the depression is in no way caused solely by the injector effect, but in the average angle of attack range it is the decisive factor. At larger angles of attack the perpendicular forces in all of the model configurations tend towards a common linearly increasing function.

#### 8. Fuselage with Single Jet

In what follows the influence of three important test parameters, i.e. relative jet intensity  $\phi = q_j/q_\infty$ , jet diameter  $d_j$  or  $d_j/D$  and the angle of attack  $\alpha$ , on the close interference effect of a single jet next to the fuselage are studied in detail.



### 8.1. Influence of the Relative Jet Intensity $\phi$

The isobar diagrams in Fig. 38 show the pressure distribution on the cylindrical portion of the fuselage projected in the plane of the drawing for the relative jet intensities  $\phi = 290$  to 36. The jet/fuselage diameter ratio is  $d_j/D = 0.3$ . The local static surface pressures were made dimensionless with the dynamic pressures of the oncoming flow. In all of the arrangements small high-intensity low pressure fields form on both sides of the jet orifice. These fields run almost symmetric to the y-axis and have nearly the same magnitude. They arise due to the overlapping of the displacement effect and the injector effect, as already discussed in detail in Section 7. At a somewhat greater distance from the jet, at an azimuth angle of about  $\psi = 80^\circ$ , the low pressure region in the arrangement with a large value of  $\phi$  ( $\phi = 290$ ,  $v_\infty = 20$  m/s) surrounds the entire jet orifice and also extends far upstream. From here the influence of the injector effect of the jet prevails, since the dipole-like distant effect of its outward displacement of  $1/r_j^2$  dies off faster than its sink effect which is proportional to  $1/r_j$ . /37

If we go to smaller  $\phi$  values, either by increasing the oncoming flow velocity or by decreasing the jet Mach number the influence of the injector effect of the jet with respect to the surrounding flow subsides more and more. The pressure region in front of the jet, which also already exists with large  $\phi$  values and appears as positive pressure in the above portion of the fuselage, gradually spreads out towards the front and sides and thus divides the closed low pressure region around the jet orifice which exists in the case of large relative jet intensities. The wake spreads out at the same time (see flow line diagrams in Figs. 28 and 29). Fig. 39 shows how the normal force changes along the fuselage during this process. A detailed

analysis of this was already given in Section 7. The reduction in the size of the positive pressure regions decreasing monotonically with  $\phi$  in front of the jet due to the injector effect also determines the shape of the  $c_N$  curves in Fig. 40. The negative perpendicular force coefficients for the three fuselage lengths  $L = 4 d_j, 8 d_j$  and  $12 d_j$  (in each case the jet is positioned in the middle) tend gradually towards a limit value with increasing  $\phi$ . This process can clearly be seen in Fig. 41 where the perpendicular force coefficient  $c_{Nj}$  is plotted over the dynamic pressure of the oncoming flow. The coefficient  $c_{Nj}$  was made dimensionless with the dynamic pressure of the jet  $q_j$ , which was the same in all of the arrangements. Finally, at  $q_\infty = 0$  with the pure injector effect of the jet the limit value of its interference effect is obtained.

Fig. 42 shows that with increasing  $\phi$  the center of gravity of the depression moves upstream due to the decrease in the positive pressure regions in front of the jet and the increased intake of the jet wake. A nose-heavy moment develops most quickly with short relative fuselage lengths.

## 8.2. Influence of the Jet Diameter

An important geometric parameter is the ratio of the jet diameter to the fuselage diameter, since jets with small orifice diameters have both a smaller displacement effect and a weaker absolute injector effect than jets with larger orifice diameters. It will have to be shown to what extent the jet diameter can be eliminated by using appropriate graphs.

/38

Fig. 43 shows the pressure distribution on a portion of the fuselage projected on plane for the following three jet diameters:  $d_j = 45, 37.5$  and  $30$  mm. The jet Mach number is  $M_j = 1$  in all cases, hence the total momentum is different. The configuration

of the isobar diagrams has already been discussed in the above section so that here we are only interested in the differences between the three diagrams. It is clear that the suction regions around the jet orifice spread out in all directions when the jet diameter is increased, and indeed almost proportionally to the diameter ratio. This is due to the injector effect, the intensity of which is also proportional to the jet diameter. Thus for plotting the perpendicular force along the fuselage in Fig. 44 the dimensionless fuselage axis coordinate  $\xi$  was chosen as the abscissa. In this type of graph the curves for all three jet diameters coincide with the exception of the region around the jet orifice. Within the actual jet  $c_p = \text{const.} \cdot d_j^2$  in keeping with the displacement effect of the jet. This agreement is also valid for the curves in Fig. 45 with  $\phi = 36$ , i.e. for higher on coming flow velocities. Deviations from this show up only in the jet wake. There as the jet diameter becomes smaller due to the decreasing suction effect -- which without cross flow with  $d_j = 30$  mm is only 2/3 of the suction effect of the large jet ( $d_{j1} / d_{j3} = 30/45$ ) -- the wake space spreads out more downstream. This process already showed up to a lesser degree with the large jet diameter ( $d_j = 45$  mm) when  $\phi$  was reduced in Fig. 39. The fact that the perpendicular force coefficient in Fig. 46 changes less over  $d_j/D$  when  $\phi = 36$  than when  $\phi = 290$  is also due to the spreading out of the jet wake when the jet diameter is decreased.

Fig. 47 contains an interesting comparison. In this figure the total jet momentum for all the jet nozzle diameters was held constant by suitable adjusting the jet Mach number. Therefore the jet with the smallest orifice diameter has the greatest specific momentum ( $M_j = 1$ ). In the jet itself the gradation in negative  $c_p$  values proportional to  $d_j^2$  appears once more. By contrast, the different injector effect of the three jets can clearly be seen in the variation in the curves in front of the

jet along the relative model length  $x/d_j$ .

### 8.3. Influence of the angle of attack

/39

Isobar diagrams, as in Figs. 48, 49 and 50, were determined for each of six different angles of attack. Here however they are only shown in the form of partial integration ( $\Delta c_{N\alpha} = f(\xi)$ ) and the full integration ( $\Delta c_{N\alpha} = f(\alpha)$ ). The change in pressure coefficients of the separate fuselage bulkheads as a result of the angle of attack setting is expressed by the following equation:

$$\Delta c_{p\alpha} = c_{p\alpha} - c_{p\alpha=0} \quad (12)$$

Accordingly, the following equation is valid for the change in perpendicular force coefficients:

$$\Delta c_{N\alpha} = c_{N\alpha} - c_{N\alpha=0} \quad (13)$$

For large angles of attack  $\Delta c_{N\alpha}$  increases with  $\alpha$  in Fig. 53 for all of the experimental setup. Of course the gradients for the various jet diameters and jet intensities are quite different. As comparison of the corresponding isobar diagrams shows, this increase is caused primarily by events on the underside of the fuselage. The gradient is without exception noticeably steeper than in the "fuselage minus jet" arrangement in Fig. 37. Hence it must be caused by the jet. More detailed analysis of changes in  $\Delta c_{p\alpha}$  in figs. 51 and 52 for  $d_j/D = 0.3$  shows that the following effects are at the bottom of this. Due to the injector suction effect the wake behind the jet, as already mentioned, is practically consumed. This causes the outer air behind the jet to flow together and a pressure region forms on the above underside of the fuselage which increases with the angle of attack. For small jet diameters this process occurs only to a

limited extent, since in this case the wake spreads out further downstream as a result of the smaller suction effect of the jets. This is clearly shown by the low pressure fields in the isobar diagrams for  $\alpha = 0^\circ$  (Fig. 48). This effect is especially pronounced in the case of the small jet diameter  $d_j/D = 0.2$ , in which a narrow low pressure region behind the jet extends to the end of the fuselage.

For angles of attack between  $-6^\circ$  and  $6^\circ$ ,  $\Delta c_{N\alpha}$  decreases constantly for  $\phi = 290$ , even though the effect described above for large values of  $\alpha$  is already operative. It is concealed, however, by the influence of the suction points on both sides of the jets. These reach a maximum at  $\alpha = 6^\circ$ . This behavior remains to be explained and should be investigated in a future separate study. It can be assumed, however, that the injector effect at angles of inclination of  $\theta > 90^\circ$ , in which the jet is directed against the oncoming flow, tends towards a limit value. A similar trend was already shown by the drift curves in Fig. 15. Here a limit value was reached at  $\theta \approx 99^\circ$ .

Under the test conditions where  $\phi = 36$ , in which the modified 40 displacement effect prevails because of the injector effect, the  $\Delta c_{N\alpha}$  curve rises over the entire range of the angle of attack. This curve is similar to that for a fuselage with a cylinder attached in place of a jet (Fig. 37).

#### 8.4. An Approach to an Analytical Determination of Changes in Perpendicular Force Along the Fuselage Body

From the measured changes in perpendicular force along the dimensionless fuselage axis coordinate  $\xi$  it can be seen that there are regularities between the interference effect and both its relative jet intensity  $\phi$  and the jet/fuselage diameter ratio ( $d_j/D$ ). However since the mixing of the jet with the cross flow

in the immediate vicinity of the fuselage induces extremely complex three-dimensional flow conditions, it is hardly possible to calculate the changes in perpendicular force solely on the basis of theory. Even in the case of simple smooth plates such an approach only results in unsatisfactory agreement with experimental results [31]. Nevertheless, in order to get some idea of the setting up of suitable functions for describing changes in  $c_p$  we will use an analogy with the pressure distribution on the stagnation point flow line ( $\eta = 0$ ) in front of a cross blown cylinder. On the basis of test findings the function set up in this way must be modified by appropriate coefficients.

In using this method of calculation it is helpful to subdivide the length of the fuselage into several partial sections. Within the individual regions the values of  $c_p$  must be assumed to vary within a certain range, since the  $c_p$  curve is discontinuous from one section to another.

Section 1:  $-\infty < \xi < -0,5$  (in front of the jet)

Section 2:  $-0,5 < \xi < +0,5 + f(d_j; \phi)$  (jet locus and wake portion)

Section 3:  $f(d_j, \phi) + 0,5 < \xi < +\infty$  (behind the jet)

The portion of the fuselage  $\Delta\xi = f(d_j, \phi)$  here describes the spreading out of the wake.

It is now assumed that the change in  $c_p$  in Section 1 in front of the jet is proportional to the change in pressure on the stagnation point flow line ( $\eta = 0$ ). Again, as in Section 7 of this paper, an infinitely long rigid cylinder of the same diameter is used in place of the jet. The following equation is valid for the potential of the stagnation point flow line of

the infinitely long line dipole:

$$\phi_D = \frac{m}{2\pi \cdot x} \quad (14)$$

From this we can calculate the velocity as:

/41

$$v_{xD} = \frac{\partial \phi_D}{\partial x} = -\frac{m}{2 \cdot \pi \cdot x^2} \quad (15)$$

With the dipole moment  $m = 2\pi \cdot r_j^2 \cdot v_\infty$  we finally obtain:

$$v_{xD} = -v_\infty \cdot \frac{r_j^2}{x^2} \quad (16)$$

Likewise, from the potential of the stagnation point flow line of the infinitely long line sink:

$$\phi_J = \frac{q}{2\pi} \cdot \ln \frac{x}{r_j} \quad (17)$$

we get the velocity:

$$v_{xJ} = \frac{\partial \phi_J}{\partial x} = \frac{q}{2\pi \cdot x} \quad (18)$$

After putting in the sink intensity  $q = k \cdot \pi \cdot r_j \cdot v_j$  the velocity becomes:

$$v_{xJ} = \frac{k}{2} \cdot v_j \cdot \frac{r_j}{x} \quad (19)$$

If the oncoming flow velocity  $v_\infty$  is then combined with these two velocities we get the velocity distribution on the stagnation point flow line:

$$v_{xges} = v_\infty - v_\infty \cdot \frac{r_j^2}{x^2} + v_j \cdot \frac{k}{2} \cdot \frac{r_j}{x} \quad (20)$$

---

1. The mnemonic subscript "ges" stands for "velocity."

or with the dimensionless coordinate  $\xi = x/d_j$  and with  $\lambda$  for the velocity ratios  $v_j/v_\infty$  we get

$$v_{xges} = v_\infty \left[ 1 - \left(\frac{1}{2\xi}\right)^2 + \lambda \cdot \frac{k}{2} \cdot \left(\frac{1}{2\xi}\right) \right] \quad (21)$$

The pressure distribution follows from the Bernoulli equation:

$$\Delta p = p - p_\infty = \frac{\rho}{2} (v_\infty^2 - v_{xges}^2) \quad (22)$$

Since, according to the equation set up, the change in /42  
perpendicular force in Section 1 is supposed to be proportional to the pressure distribution on the stagnation point flow line we obtain the following from equations (22) and (21) by introducing the term  $\lambda \approx \sqrt{\phi}$ :

$$c_p = \frac{\Delta p}{q_\infty} \sim \underbrace{k \cdot \sqrt{\phi} \left[ \left(\frac{1}{2\xi}\right)^3 - \left(\frac{1}{2\xi}\right) \right]}_I - \underbrace{\left[ \left(\frac{k}{2}\right)^2 \cdot \phi - 2 \right] \left(\frac{1}{2\xi}\right)^2 - \left(\frac{1}{2\xi}\right)^4}_{II} \quad (23)$$

The equation contains a total of 4 addends in which the dimensionless fuselage coordinate  $\xi$  appears with negative exponents. The correct intensity distribution between the terms must first be determined on the basis of measurements.

It turns out to be convenient to consider the  $\xi$  terms with even exponents just like those with odd exponents. Close to the jet the terms with even exponents determine the shape of the  $c_p$  curve. In the limiting case of  $\xi = -0.5$  (forward edge of the jet)  $c_p = II$ , whereas for large distances from the jet  $c_p \approx I$ . To determine the coefficients of the two partial functions I or II appropriate values are taken from the measurement shown in Fig. 39. In particular, this determination is



made as follows: for  $\xi = -6$  (the largest measured value) the component given by the partial function II is negligibly small in comparison with the component given by I. Moreover, in the partial function I the  $\xi$  term of the third degree is negligibly small in comparison with the  $\xi$  term of the first degree so that for  $c_p$  we obtain the simple equation

$$c_p = -\frac{k \cdot \sqrt{\phi}}{2\xi}, \quad (24)$$

From this  $k$  can be calculated and introduced into the partial function II. For section 1 we get

$$k_1 = -0,011.$$

At the edge of the jet ( $\xi = -0.5$ ) the measurement requires that the partial function II is composed as follows in order to calculate  $c_p$ :

$$c_p = -\left(\frac{1}{2\xi}\right)^2 \cdot \left[ \left(\frac{k}{2}\right)^2 \cdot \phi - k' + k'' \left(\frac{1}{2\xi}\right)^2 \right], \quad (25)$$

whereby  $k'$  should conveniently be equal to about  $-0.1$  and  $k'' \approx 0.001$ . Even at points which are just slightly forward of the jet the  $\xi$  term with  $k''$  is negligibly small. It will be left out of the following equations.

Thus for the pressure coefficients in section 1 we get the 43 following equation

$$c_{p1} = -0,011 \cdot \sqrt{\phi} \left[ \left(\frac{1}{2\xi}\right)^3 - \left(\frac{1}{2\xi}\right) \right] - \left[ (0,0055)^2 \cdot \phi + 0,1 \right] \cdot \left(\frac{1}{2\xi}\right)^2. \quad (26)$$

In section 3 behind the jet the  $c_p$  values are calculated as follows using a similar mathematical formula:

$$c_{p3} = -0,002 \cdot \sqrt{\phi} \left[ \left(\frac{1}{2(\xi-\Delta\xi)}\right)^3 - \frac{1}{2(\xi-\Delta\xi)} \right] - \left[ 0,001^2 \cdot \phi + 0,19 \right] \cdot \left(\frac{1}{2(\xi-\Delta\xi)}\right)^2. \quad (27)$$

Here the term  $\Delta\xi = \Delta x/d_j = f(d_j, \phi)$  takes into account the spreading out of the jet wake as a function of the jet diameter and of the relative jet intensity. The coordinate shift  $\Delta\xi$  is shown in diagram form in Fig. 54. The pressure coefficients in the locus of the jet are proportional to  $d_j^2$  (displacement effect) and are calculated from measured values according to the following equation:

$$c_{p2} = (\phi \cdot 10^{-4} - 0,035) - 1,73 \cdot \left(\frac{d_j}{D}\right)^2 \quad (28)$$

They change only slightly with the relative jet intensity  $\phi$ . The component of the second term of the equation essentially determines the magnitude  $c_p$ . Its constant (1.73) takes into account the modified displacement effect of the jet due to the injector effect and is considerably larger than in the model configuration with solid bodies used in place of the jet, i.e.  $\phi = 0$  (see comparison curves for  $c_p$  in Fig. 36).

By means of equations (26), (27) and (28) the perpendicular force coefficient of a cylindrical fuselage body with a single jet is calculated to be:

$$c_N = \frac{\pi \cdot d_j}{D} \left[ \int_{-\infty}^{-0,5} c_{p1} \cdot d\xi + \int_{-0,5}^{0,5+\Delta\xi} c_{p2} \cdot d\xi + \int_{0,5+\Delta\xi}^{\infty} c_{p3} \cdot d\xi \right] \quad (29)$$

Fig. 46 shows that there is quite good agreement between the measured points and the calculated values.

In summary, it can be stated that the change in perpendicular force along the fuselage in front of and in back of the jet can be calculated using the derived functions, whereby empirically determined coefficients modify the original function. The outer flow moving perpendicularly to the jet acts in such a way that with increasing flow velocity  $v_\infty$  the size of the low pressure /44

regions in front of the jet becomes smaller and smaller. The perpendicular forces in the jet locus itself change only slightly with  $\phi$  in the range of  $\phi$  studied here. The equation is valid for the relative jet intensities studied of  $\phi = 36$  to  $\phi = 290$ , the angle of attack  $\alpha = 0^\circ$  and a jet/fuselage diameter ratio of  $0.2 \leq d_j/D \leq 0.3$ . For angles of attack  $\alpha \neq 0^\circ$  a  $\Delta c_{N\alpha}$  component from Fig. 53 must be added to the perpendicular force coefficients determined using equation (29).

## 9. Fuselage with Double Jet

In the double jet arrangements, along with the flow mechanics and geometric test quantities  $\phi$ ,  $\alpha$  and  $d_j/D$  studied in detail in Section 8 there appears another important parameter, which is the distance  $L_j$  between the two jets. The importance of this parameter and the degree of interaction between the two jets are shown quite impressively by the isobar diagrams in Figs. 55 and 56. In comparison with the single jet ( $L_j/D = \infty$ ), with  $\phi = 290$  the addition of a second jet also causes changes in the pressure fields in the vicinity of the forward jet. This is clearly shown by the changes in isobar configuration as the distance between the two jets is increased. The distance was changed in several steps between  $L_j/D = 1.5$  and  $L_j/D = \infty$  (single jet). Even with  $L_j/D = 4$ , which with  $d_j/D = 0.3$  corresponds to a distance between the jets of more than 13 jet diameters, it is still possible to find differences in the isobar diagram around the forward jet in comparison with the isobar diagram for a single jet.

Comparison of individual diagrams reveals the following:

- 1) the suction regions around the orifice of the forward jet spread out due to the injector effect of the rear jet, whose oncoming flow is severely obstructed by the first jet;
- 2) the low pressure areas around the rear jet spread out

less than in the case of the single jet. This last point is due primarily to the smaller oncoming flow velocity as a result of the shadowing caused by the forward jet which has already been discussed in Section 6.2. To a small extent this is also due to the strong downward movement of the flow induced by the forward jet. This decreases the difference in direction between the two flows.

At higher oncoming flow velocities, i.e. for smaller  $\phi$  values (Fig. 56), each of the two jets develops its own pressure field similar to a single jet even for separating distances of  $L_j/D = 2$ . The influence of the forward pressure field due to the injector /45 effect of the rear jet can no longer be measured due to the substantial interference component of the displacement effect at this jet intensity.

Figs. 57-59 show perpendicular force curves for changes in  $c_p$  along the cylindrical portion of the fuselage for different distances between the jet axes with  $\phi = 290$  and  $36$  and with  $d_j/D = 0.3$  and  $0.2$ . The loci of the two jets are clearly marked on the upper edge of the graphs. In order to complete the spacing series the  $c_p$  curve for the single jet must still be plotted. Its curve corresponds to an "infinite" space between the two jets. In the three diagrams the length of the  $x/d_j$  axis of the cylindrical portion of the fuselage shown corresponds to the longest adjustable version  $L_j/D = 4$ . With the shorter fuselage versions the  $c_p$  are also drawn on the jet axis locus of the long version so that there is a gap between the two halves (each half representing the region around one of the jets). The larger this gap, the shorter the fuselage version in question. In this method of representation the influence of  $L_j$  on the changes in perpendicular force is easier to see. The normal forces, which without exception are negative down to the tail section of the fuselage, differ quite distinctly for different

distances between the jets, especially in Fig. 57 with  $\phi = 290$  and  $d_j/D = 0.3$ . (The positive perpendicular forces on the tail should not be regarded as a pure interference effect, but rather they are due to the particular shape of the model tail.) As the jets are moved apart the minimum values of  $c_p$  increase by about the same amount on the locus of the forward jet and in the region between the two jets, and as expected they slowly approach the perpendicular force curve for the single jet. In the forward half of the model the difference between the curves for the single jet is a measure of the magnitude of interference of the rear jet on the forward jet, primarily due to the injector effect (downward current). Similarly the degree of shadowing of the rear jet (smaller local oncoming flow velocity and hence weaker displacement effect) can be inferred from the differences between the rear section of the  $c_p$  curve and the curve for the single jet. It turns out that the extreme values of  $c_p$  on the locus of the rear jet decrease as the distance between the two jets is increased and at  $L_j/D = 4$  they reach the value of the single jet. The shadowing effect becomes smaller and the rear jet therefore gradually begins to behave like a single jet. By contrast, up to this distance between the jets the interference effect of the rear jet on the forward jet due to the injector effect has not died away. This could already be seen in Fig. 55. On the other hand, with the smallest jet diameter ( $d_j/D = 0.2$ ) in Fig. 57, even when  $L_j/D = 1.5$  only a small amount of interaction between the two jets in the jet loci can be detected. A depression remains /46 only in the area between the two jets evidently due to the fact that the forward jet obstructs the flow of injector air to the rear jet. With  $\phi = 36$  in the arrangement with the larger oncoming flow velocity and thus greater displacement effect of the jets only the shadowing effect of the forward jet still exists. The isobar diagrams already showed that starting from  $L_j/D = 2$  each of the two jets forms its own pressure field,

since, as expected, at this point the interference component of the injector effect of the jet falls off sharply relative to the interference component of its displacement effect.

By subtracting the pressure coefficients of the single jet, which is not influenced by a second jet, it is possible to obtain reliable quantitative data on the interference components of the two jets (Fig. 61). The diagram on the left shows to what extent the depression in the locus of the forward jet is increased by the rear jet. The minimum pressure coefficient of the single jet is used as the reference quantity. The increase in the depression is greatest at  $\phi = 290$  due to the prevailing injector effect of the jets. However it drops off very sharply when the distance between the two jets  $L_j/D$  is increased. At  $\phi = 36$  -- here the component of the displacement effect of the jets predominates -- hardly any increase in the depression on the locus of the forward jet can be detected even when the distance between the jets is small. The diagram on the right shows the increase in  $c_p$  on the rear jet due to shadowing in comparison with the single jet. The distance between the jets here more strongly effects the shape of the curve than in the case of the forward jet. The different slopes of the curves for the three jet intensities, whereby the increase in  $c_p$  is greatest at  $\phi = 36$  as the distance between the jets is decreased, are due to the different degrees to which the jet mixes with the outer flow directly behind the orifice. In the models using a solid body in place of the jet (Fig. 60) the wind shadow effect is much greater still, since the solid body has no injector effect which sucks in and reduces the size of the wake.

Figs. 62 and 63 show the changes in the perpendicular force plotted over the distance between the double jets for different relative jet intensities and for  $\alpha = 0^\circ$ . As expected from the

results of Fig. 61, the integral value of the depression increases as the distance between the jets is increased. When  $d_j/D = 0.2$  the change in  $c_N$  with the distance between the jets is less than when  $d_j/D = 0.3$  because there is less interaction between the jets (Fig. 58).

For a quick and useful estimation of the jet-induced perpendicular forces on a fuselage body with double jets it is convenient to combine the effects of the individual parameters in one empirical formula. Because of the strong interdependence of the parameters it is not possible to make a simple combination of the parameters. On the basis of the curves shown in Figs. 62 and 63 and other data not shown here [32,33] we obtain the following estimation formula:

$$c_N = a_1 \cdot b_1 + a_2 \cdot b_2 \cdot \phi \quad (30)$$

The expressions  $a_1$  and  $a_2$  take into account the effect of the jet/fuselage diameter ratio and  $b_1$  and  $b_2$  stand for the terms combining  $d_j/D$  and the distance between the jets  $L_j/D$ . Specifically, these terms are written out as follows:

$$\begin{aligned} a_1 &= -(0.1 + 0.75 \cdot \frac{d_j}{D}) & a_2 &= (0.0004 - 0.0057 \frac{d_j}{D}) \\ b_1 &= (\frac{L_j}{D})^{(2d_j/D - 0.12)} & b_2 &= (\frac{L_j}{D})^{(0.85 - 2.38 d_j/D)} \end{aligned}$$

Equation (30) is valid for relative jet intensities ranging between  $\phi = 36$  and  $290$ , a jet/fuselage diameter ratio of  $0.2 \leq d_j/D \leq 0.3$  and a distance between the jets of  $1.5 \leq L_j/D \leq 4$ . For a fuselage angle of attack of  $\alpha \neq 0^\circ$  the  $\Delta c_{N\alpha}$  values can be obtained from Figs 64-67. These contain a wide parameter spectrum.

Fig. 68 shows the pitching moment coefficients of the double jet fuselage as a function of the distance between the jets. By definition the moment reference point lies in the intersection of the forward jet axis and the fuselage axis so that the pitching moment must increase as the distance between the jets becomes greater. At  $d_j/D = 0.3$   $c_M$  increases faster over  $L_j/D$  because of the larger depression on the rear jet locus (Figs. 57 and 58) than when the jet diameter is small ( $d_j/D = 0.2$ ).

#### 10. Fuselage with Wing

An important design parameter for aircraft is the position of the wing with respect to the power units. This parameter also proves to be influential with regard to jet interference. Five wing positions were studied. These are shown in detail in Fig. 4. In keeping with the purpose of the study the pressure distribution was determined only on the fuselage itself and not on the wings.

Depending on the position of the wing very different pressure fields are formed on the fuselage (Figs. 69 and 70) in comparison with the test setups without wings (Figs. 55 and 56). Particularly striking in the case of the forward and rear wing positions are the large low pressures in the vicinity of the jet emerging underneath the wing in each case. Here the wing obstructs the flow of injector air from the top of the fuselage so that the jets must take in more air from their immediate surroundings, i.e. from the underside of the wing and fuselage as well as from the forward outer field. /48

According to Figs. 69 and 70 the stagnation point for all five wing positions is located on the top of the wing -- in spite of the geometric angle of attack of  $\alpha = 0^\circ$  -- as a result



of the jet-induced downward current. In the portion of the fuselage in front of the wing this likewise implies a considerably more negative effective local fuselage angle of attack.

On top of the wing only its displacement appears due to a weak low pressure field on the top of the fuselage. The graphs in Figs. 71-74 show the change in perpendicular force caused by the wing

$$\Delta c_{pF} = c_{pF} \text{ (with wing)} - c_p \text{ (without wing)} \quad (31)$$

for several wing positions and relative jet intensities. According to this partial integration the wing induces additional low pressures on the underside of the fuselage mainly in the region of the leading edge of the wing, whereas at the respective point on the trailing edge of the wing the changes are considerably smaller. In order to explain this we will use the following simple case as an analogy.

The pressure distribution on a wing set at a certain angle of attack in an infinitely large parallel flow is mainly determined by the angle of attack (with the exception of very small angles of attack). The thickness distribution of the wing does not have all that much effect in this matter as long as the thickness is not very great. As everyone knows, a strong low pressure forms on such a wing in the vicinity of the leading edge. This low pressure quickly fades away towards the trailing edge and at the trailing edge itself sinks practically to 0. Hence no pressure difference can be detected on the trailing edge because the "Kutta-Joukowski" flow condition must be met for a well designed airfoil wing. Basically the main physical features of this picture also apply to a wing in the presence of lift jets. The analogy consists of

the fact that the lift jets induce a downward component in the outer flow in their immediate vicinity and also at greater distances due to their injector effect. As a result the wing is in a more or less strong downward flow. In our analogous situation this implies a wing with a negative angle of attack. Thus we can expect that with such a wing the familiar strong low pressure field, which dies away towards the trailing edge of the wing, will appear at the point of the leading edge of the wing and/or above or below it. Quantitative deviations in this viewpoint are to be expected, since the downward component of the oncoming flow is at maximum in the vicinity of the jet axis and decreases in front of or behind the axis.

/49

To be sure there are quantitative differences between the two flow configurations, but these do not adversely affect the basic agreement of the physical picture.

Thus due to the injector effect of the lift jets even at  $\alpha = 0^\circ$  (geometric) the fuselage is in a downward directed flow with an inclination which differs locally. Because of the wing additional velocities are induced along the axis of the fuselage and perpendicular to it. For the same angle of attack these velocities are directed downward in front of the wing and upward behind the wing. Thus a fuselage with a wing and lift jets finds itself in a flow with a very different angle of attack distribution along the axis of the fuselage. In order to determine this the method given in [35] must be further developed. According to this the local angle of attack is composed of the following elements:

$$\alpha(\xi) = \alpha_\infty + \alpha_w(\xi) + \alpha_j(\xi), \quad (32)$$

whereby  $\alpha_j(\xi)$  stand for the local downwash angle induced by the

lift jets.

Using the  $\Delta c_{pF}$  curves (change in local pressure coefficients due to the effect of the wing) shown in Fig. 74 it is possible to determine the variable  $\alpha_j(\xi)$  distribution along the fuselage axis. The test models used were those in which the wing was positioned in front of or behind a single jet. The effect of the wing, i.e. increase in the depression, is greatest when the leading edge of the wing is located in the immediate vicinity of the lift jet. This is understandable if one considers that the jet-induced downward component of the outer flow ( $\alpha_j(\xi)$ ) is at a maximum in the vicinity of the jet locus. When the wing is positioned in front of the jet the leading edge of the wing is far removed from the jet locus and there finds itself in a range of smaller downwash angles  $\alpha_j(\xi)$ . Thus the maximum negative  $\Delta c_{pF}$  value is considerably smaller and only about half as great as in the test setup with the lift jet in front of the wing. In general, the effect of the wing on the pressure distribution on the fuselage extends over a section of the fuselage as long as the thickness of the wing with a maximum close to the leading edge of the wing.

In the double jet fuselage model (Figs. 71-73), in addition /50 to this position-dependent low pressure field with a maximum close to the leading edge of the wing, the wing also causes changes in pressure around the orifice of the forward lift jet. These pressure changes, which for the most part cause a reduction in the suction points here, are greatest when the wing is directly over or a short distance in front of the rear lift jet (lower isobar diagram in Figs. 69 and 70). Thus they are induced by the rear jet. In both wing arrangements the incoming flow for the rear jet is particularly cut off and as a result it is forced to take in more air from the outer field in front of it and thus at the same time increasing its down-

ward component. This results in smaller inclination angles between the forward lift jet and the outer flow ( $\theta < 90^\circ$ ) and thus smaller low pressures at the jet orifice. Both isobar diagrams show that in this case the stagnation point is further aft of the leading edge of the wing than in the case of the other wing positions.

Finally, Fig. 75 shows that the pressure changes on the fuselage induced by the wing for positive and negative angles of attack are very similar in their depression distribution for all angles of attack and can be approximately described by the following equation

$$\Delta c_{pFa} = c \cdot f(\xi) \cdot \alpha . \quad (33)$$

The result indicates that the distribution of the jet-induced downwash angle  $\alpha_j(\xi)$  along the fuselage axis is nearly independent of the angle of attack of the fuselage. This information is very important in estimating the interference effect of the wing on the fuselage. For this reason the  $c_{NF}$  curves for the test models with the wing in Figs. 76-78 also differ from those without a wing primarily in terms of a different slope. With negative and small positive angles of attack for the fuselage the effect of the wing increases the negative perpendicular forces on the fuselage, since  $\alpha(\xi)$  is negative there, whereas for greater angles of attack with positive pressure fields in the region of the leading edge of the wing the effect of the wing considerably increases the integral perpendicular force on the fuselage.

For a quick estimation of the perpendicular force on a fuselage with a wing the effects of the wing position and relative jet intensity  $\phi$  can be combined in an approximate fashion in the following empirical formula:

$$c_{NF} = c_{NF0} + c_1 \cdot \alpha + c_2 \cdot \alpha^2 + c_3 \cdot \alpha^3 + c_4 \cdot \alpha^4 \quad (34)$$

with

/51

$$\begin{aligned} c_1 &= 4.135 & c_3 &= 18.86 \\ c_2 &= -0.363 & c_4 &= 24.68. \end{aligned}$$

The first term of the equation ( $c_{NF0}$ ) represents the perpendicular force coefficient at an angle of attack of 0 and is dependent on the distribution of the downwash angle  $\alpha_j(\xi)$  along the axis of the fuselage which is important for the wing effect. This in turn depends on the position of the wing and the relative jet intensity  $\phi$ .

From the measurements we get the following values for  $c_{NF0}$ :

$c_{NF0}$	Wing Position		
	$x_v/D$	$z_o/D$	$\phi$
-1,29	-1	0	290
-1,23	0,5	0	290
-1,43	2,5	0	290
-1,23	0,5	-0,25	290
-0,93	0,5	0,25	290
-1,01	0,5	0	72
-0,92	0,5	0	36

At an angle of attack of  $\alpha = 0^\circ$  the following relationship exists between the perpendicular force coefficients for the test models without a wing (after equation (19)) and with a wing:

$$c_{NF0} = c_N + \Delta c_{NF0} \quad (35)$$

The term  $\Delta c_{NF0}$  can be determined by integrating the  $\Delta c_{pF}$  curves in Figs. 71-74. It should be pointed out that with this data it is fundamentally possible to determine the downwash distribution along the axis of the fuselage using the equation for lift distribution on the fuselage according to Schlichting [35].

The variable gradients of the  $c_M$  curves in Figs. 79 and 80 are due to the fact that the position of the moment reference point (intersection of the forward jet axis and the fuselage axis) was the same for all of the wing positions. Therefore the test setup with the wing positioned above the rear lift jet ( $x_V = 2.5$ ;  $z_0 = 0$ ) also had the greatest changes in  $c_M$  over  $\alpha$ . Finally, we can infer from Fig. 81 that the  $c_M$  values for the three jet intensities  $\phi = 290, 72$  and  $36$  can be combined in one curve. This is easy to understand, since the interference component of the wing changes considerably more with the angle of attack (change of sign) than the interference component of the jets. /52

As a result of these studies it can be concluded that in terms of its interference effect on the fuselage the wing position between the lift jets is the most appropriate from a practical standpoint. In the lower angle of attack range the wing induces only a small additional downward pressure, and at large angles of attack it induces a high increase in  $c_{NF}$ . In order to determine the total jet interference the studies should be extended to include the wings.

#### 11. Effect of the Ground

From force measurements on complete models with lift jets it is known that the pitching moment in particular changes sharply close to the ground.

The effect of the ground on the pressure distribution on the model fuselage was studied for a few test arrangements with a single jet and multiple jets. In these experiments the dimensionless distance from the ground was varied in a range from  $0.5 < h/D < 3.8$ , while the jet velocity ( $M_j = 1$ ), the oncoming flow velocity ( $v_\infty = 20$  m/s) and the angle of attack ( $\alpha = 0^\circ$ ) were kept constant. Figs. 82 and 83 show the change in  $c_p$  due to the effect of the ground. This change is represented in the following form:

$$\Delta c_{pB} = c_{pB} \text{ (with ground)} - c_p \text{ (without ground)} \quad (36)$$

In the single jet setup (Fig. 82) the negative perpendicular forces spread out in a fan shape in the region of the model in front of the jet as the distance from the ground is decreased. This is due to the fact that during this process the influx of injector air to the jet is more and more obstructed as a result of the vertical reduction in the size of the intake area. Thus the influx velocity of the injector air increases and causes a drop in static pressure on the underside of the fuselage. The effect of the ground in back of the jet is only small and practically negligible. These effects subside with increasing oncoming flow velocity.

With the addition of another jet (Fig. 83) the effect of the ground acts very differently in the vicinity of the two jet loci. While the additional negative perpendicular forces induced by the ground on the forward jet show up primarily on the portion of the fuselage in front of the jet, just as in the case of the single jet, around the rear jet they are nearly symmetrical to the jet axis. With dimensionless distances above the ground of less than  $h/D = 1.5$  the  $c_p$  values around the rear jet fall off considerably more sharply than in the forward section of the fuselage. Consequently the model becomes very

tail heavy. In addition to the effects present in the case of the single jet another decisive factor in this sharp rise of low pressures in this area is the strong shadowing effect of the forward jet. Even at dimensionless distances above the ground of  $h/D < 1.7$  we get the well known fountain formation in the area between the two jets. At  $h/D = 0.83$  this shows up clearly as positive pressure on the fuselage.

Figs. 84 and 85 show these separate phenomena in integral form for different distances between the jets. The drop in  $\Delta c_{NB}$  as the distance from the ground is decreased is greater in the double jet setup than in the single jet arrangement due to the large interference component of the rear jet. The change in the pitching moment increases close to the ground as the distance between the jets is increased, since the depression maximum in each case is located in the vicinity of the rear jet.

## 12. Summary

In V/STOL aircraft the jets show a strong interference effect with the airframe and the ground. Because of the large number of parameters basic fundamental studies are required on a variable model (MAT model). In the present work flow processes (velocity and direction distribution) are studied on single and double lift jets in a cross flow along with their reactions on the lift forces and moments of the airframe. These effects are described in detail. The main emphasis of the work centers around the findings of systematic pressure distribution measurements on the surface of the fuselage.

The number of test parameters is relatively large. These include the following: the angle of attack, jet velocity and oncoming flow velocity as well as the geometric parameters including jet diameter, distance between the jets, the position



the wing in relation to the jets and the fuselage and the distance above the ground.

The most important causes of jet interference are the following phenomena:

1. The injector effect with its suction activity and the downward current of the jet.
2. The flow around the jet with displacement, drift, cross-section deformation and jet wake.
3. The interaction of the double jets due to shadowing and obstruction of the influx of sucked in secondary air

/54

Because of the cross wind the jets are deflected and blown towards the rear. This drift is almost exclusively a function of the relative jet intensity  $\phi$ , whereby the forward jet reacts more strongly than the rear jet which lies in the wind shadow. Mathematical relationships were found for the path coordinates of the two jets.

The relative jet intensity also proves to be the most important parameter with regard to the short-range effect of the jets, in particular in the area in front of the jet. The influence of the jet diameter is restricted to the immediate region of the jet itself, while greater changes in pressure appear primarily on the portion of the fuselage behind the jet due to the influence of the angle of attack. By means of an approximation method an equation was obtained for the changes in perpendicular force with the help of empirical constants. This made it possible to calculate the perpendicular force and the pitching moment.

In the double jet arrangements there is a strong interaction

between the two jets. This causes the model to become increasingly tail heavy when the distance between the jets is increased.

The influence of the wing increases the downward pressure of the fuselage for negative and small positive angles of attack. This is because in this  $\alpha$  range the effective angle of attack of the model is negative due to the jet-induced downward current. At greater angles of attack low pressure fields form in the vicinity of the forward edge of the wing on the fuselage which considerably increase the integran perpendicular force on the fuselage. With respect to the interference effect of the wing on the fuselage the most appropriate wing position in practice proves to be that between the lift jets.

In wingless models the effect of the ground first becomes noticeable at distances above the ground  $h/D < 1.8$ . In contrast to the single jet, the double jet arrangement causes a strong increase in the negative normal forces and the pitching moment, since as the distance to the ground becomes smaller strong low pressure fields form at the rear jet due to the wind shadow effect of the forward jet.

Günter Viehweger, Ph.D. Engineering  
Low-speed wind tunnels, central  
office Linder Höhe, 5000 Cologne  
90.

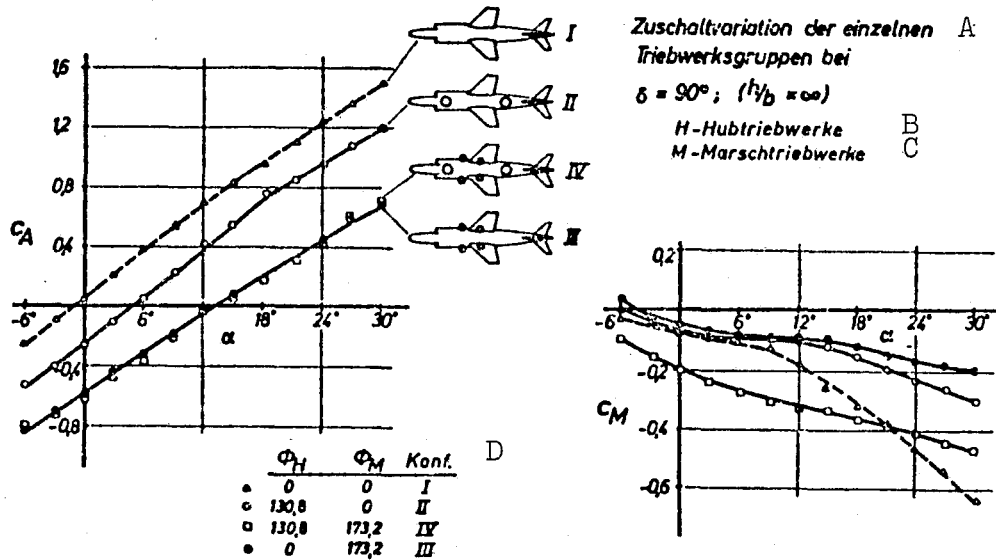
## REFERENCES

1. Schulz, G. and G. Viehweger, "Secondary forces on a VTOL aircraft during hover and transition flight taking into consideration the effect of the ground," WGK-Jahrbuch, 152-161 (1967).
2. Barche, D. and G. Krenz, "Jet effect on V/STOL aircraft during transition and high-speed flight," Luftfahrt-technik-Raumfahrttechnik 15/5, 126-132 (1969).
3. Seibold, W., "Studies on secondary forces produced by lift jets on VTOL aircraft," WGL-Jahrbuch, 257-275 (1962).
4. Jordinson, R., "Flow in a jet directed normally to the wind," ARC R+M, 3074 (1958).
5. Gordier, R.L., "Studies on fluid jets discharging normally into moving liquid," Univ. of Minnesota, T.P. No. 28, Series B (1959).
6. Williams, J. and Wood, M.N., "Aerodynamic interference with Jet-Lift V/STOL aircraft under static and forward-speed conditions," R.A.E. Technical Report No. 66403 (1966).
7. Seidel, M., "Studies on the influence of an inclined jet on the aerodynamic characteristics of a tail unit," Z. Flugwissenschaften 19/1, 13-29 (1971).
8. Wooler, P.T., G.H. Burghardt and J.T. Gallagher, "Pressure distribution on a rectangular wing with a jet exhausting normally into an airstream," J. Aircraft 4, 537-543 (1967).
9. Schmidt, H., "Deflection of a round turbulent free jet by a cross wind," DFLRB [German Aerospace Research and Test Center] Internal Report 061-72 A 24.
10. Keffer, J.F. and W.D. Baines, "The round turbulent jet in a cross wind," J. Fluid Mech. 15, 481-496 (1963).
11. Chang, H.C., "Rolling up of a cylindrical jet due to a cross wind," Dissertation, U. of Göttingen (1942).
12. Ricou, F.P. and D.B. Spalding, "Measurements of entrainment by axis-symmetrical turbulent jets," J. Fluid Mech. 11, 25-32 (1961).

13. Schulz, G. "Calculation using singularities of the pressure distribution on an aircraft fuselage with discharging lift jets," DLGR [German Aerospace Society] 70 - 056 (1970).
14. Volger, R.D., "Surface Pressure Distribution induced on a flat plate by a cold air jet issuing perpendicularly from the plate and normal to a low-speed freestream flow," NASA TN D-1629 (1963).
15. Soullier, A., "Testing at Sl.MA for basic investigations on jet interaction. Distribution of pressures around the jet orifice, April 1968," NASA TTF - 14066 of 1974 -- translation.
16. Ousterhout, D., "An experimental investigation of a cold jet emitting from a body of revolution into a subsonic free stream," NASA - CR - 2089 (Aug. 1972).
17. Bradbury, L.J.S., "The static pressure distribution around a circular jet exhausting normally from a plane wall into and airstream," ARC C.P. 822 (1955).
18. Crowe, C.T. and H. Riesebieter, "An analytic and experimental study of jet deflection in a cross flow," AGARD Conf. Proc. Nr. 22 (1967).
19. Vogler, R. "Interference effects of single and multiple round or slotted jets on a VTOL model in transition," NASA TND-2390, (1964).
20. Vogler, R., "Ground effects on single and multiple-jet VTOL models at transition speeds over stationary and moving ground planes," NASA TND-3213 (1966).
- 21a. Schulz, G., "The subsonic wind tunnel of the DVL [German Aerospace Test Center] in Porz-Wahn (part 1)," DVL report No. 344 (1964)
- 21b. Schulz, G. and G. Viehweger, "The subsonic wind tunnel of the DVL in Porz-Wahn (part 2)," DLR FB [German Aerospace Research Report] 65-66 (1965).
22. Viehweger, G., "Analysis of free jet interference on a cylindrical fuselage using pressure distribution measurements," Internal Institute Report I-F-70-65 of the German Aerospace Research and Test Center.
23. Tollmien, W., "Calculation of turbulent expansion effects in a free jet," ZAMM 6/6, 468-473 (1926 [sic]).

24. Schlichting, H., "Boundary layer theory," G. Brauer, Munich, 1958.
25. Reichardt, H., "Mathematical relationships of free turbulence," VDI [Association of German Engineers] Research Report 414 (1942).
26. Graefe, H.-J., "Injector effect of free jets with a high orifice Mach number," DLR [German Aerospace] Report 74-18 (1974).
27. Liem, K., "Flow effects with free lift jets," Luftfahrt-technik [Aeronautical Engineering], 198-207 (1962).
28. Leinhardt, Prechter, "Semiempirical calculation methods for the turbulent expansion of ground hot gas jets in a higher surrounding gas moving in the same direction" Technical Report 66/16 of MAN-Turbo (1966).
29. Mehmel, D., "Flow field studies of a jet in a parallel flowing cross wind," AVA [Aerodynamic Test Center] Report 67 A 53.
30. Iwanow, V.S., "Equations for trajectories of jets with acute blast," in "The theory of turbulent jets," MIT Press, Cambridge, Mass. (1963).
31. Yeh, B.T., "Calculation of the jet-induced pressure field on a flat plate," DLR-FB [German Aerospace Research Report] 73-02 (1973).
32. Viehweger, G., "Aerodynamic interference between fuselage and lifting jets emerging from its lower part," AGARD -CP-135, pp. 12-1/12-13 (1973).
33. Viehweger, G., "Studies on aerodynamic interference between an aircraft fuselage and multiple lift jets discharging from the fuselage Part III: Variation of the distance between the jets," Internal Institute Report IB 157-73 A 12.
34. Becker, M., "Studies on a rotation-symmetric free jet perpendicular to a flow," Aachen Technical University Dissertation (1972).
35. Schlichting, H. and E. Truckenbrodt, "Aerodynamics of the airplane," Springer-Verlag, Berlin, Göttingen, Heidelberg (1960).

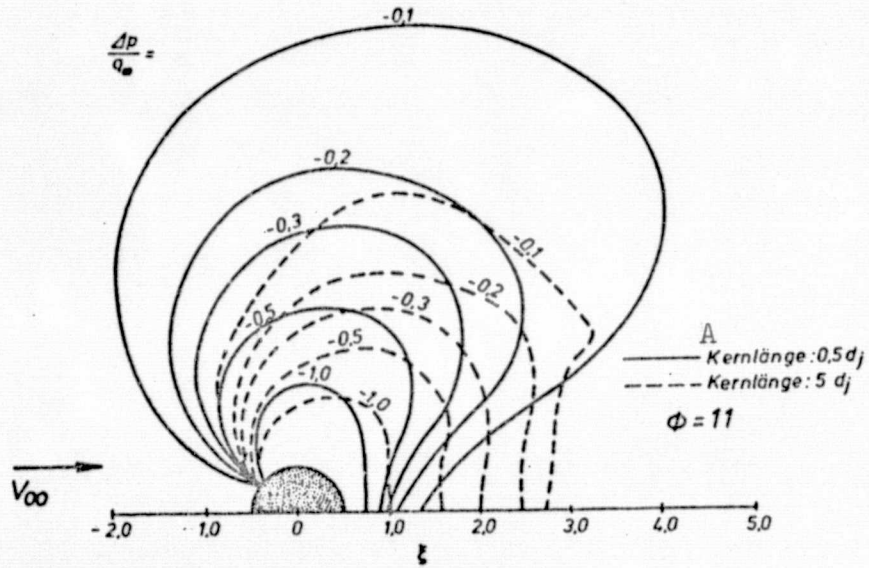
Figure 1



Secondary forces and moments on the airframe of the VAK 191 B due to the influence of the jet.

- Key: A) Various arrangements  
of the individual power  
unit groups with  
B) H = lift jets  
C) M = cruise jets  
D) Configuration

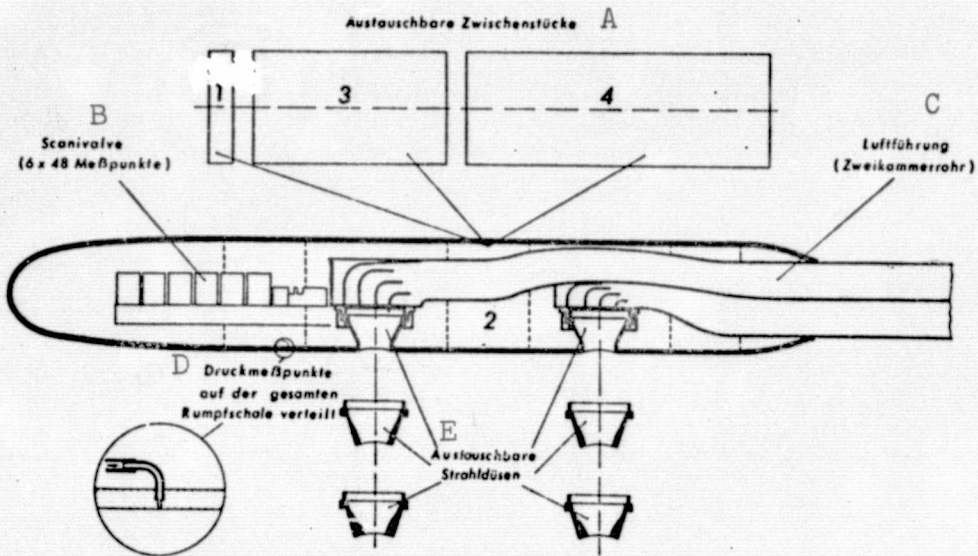
Figure 2



Pressure distribution on a flat plate longitudinal to the flow with a jet (NASA Langley).

Key: A) Core length



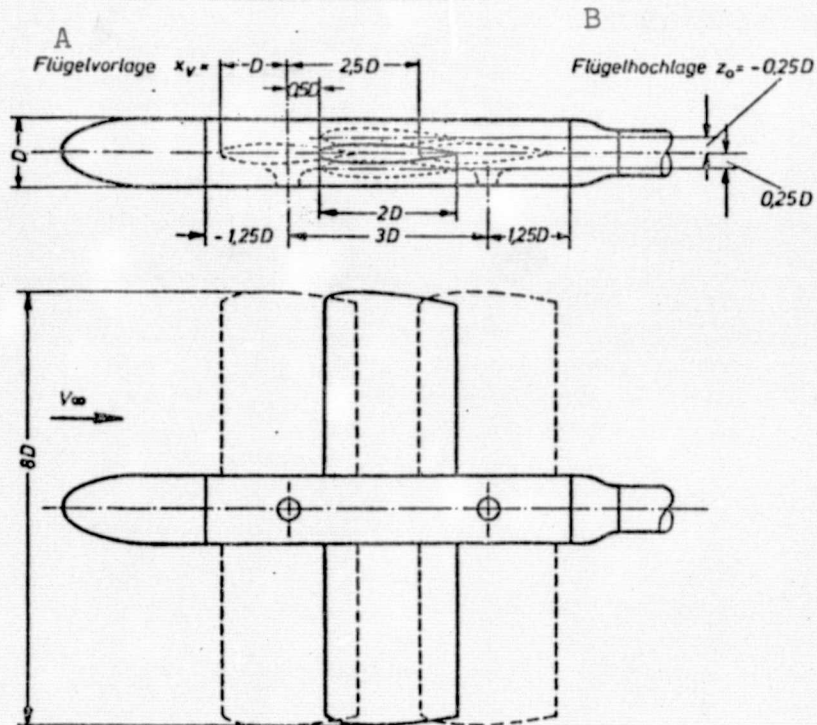


Cut away picture of the model. Interchangeable jet orifices and fuselage spacers.

Key: A) Interchangeable spacers  
 B) Scanivalve (6 x 48 measuring points)  
 C) Air line (2-channel pipe)  
 D) Pressure measurement points distributed over the total shell of the fuselage  
 E) Interchangeable jet orifices

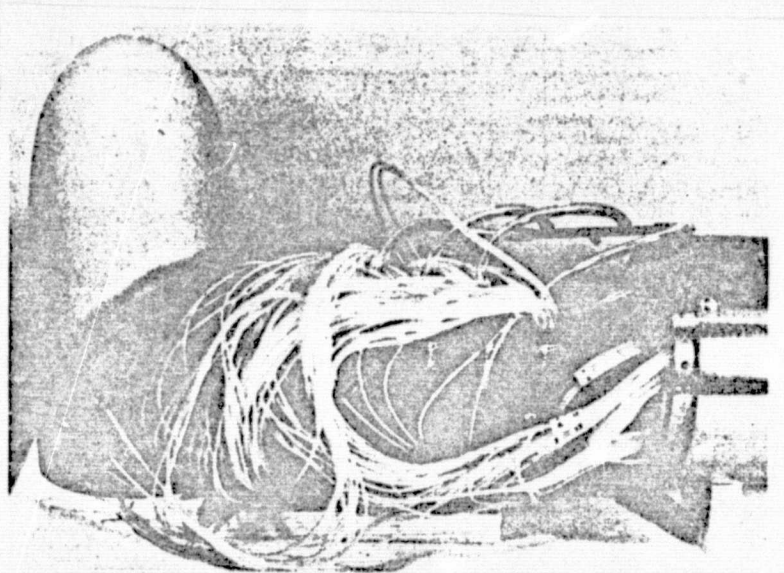


Figure 4

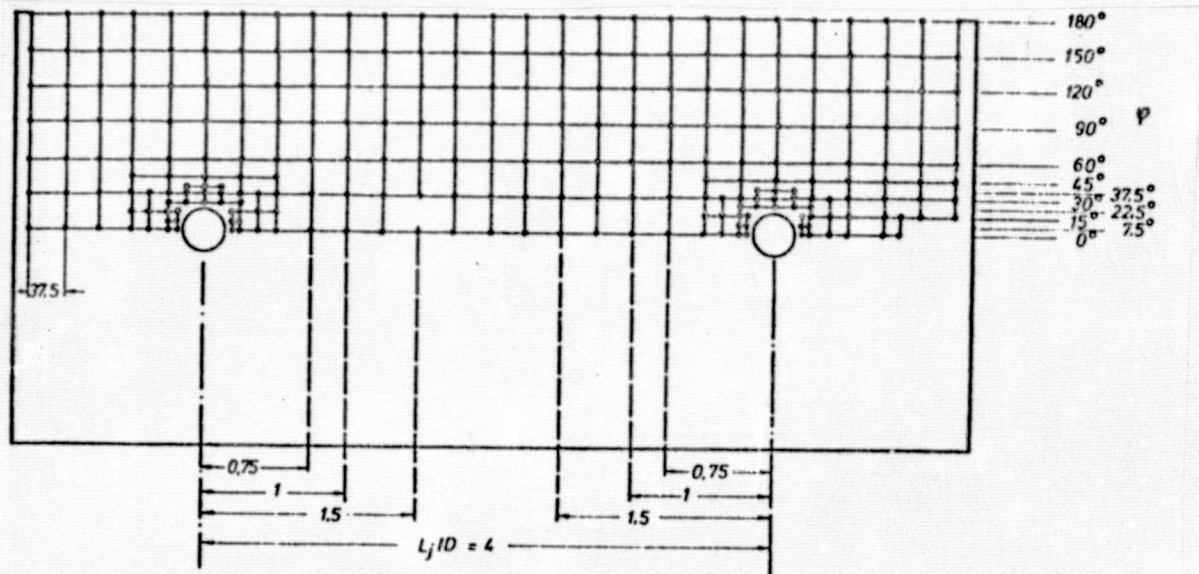


Model configuration with airfoil wing. Position of the wing with respect to the jet orifices. Fuselage diameter:  $D = 150$ .

Key: A) Horizontal position of the wing  
 B) Vertical position of the wing



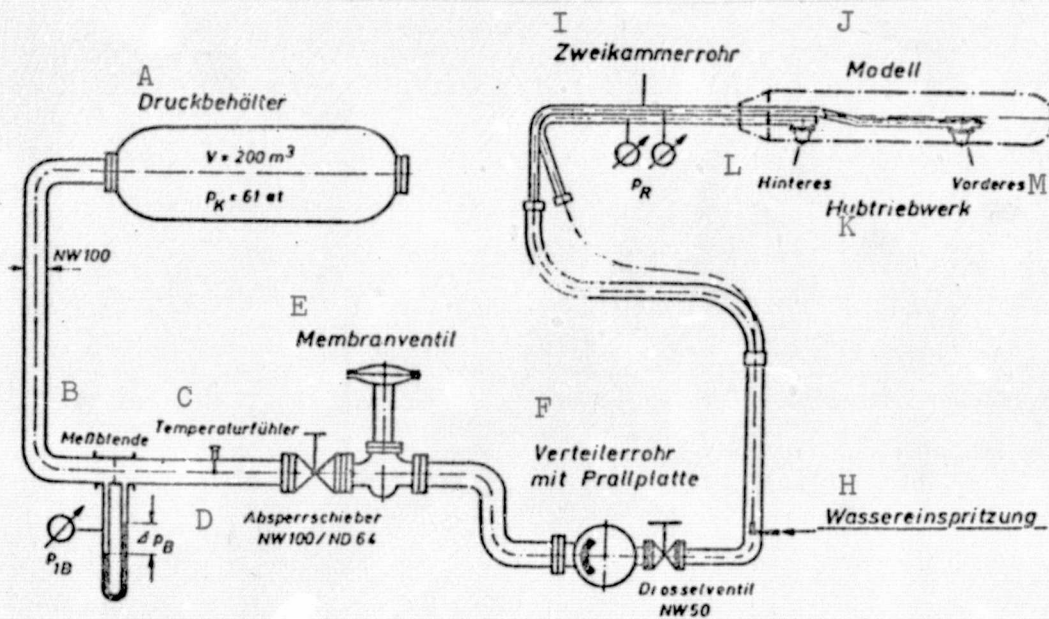
Arrangement of the scanivalve units in the fuselage nose.  
Model open.



Projection of the cylindrical central section of the fuselage for the different model versions showing the position of the pressure holes. The projection shown corresponds to the length of the fuselage with  $L_j/D = 4$ .



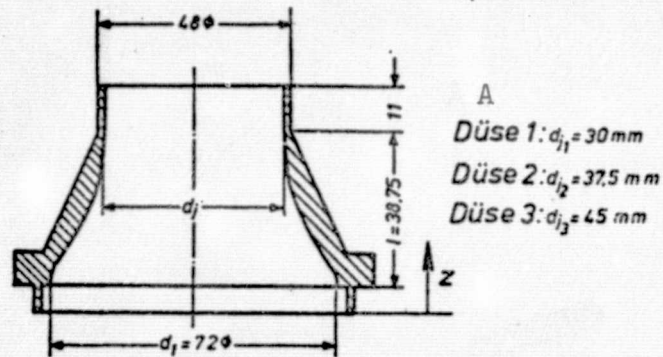
Figure 7



Compressed air system of the wind tunnel with control valve and distribution system

- |  |                    |
|--|--------------------|
| Key: A) Pressure tank                      | H) Water injection |
| B) Measuring orifice                       | I) 2-Channel pipe  |
| C) Temperature sensor                      | J) Model           |
| D) Shut off valve                          | K) Lift jet unit   |
| E) Diaphragm valve                         | L) Aft             |
| F) Distribution pipe with deflecting plate | M) Forward         |
| G) Throttle valve                          |                    |

Figure 8



B Düsenkontur:  
(nach WITOSZYNSKI)

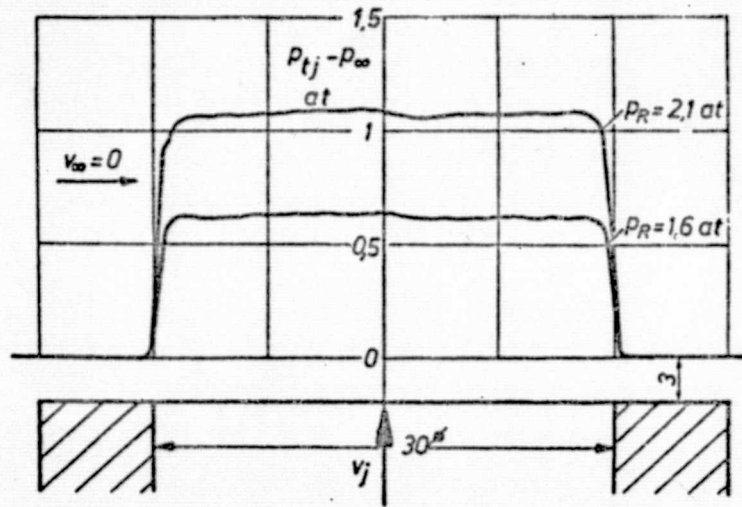
$$d_{z1} = \frac{d_j}{\sqrt{1 - \left[1 - \left(\frac{d_j}{d_1}\right)^2\right] \frac{[1 - (z^2/l^2)]^2}{[1 + (z^2/3l^2)]^3}}}$$

für:  $0 \leq \frac{z}{l} \leq 1$

Jet orifice dimensions

Key: A) Jet orifice  
B) Jet orifice contour  
(after Witoszynski)

Figure 9



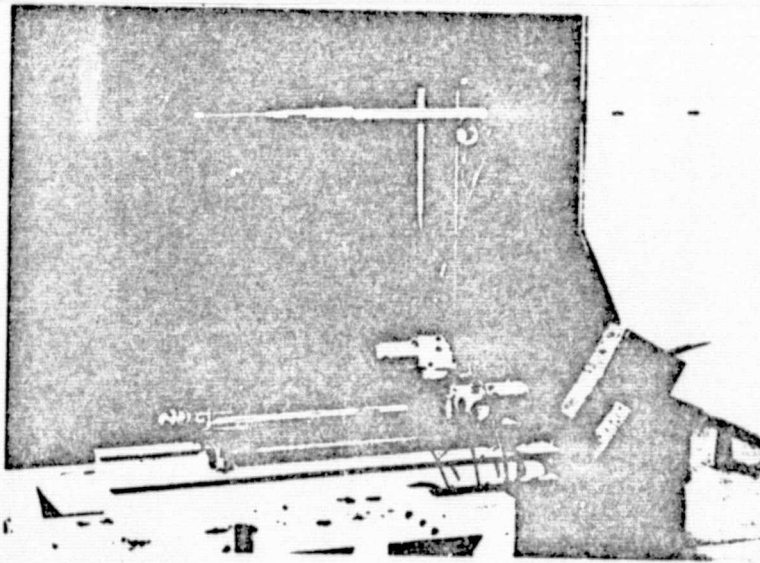
$d_j = 30 mm$ .

Calibration of the jet nozzle jet (cross section)

$d_j = 30 mm$ .

Figure 10

165

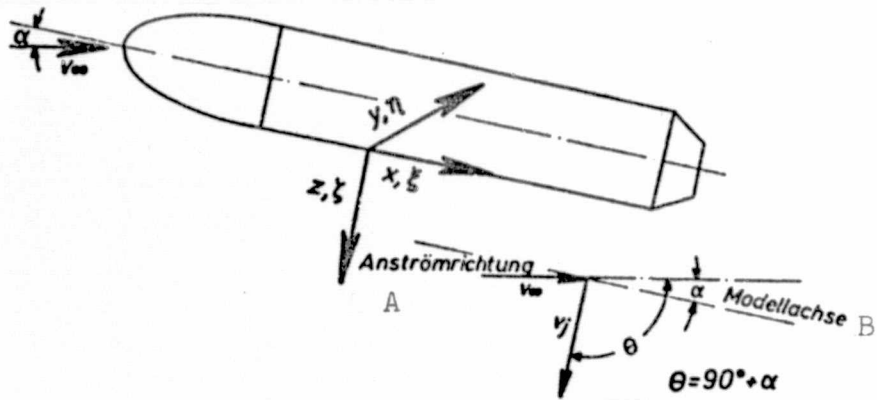


Probe-moving instrument with 5 degrees of freedom.





Figure 12a

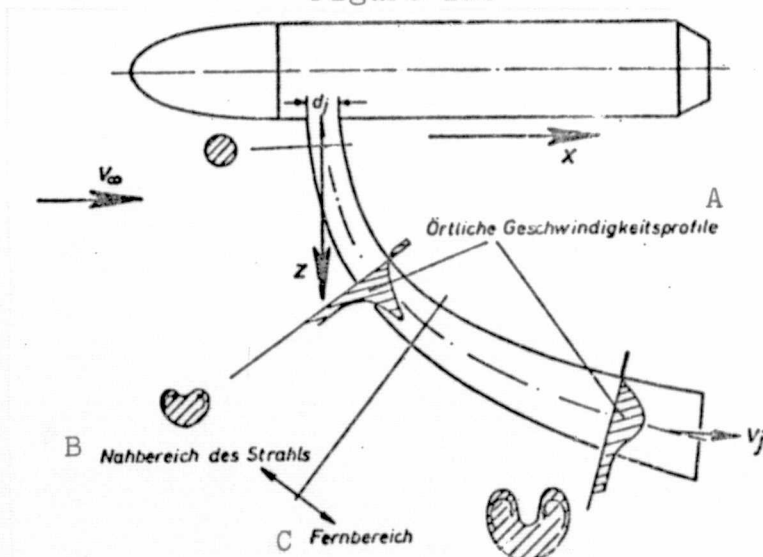


Coordinate system

Key: A) Direction of oncoming flow

B) Model axis

Figure 12b

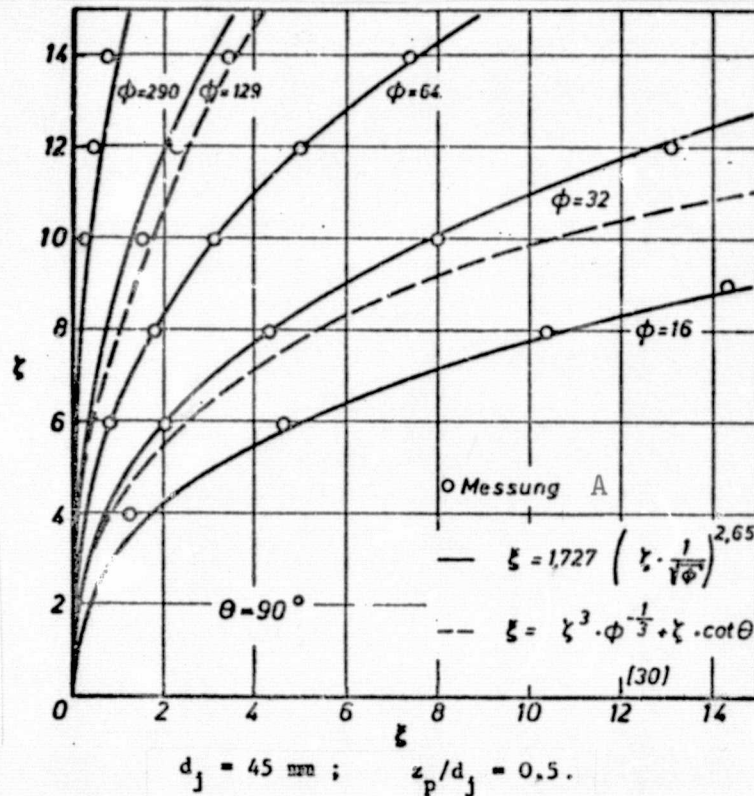


Free jet behavior in a fundamental flow.

Key: A) Local velocity profiles C) Away from the fuselage

B) Close to the fuselage





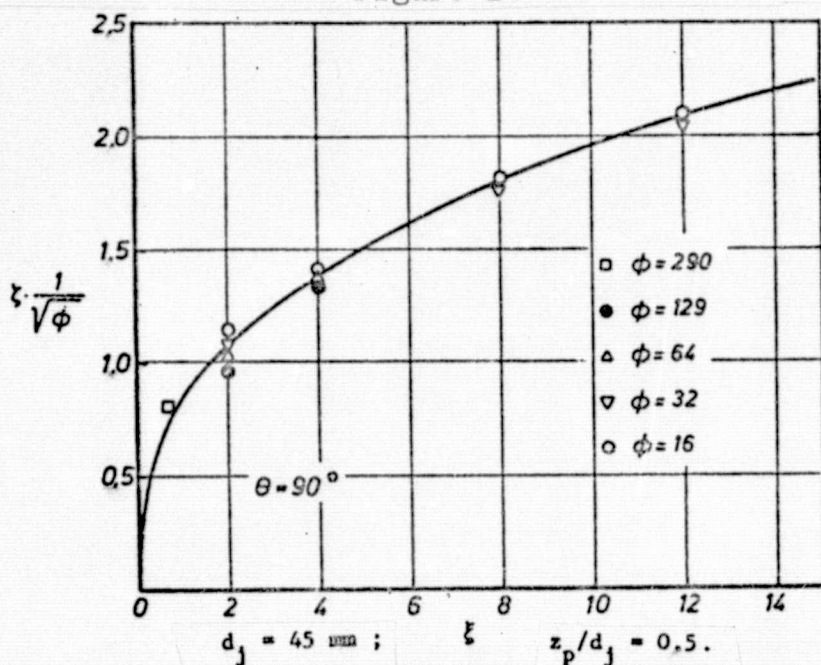
Path of the jet axis for different relative jet intensities.

$d_j = 45 \text{ mm}; \quad z_p/d_j = 0,5$

Key: A) Measurement point

REPRODUCIBILITY OF THE ORIGINAL PAGE IS POOR

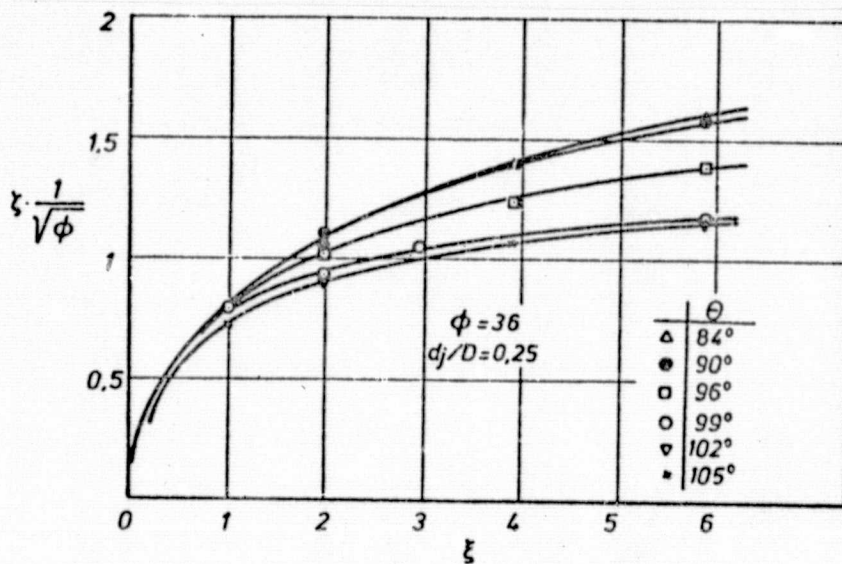
Figure 14



Path of the jet axis for different relative jet intensities.  
 $d_j = 45 \text{ mm}$ ;  $z_p/d_j = 0.5$ .

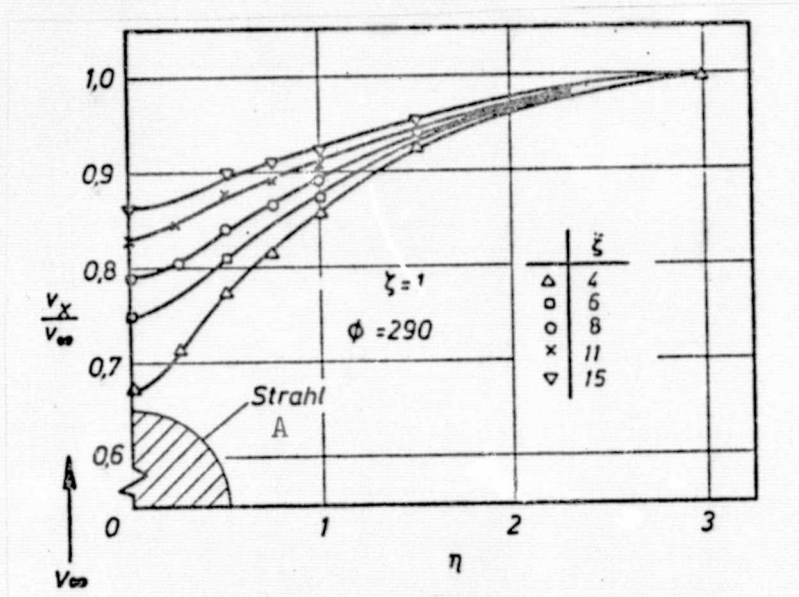
Figure 15

768



Path of jet axes with different initial angles of inclination  $\theta$ .

Figure 16

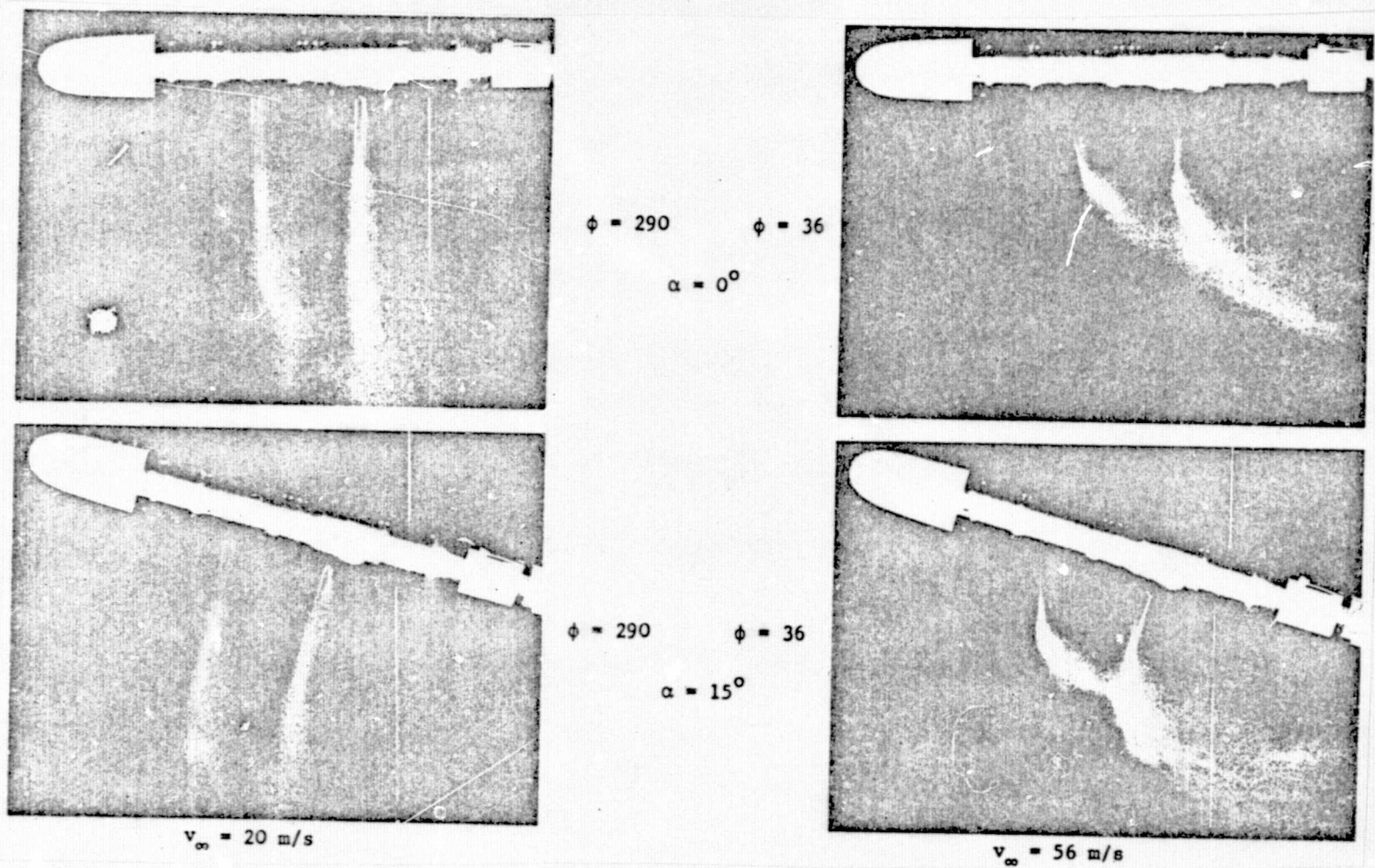


Velocity distribution in the wake of a cross blown jet  $x/d_j$  plotted over the distance from the jet axis.

Key: A) Jet

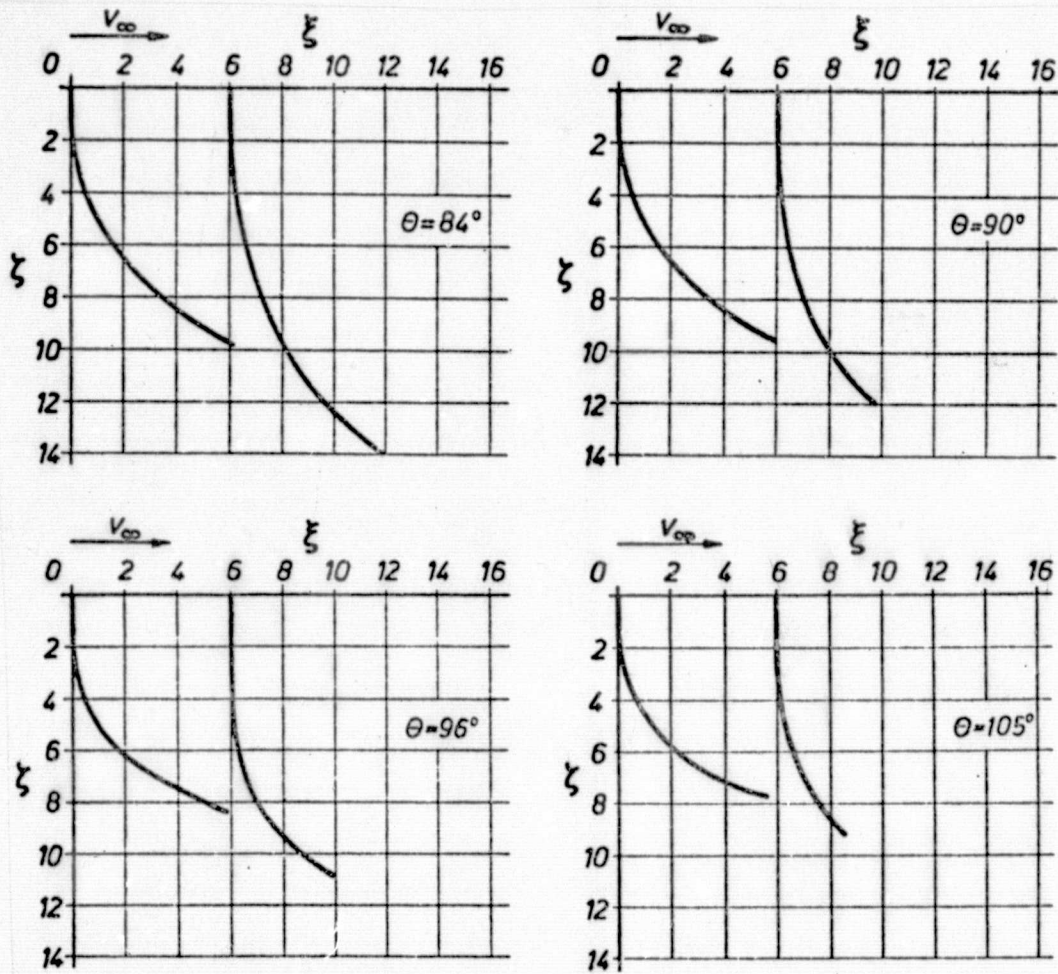


Figure 17



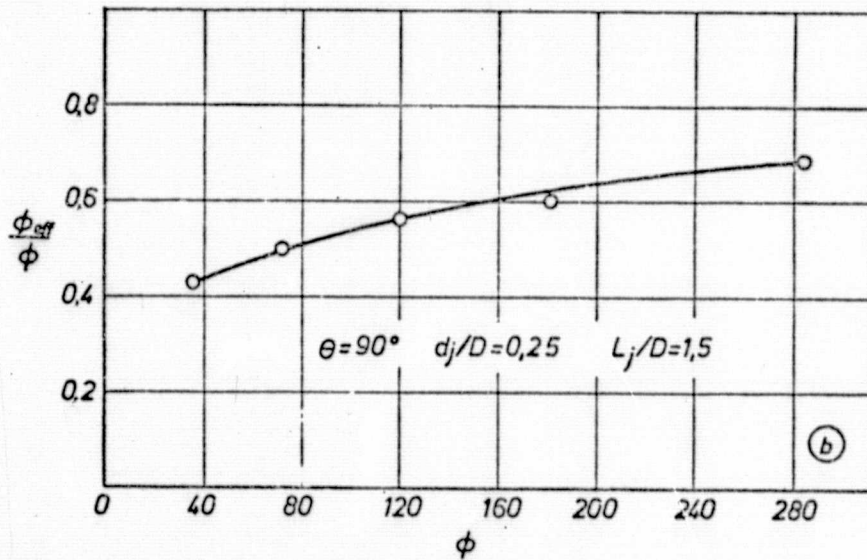
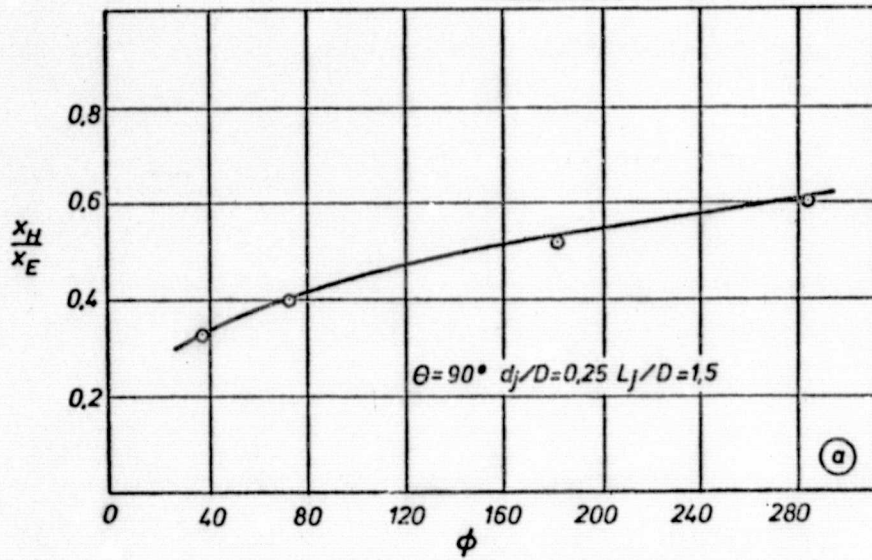
Visualization of the jets by water injection.

$$d_j/D = 0.25 \quad L_j/D = 1.5 \quad M_j = 0.$$



Axis paths of tandem jets (wind shadow effect).

$$\phi = 36 ; M_j = 1 ; d_j/D = 0.25 ; L_j/D = 1.5 ; v_\infty = 56 \text{ m/s.}$$



Wind shadow effect with double jets.

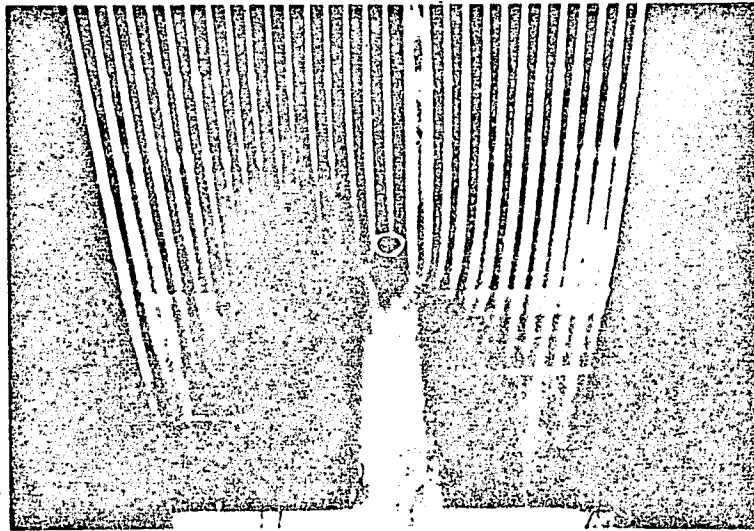
$x_E$ : Drift of the single jet

$x_H$ : Drift of the rear jet

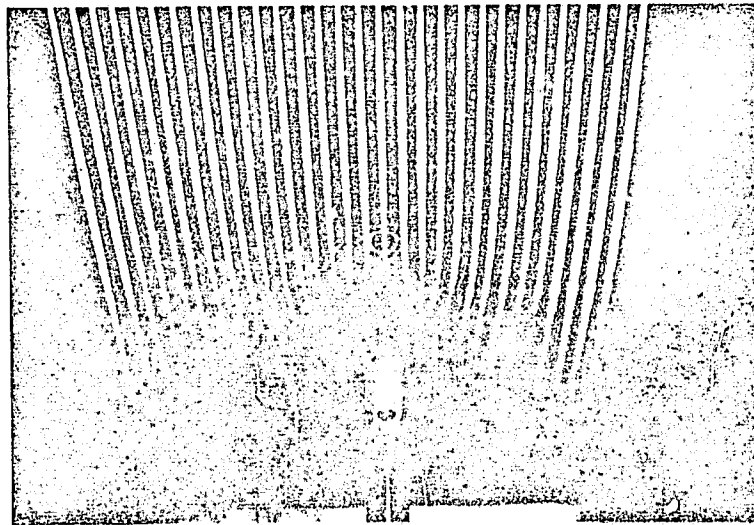
$\phi_{eff}$ : Effective relative jet intensity of the rear jet.

Figure 20

/72



$z = 1$



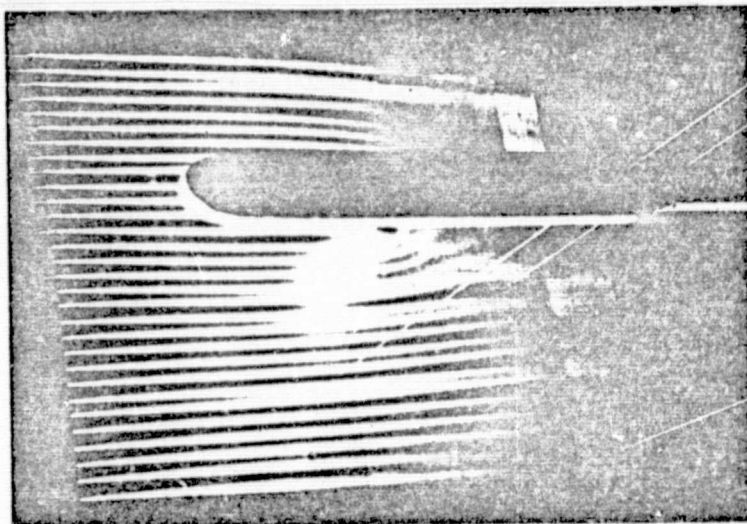
$z = 3$

The visualization of the flow around the jet by means of oil vapor.

$$\alpha = 0^\circ ; \phi = 290 ; M_j = 1 ; d_j/D = 0.3 ; v_\infty = 20 \text{ m/s.}$$

REPRODUCIBILITY OF THE  
ORIGINAL PAGE IS POOR

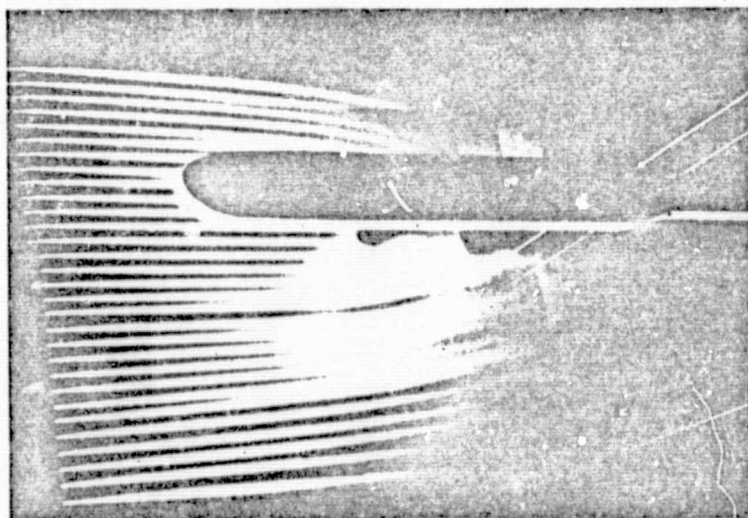




Visualization of the flow around a single jet by means of oil vapor.

$$\alpha = 0^\circ ; \phi = 290 ; M_j = 1 ; d_j/D = 0.3 ; \zeta = 1.5 ; v_\infty = 20 \text{ m/s.}$$

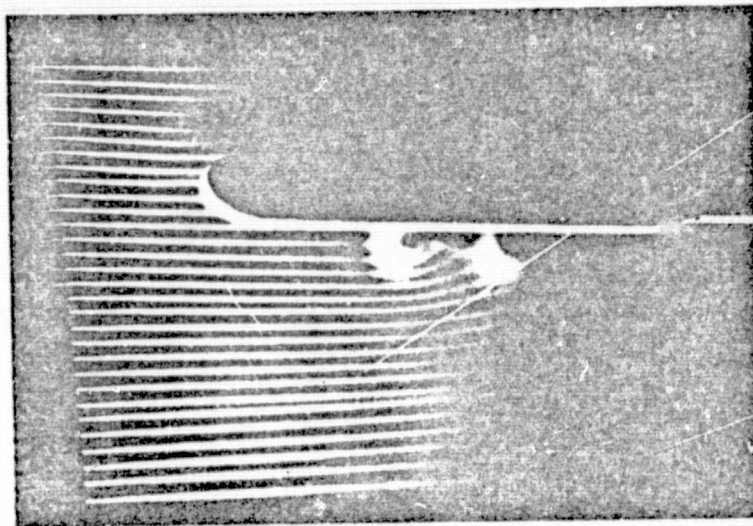
Figure 22



Visualization of the flow around a double jet by means of oil vapor

$$\alpha = 0^\circ ; \phi = 290 ; M_j = 1 ; d_j/D = 0.3 ; \zeta = 3.5 ; v_\infty = 20 \text{ m/s ; } L_j/d_j = 5.$$



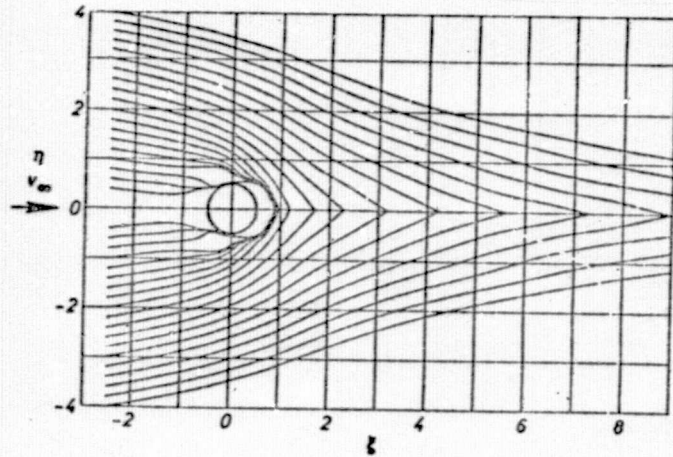


Visualization of the flow around a double jet by means  
of oil vapor

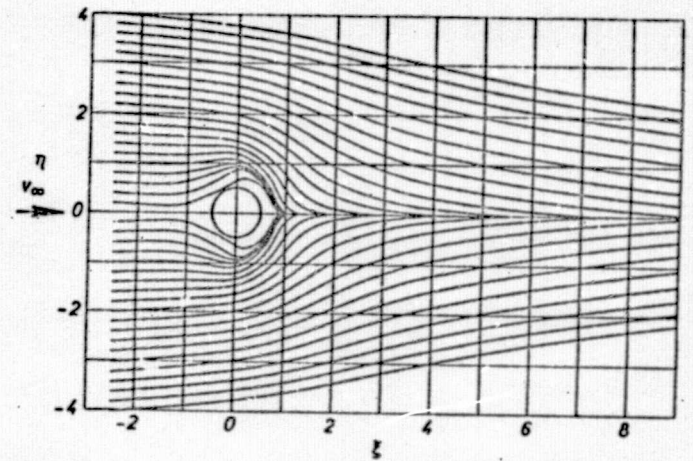
$$\alpha = 0^\circ ; \phi = 72 ; M_j = 1 ; d_j/D = 0,3 ; \zeta = 3,5 ;$$
$$v_\infty = 40 \text{ m/s} ; L_j/d_j = 5.$$

REPRODUCIBILITY OF THE  
ORIGINAL PAGE IS POOR

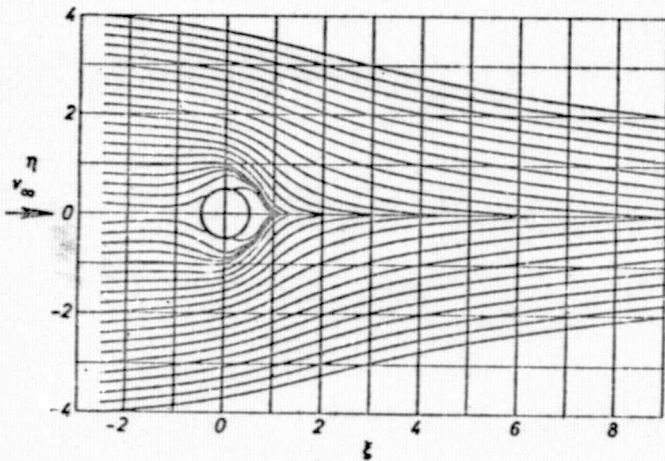
Figure 24



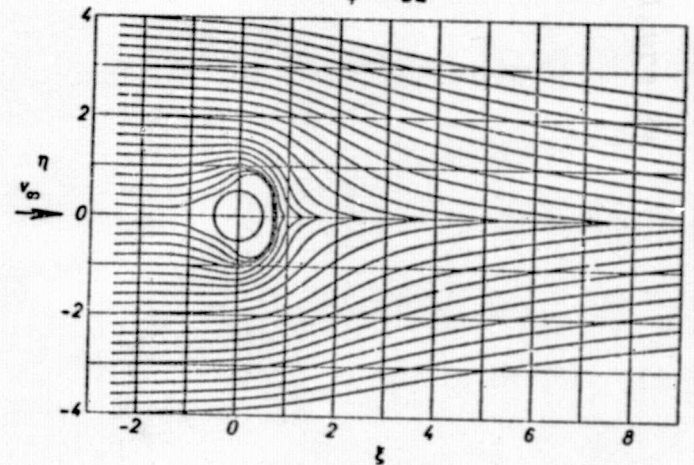
$\phi = 290$



$\phi = 32$



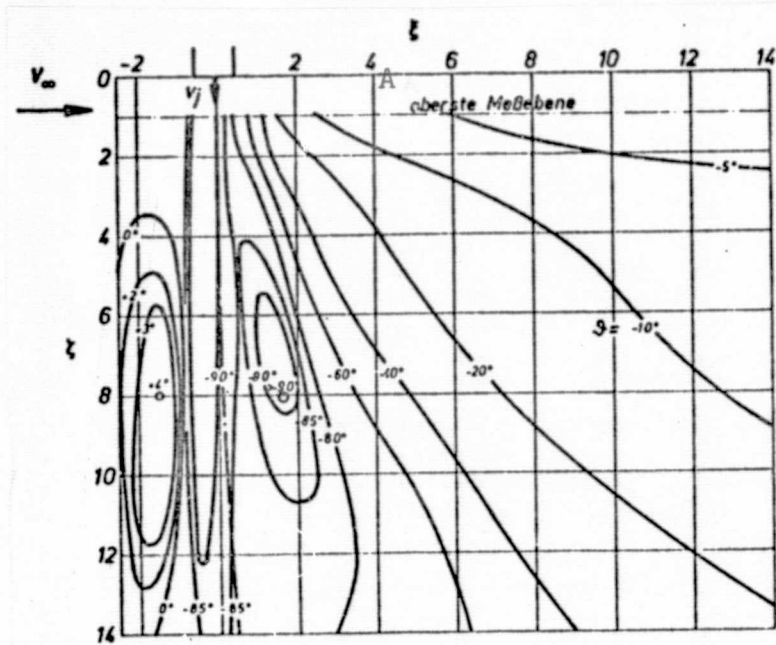
$\phi = 64$



$\phi = 16$

Flow line diagrams based on field measurements  $\zeta = 1$ ;  $\theta = 90^\circ$ .

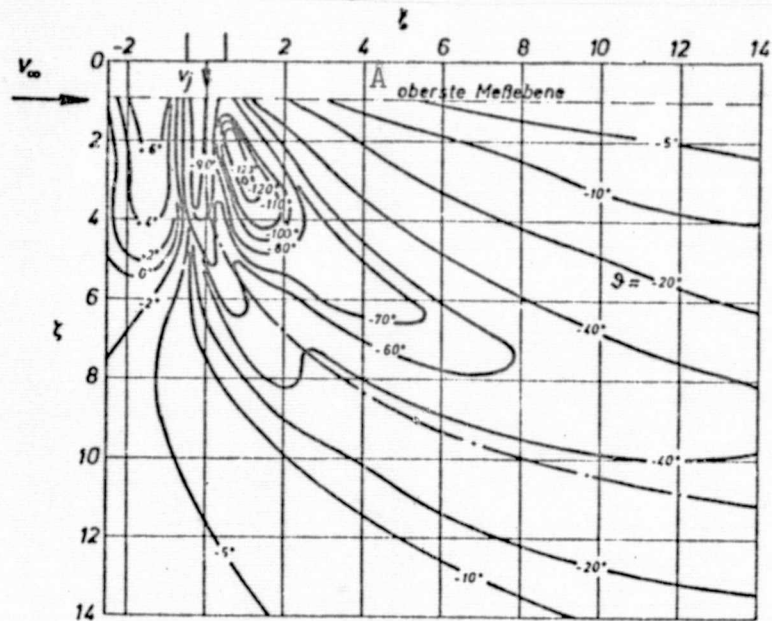
Figure 25



Free jet in a cross wind (isoclines in the longitudinal cross-section  $M_j = 1$  ;  $\phi = 290$  ;  $d_j = 45 \text{ mm}$  .

Key: A) Highest measuring plane

Figure 26

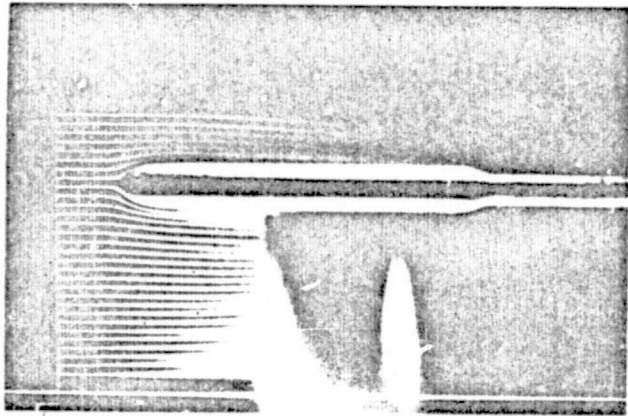


Free jet in a cross wind (isoclines in the longitudinal  
 corss-section)  $M_j = 1$  ,  $\phi = 36,25$  ;  $d_j = 45$  mm.

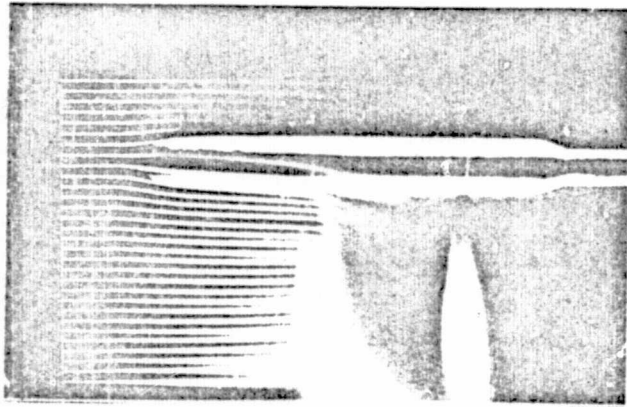
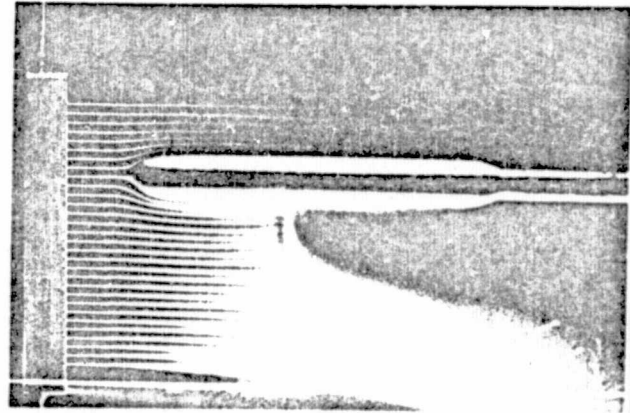
Key: A) Highest measuring plane



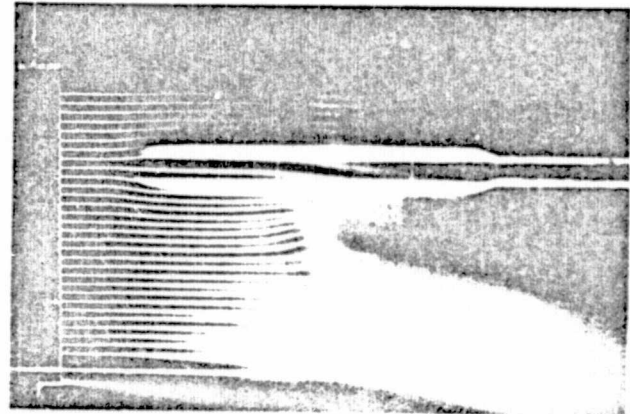
Figure 27



$\eta = 0$



$\eta = 1$



$M_j = 1 \quad \phi = 290$

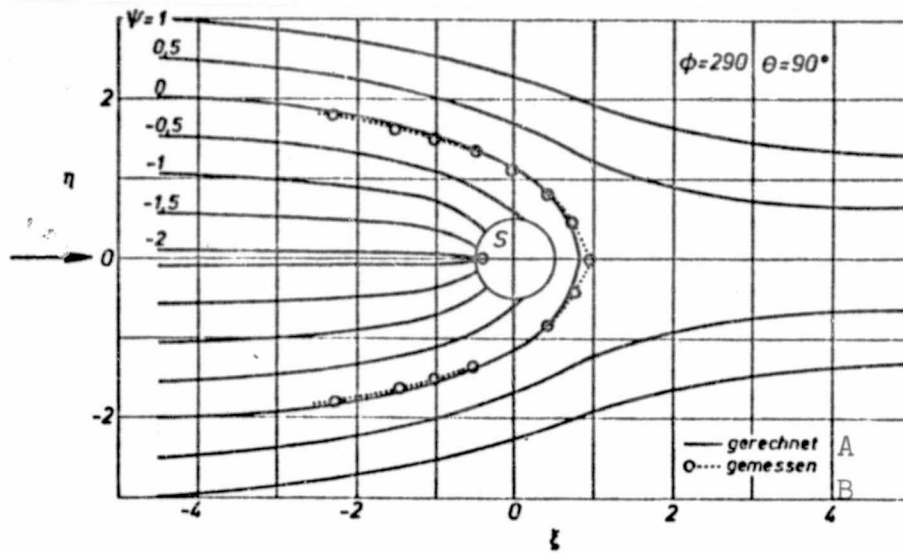
$M_j = 0.65 \quad \phi = 32$

Visualization of the flow field by means of oil mist.  
Vertical arrangement of the probe rack.

$\alpha = 0^\circ$  ;

$d_j/D = 0.3$  ;

$L_j/d_j = 10$ .



Calculated flow line diagram of the flow around a jet  
for  $\phi = 290$ .

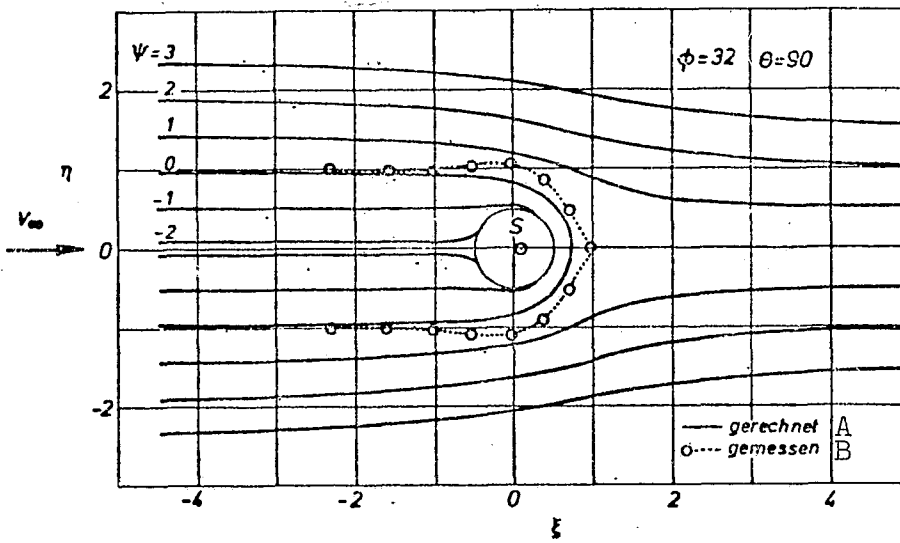
Sink point:  $\xi_0 = -0.4$ ;

Sink intensity:  $k = -0.18$ .

Key: A) Calculated

B) Measured

Figure 29



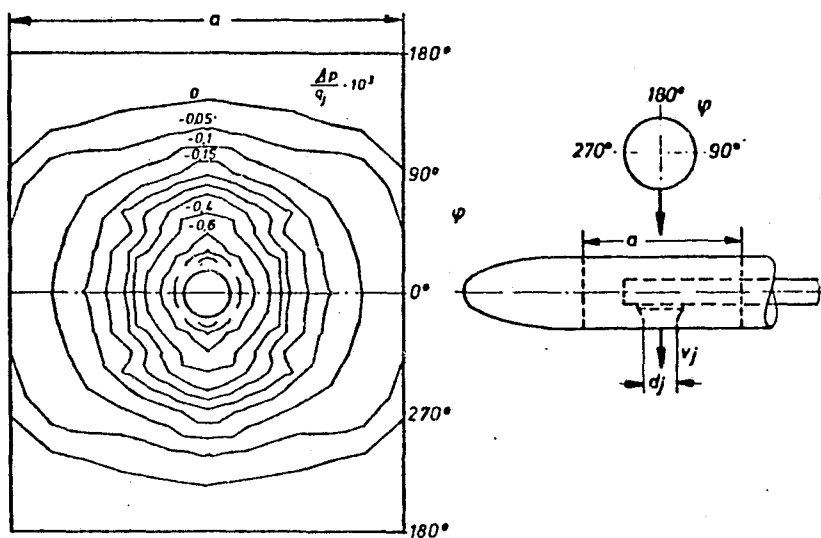
Calculated flow line diagram of the flow around a jet  
for  $\phi = 32$

Sink point:  $\xi_0 = 0.1$ ;

Sink intensity  $k = -0.24$ .

Key: A) Calculated  
B) Measured

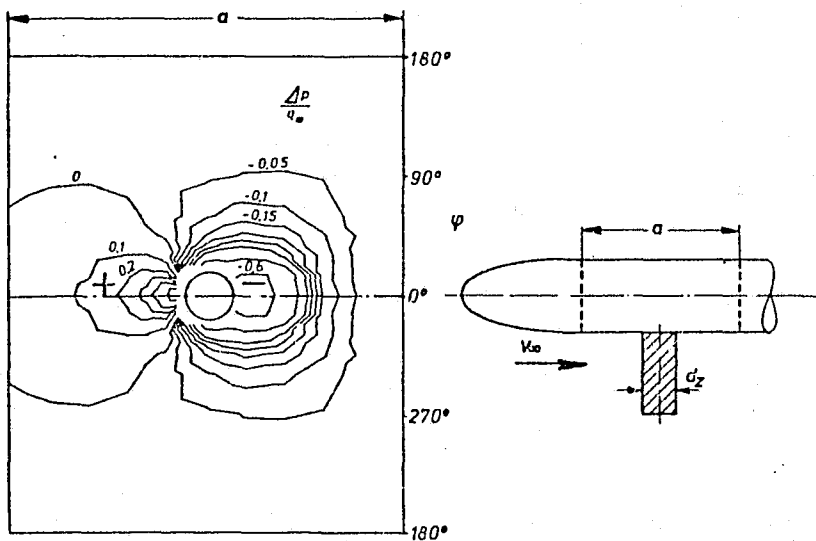
Figure 30



Pressure distribution on a fuselage with lift jet and without cross wind.

$$M_j = 1.0; \quad d_j/D = 0.3.$$

Figure 31

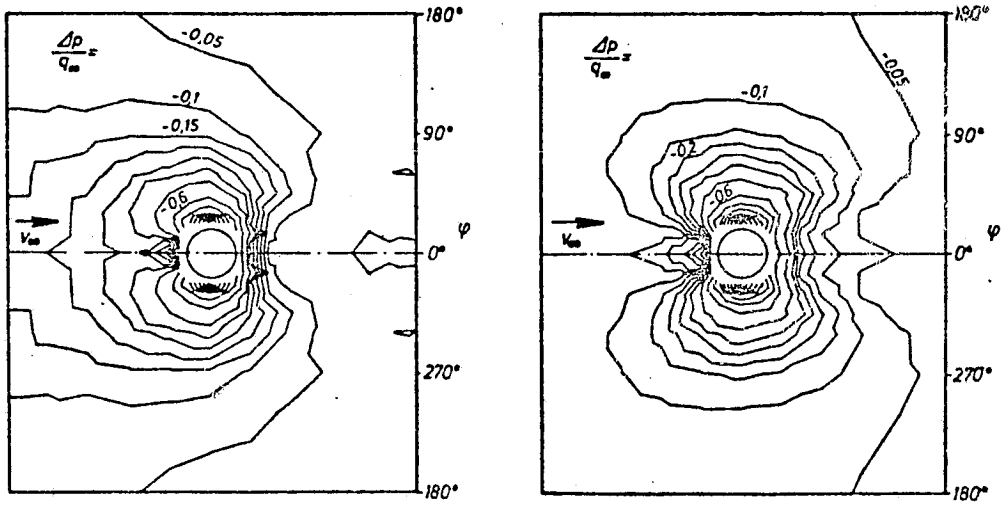


Pressure distribution on a fuselage with an attached cylinder in a cross wind.

$$dz/D = 0.3.$$



Figures 32 and 33



$\phi = 290$

$\phi = 36$

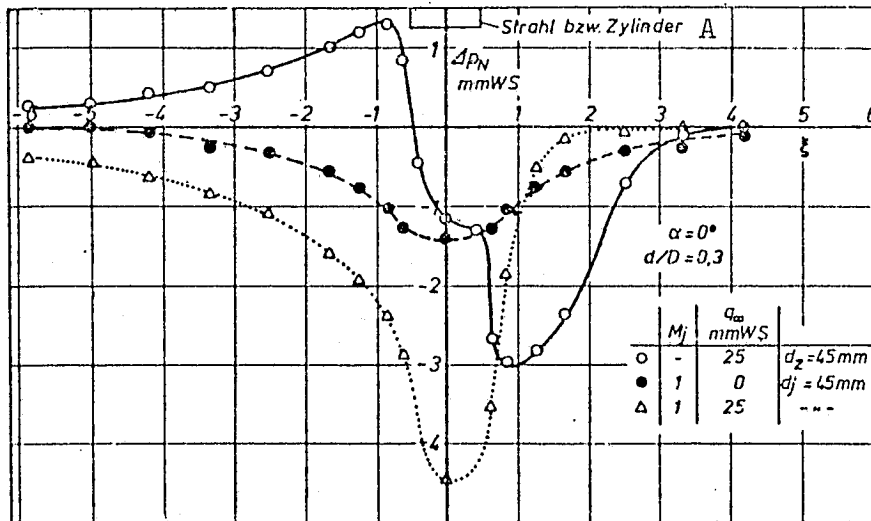
Pressure distribution on fuselage with a lift jet in a cross flow.

$\alpha = 0^\circ$

$M_j = 1$

$d_j/D = 0.3$

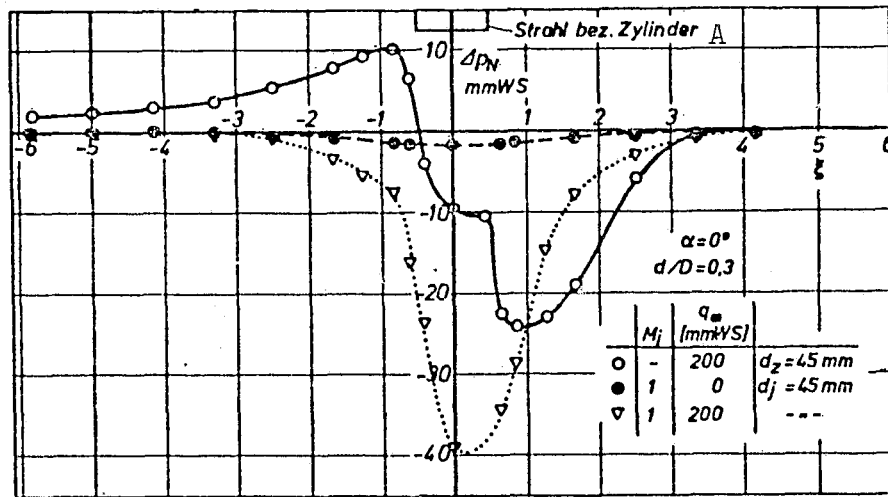
Figure 34



Graph of integral pressure components along a cylindrical fuselage for different test arrangements with a jet or jet substitute.

Key: A) Jet or cylinder

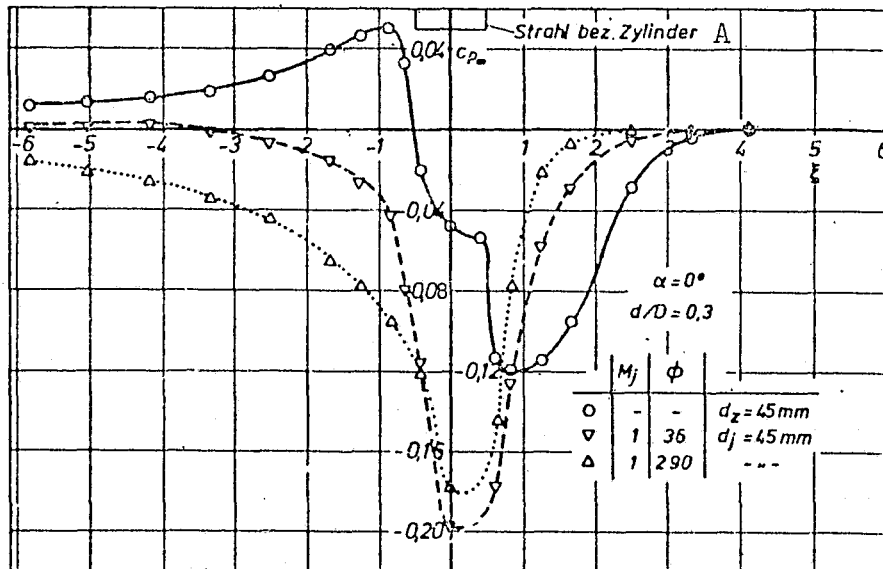
Figure 35



Graph of integral pressure components along a fuselage for different test arrangements with jet or jet substitute.

Key: A) Jet or cylinder

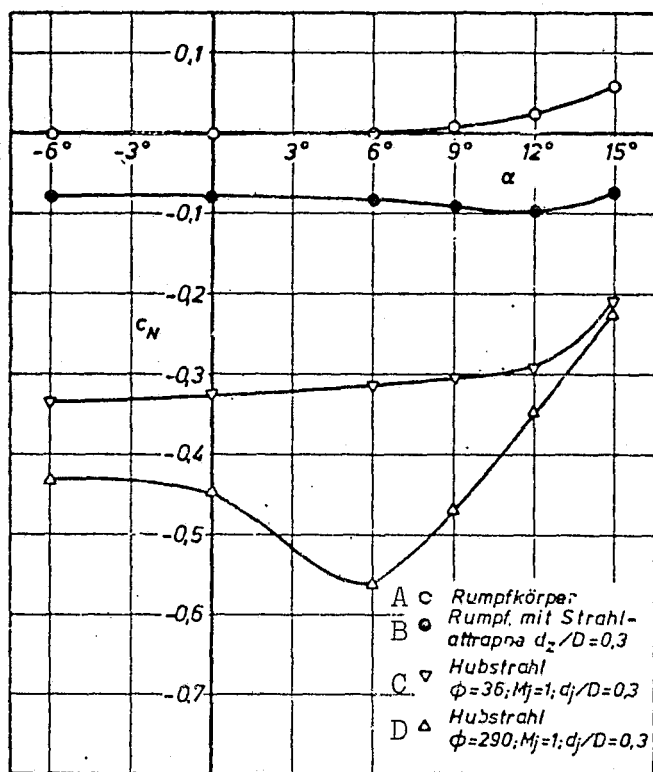
Figure 36



Graph of transverse forces along a fuselage for different test arrangements.

Key: A) Jet or cylinder

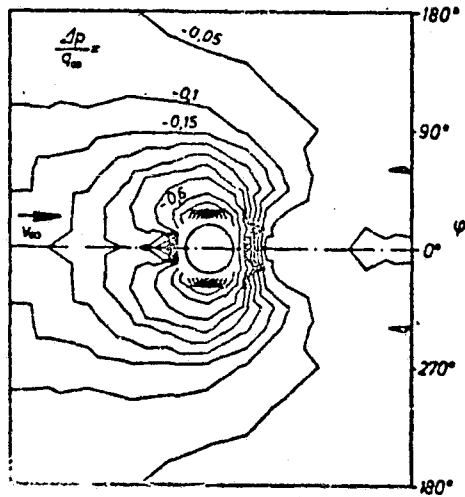
Figure 37



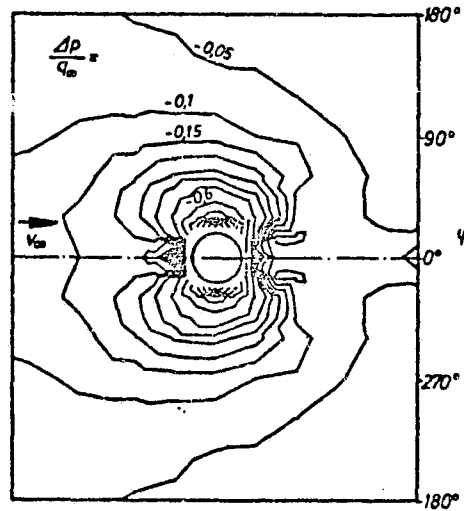
Perpendicular force coefficients of a fuselage as a function of the angle of attack for different test arrangements. Fuselage length  $L = 12d$  for symmetrical jet or jet substitute arrangements.

- Key: A) Fuselage body
- B) Fuselage with jet substitute
- C) Lift Jet
- D) Lift Jet

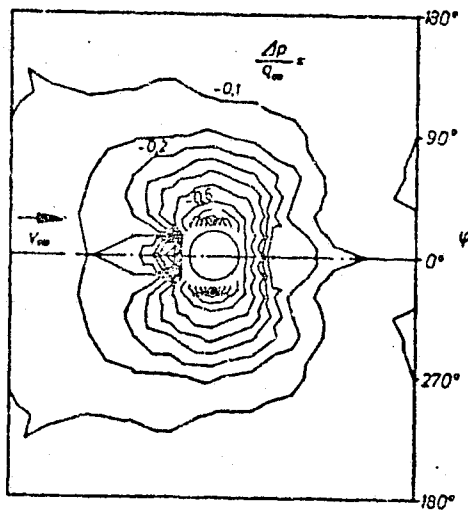
Figure 38



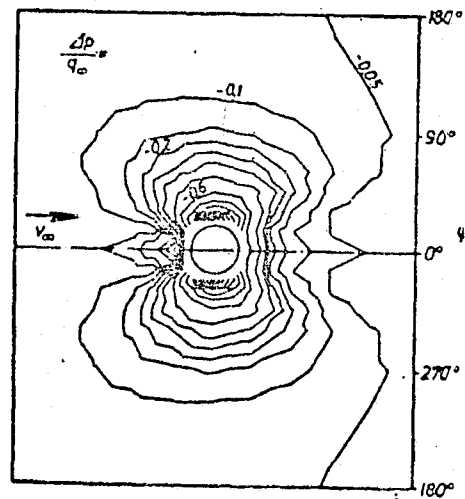
$M_j = 1$  ;  $\phi = 290$



$M_j = 0.65$  ;  $\phi = 129$



$M_j = 1$  ;  $\phi = 72$

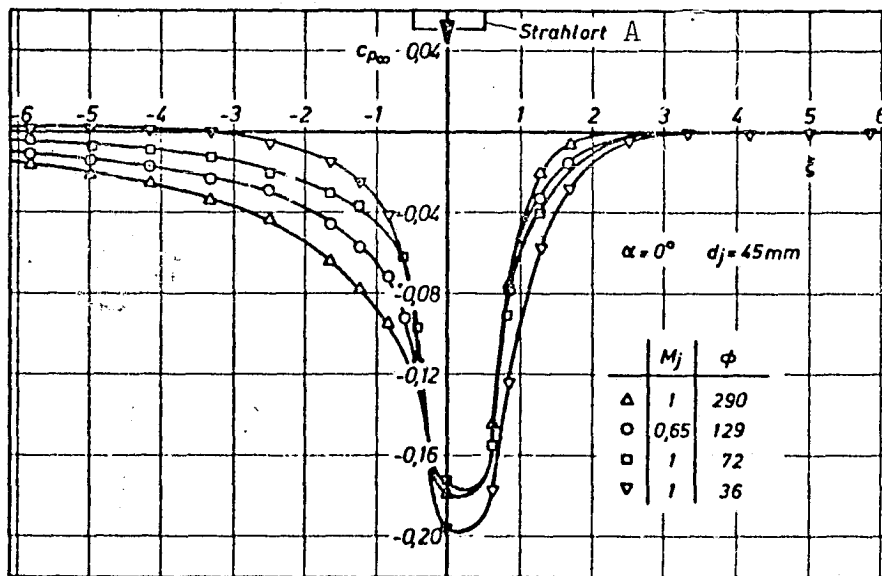


$M_j = 1$  ;  $\phi = 36$

Pressure distribution on a fuselage with a lift jet in a cross flow for different relative jet intensities.

$\alpha = 0^\circ$  ;  $d_j/D = 0.3$ .

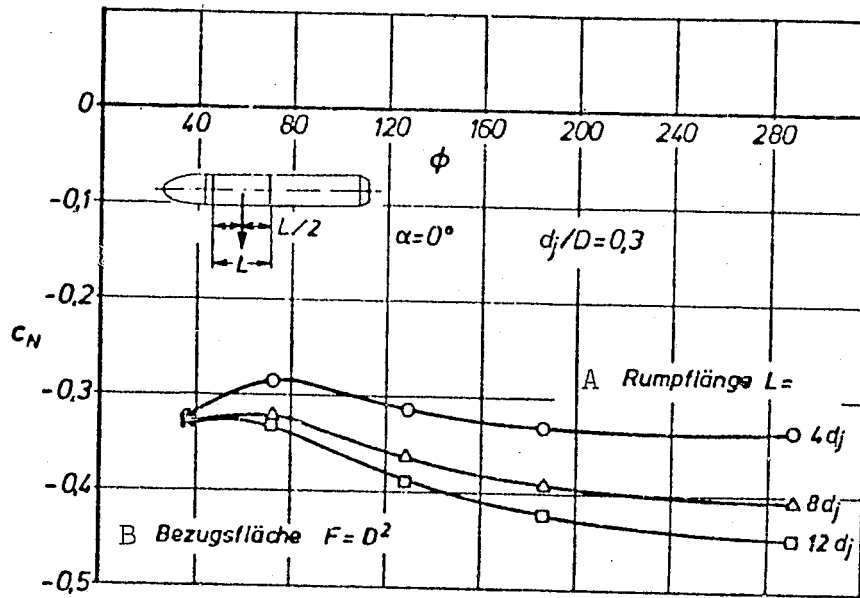
Figure 39



Graph of transverse forces along a fuselage for different relative jet intensities.  $d_j/D = 0.3$ .

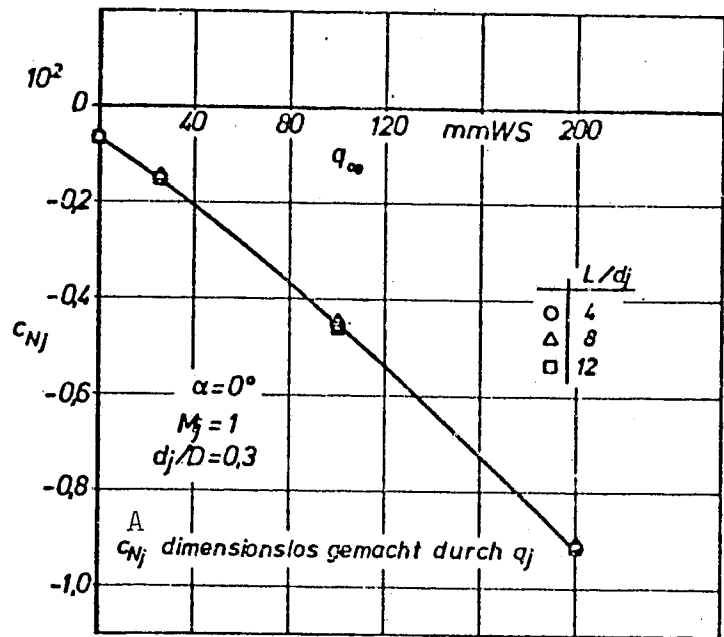
Key: A) Jet locus

Figure 40



Perpendicular force coefficients of a fuselage as a function of the relative jet intensity. The curve parameter is the fuselage length.

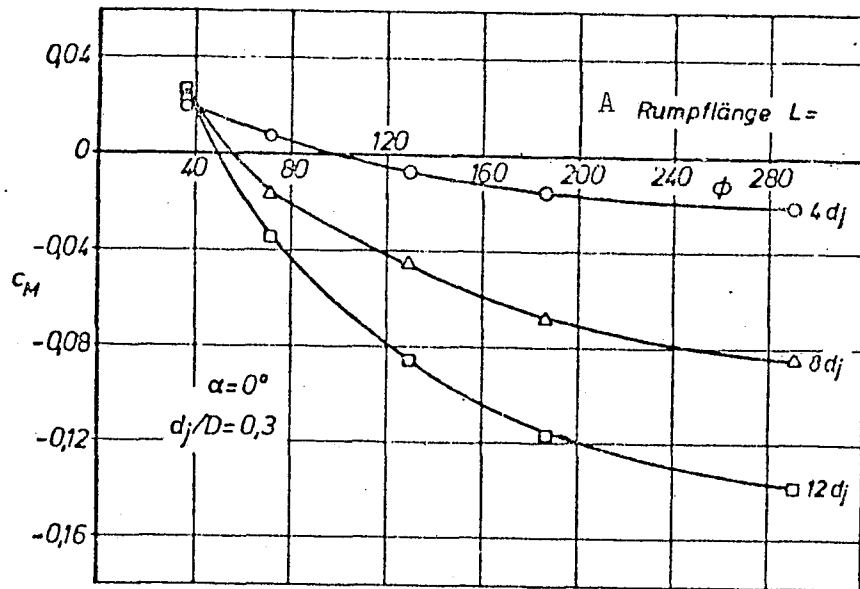
Key: A) Fuselage length  
 B) Reference surface area



Perpendicular force coefficients of a fuselage as a function of the dynamic pressure of the oncoming flow with a constant jet Mach number.

Key: A) Made dimensionless  
by  $q_j$

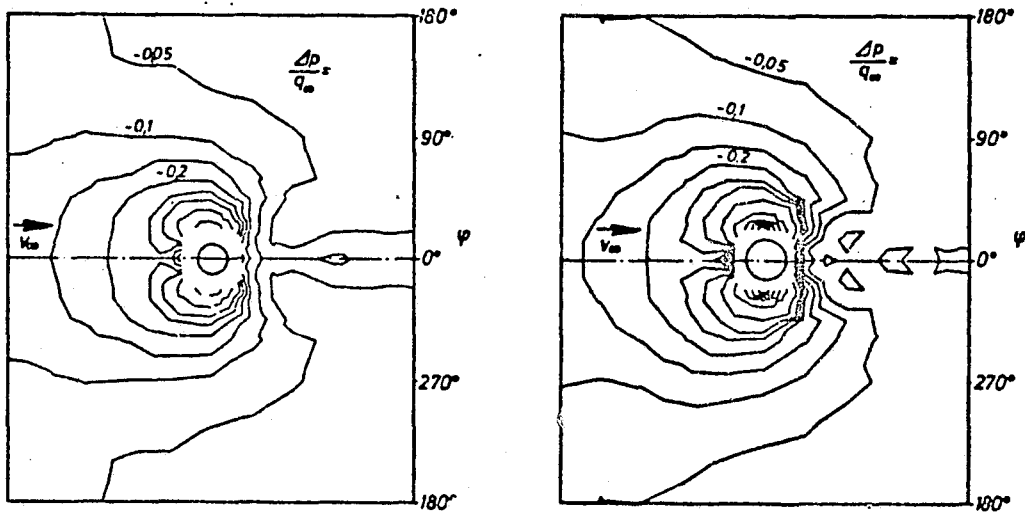
Figure 42



Pitching moment coefficients of a fuselage as a function of the relative jet intensity. The curve parameter is the fuselage length.

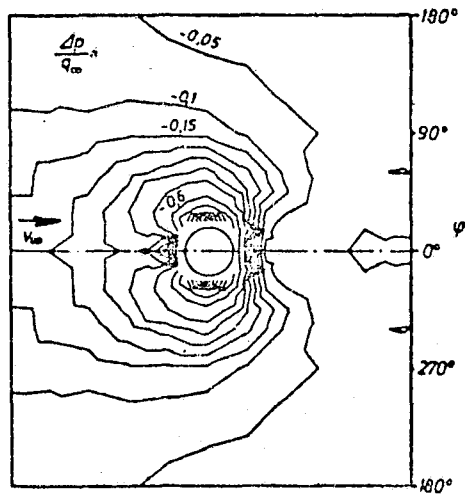
Key: A) Fuselage length





$d_j/D = 0.2$

$d_j/D = 0.25$

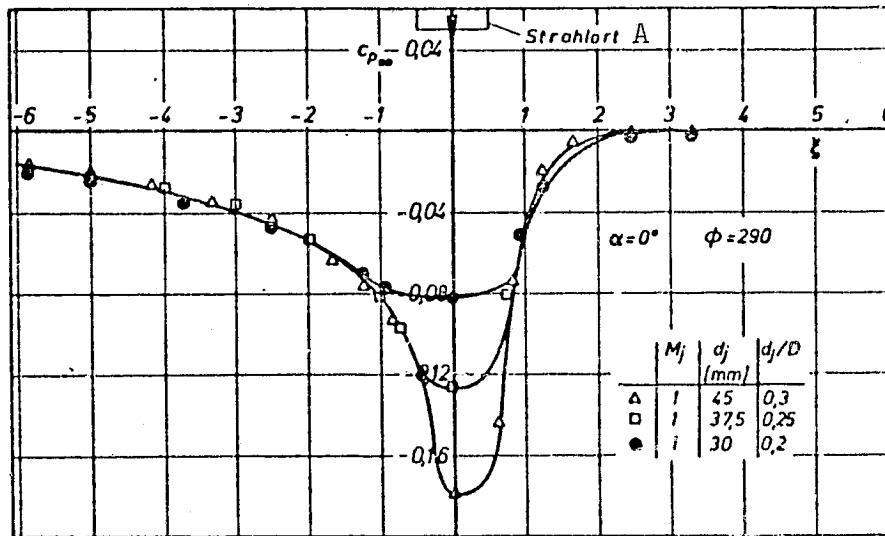


$d_j/D = 0.3$

Pressure distribution on a fuselage with a lift jet in a cross flow for different jet diameters.

$\alpha = 0^\circ ; M_j = 1 ; \phi = 290.$

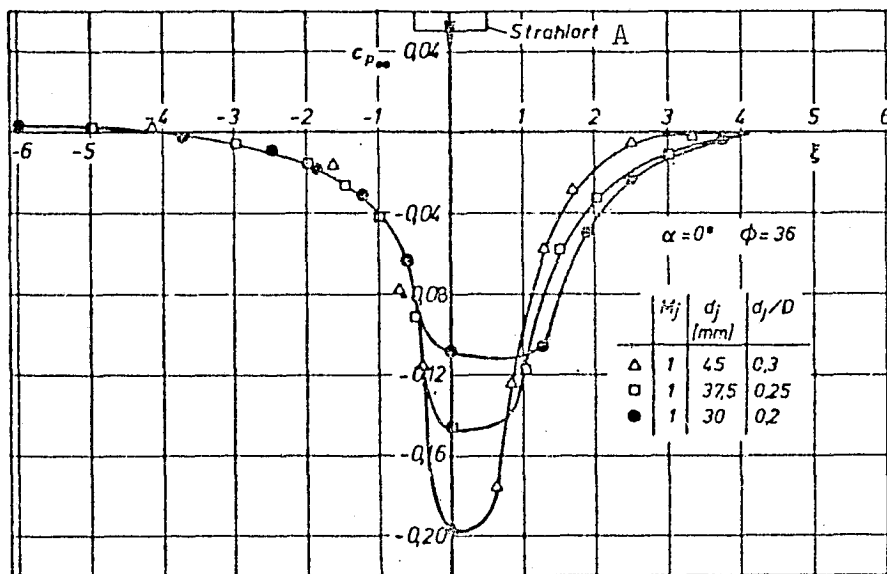
Figure 44



Graph of perpendicular forces along a fuselage for different jet diameters.

Key: A) Jet locus

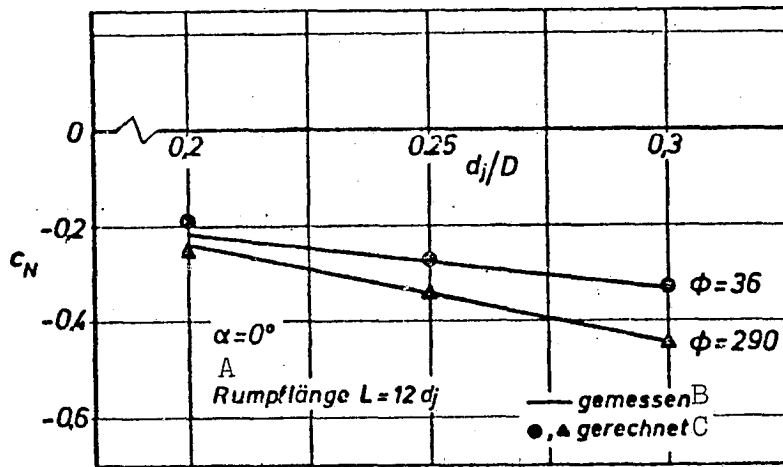
Figure 45



Graph of perpendicular forces along a fuselage for different jet diameters.

Key: A) Jet locus

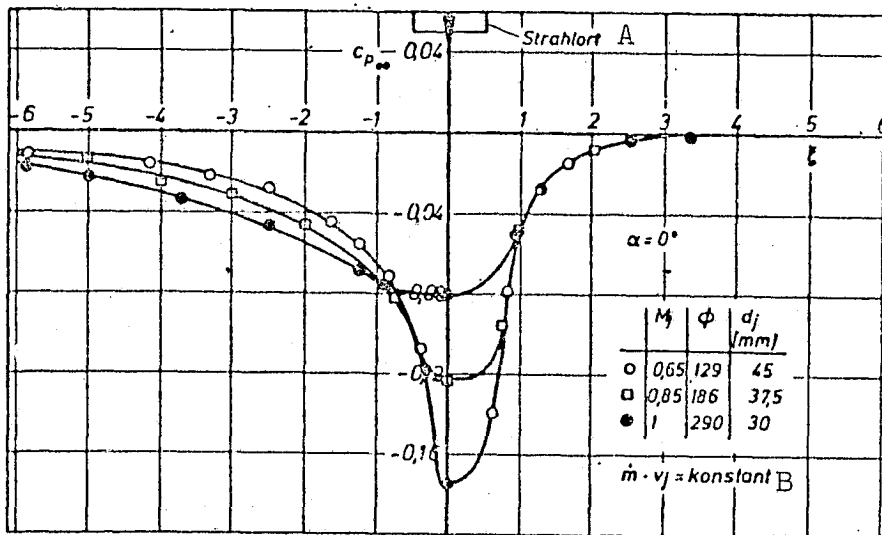
Figure 46



Perpendicular force coefficients of a fuselage as function of the jet/fuselage diameter ratio.

- Key: A) Fuselage length  
 B) Measured  
 C) Calculated

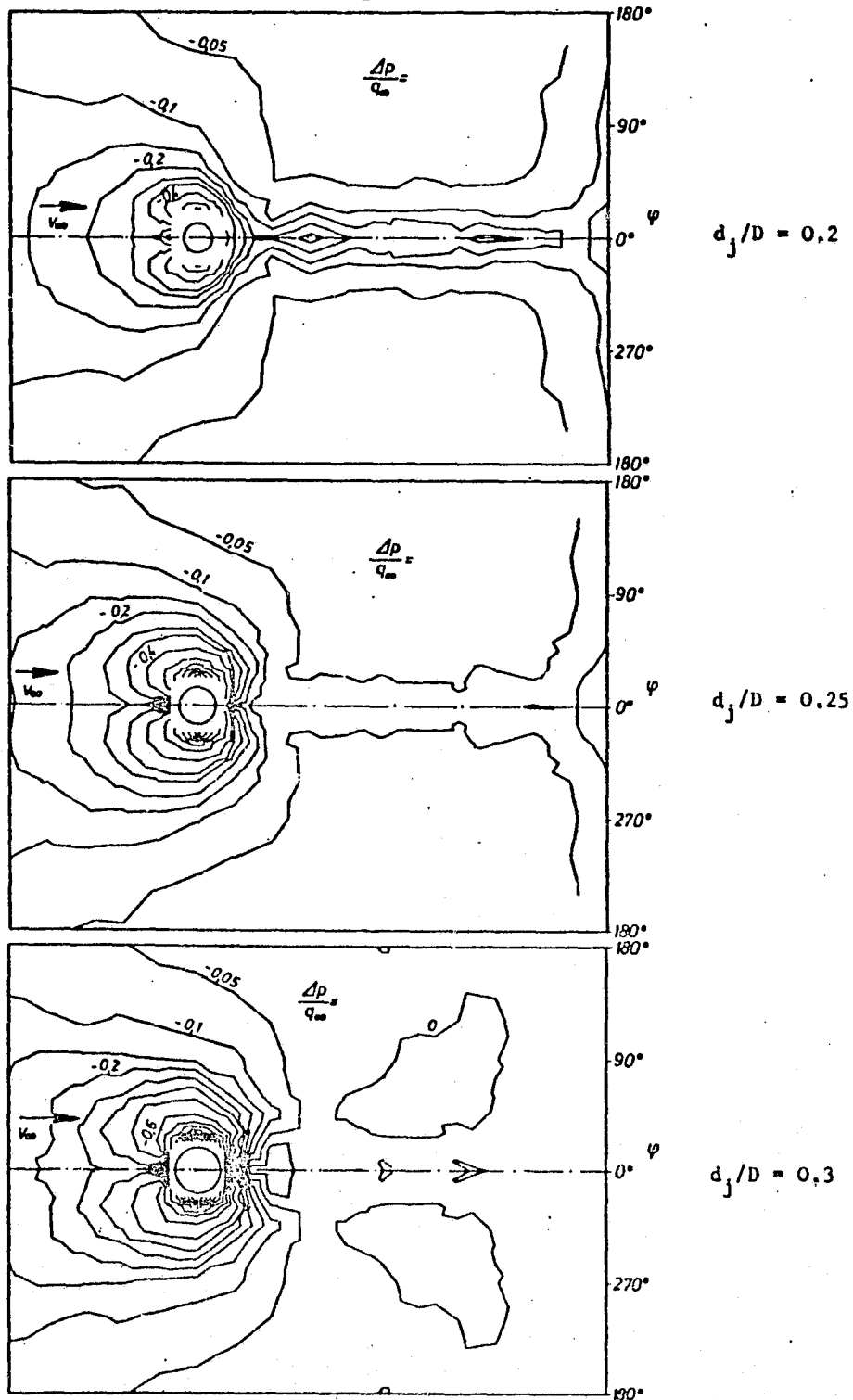
Figure 47



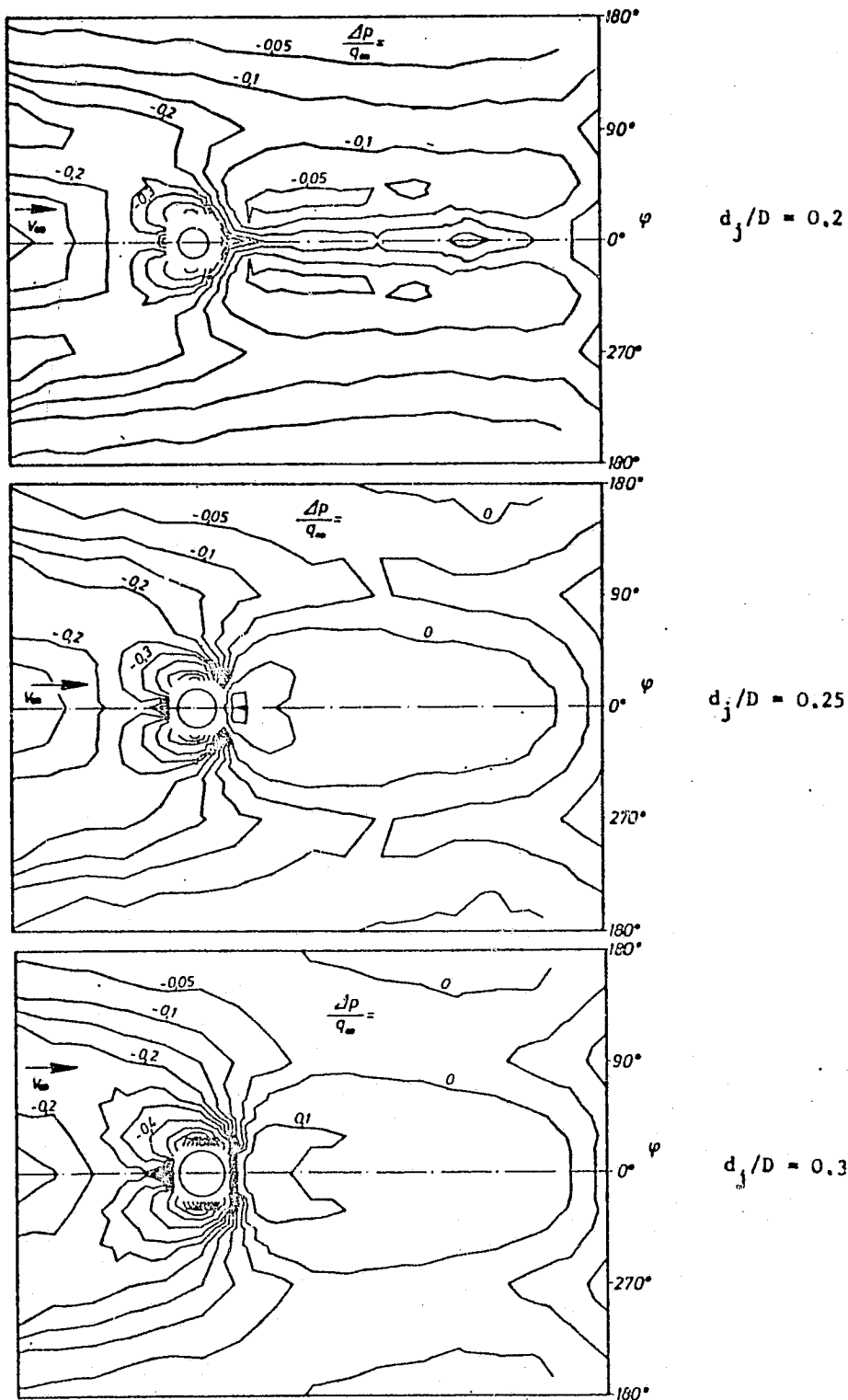
Graph of perpendicular forces along a fuselage for different jet diameters with the same jet momentum.

- Key: A) Jet locus  
 B) Constant

Figure 48



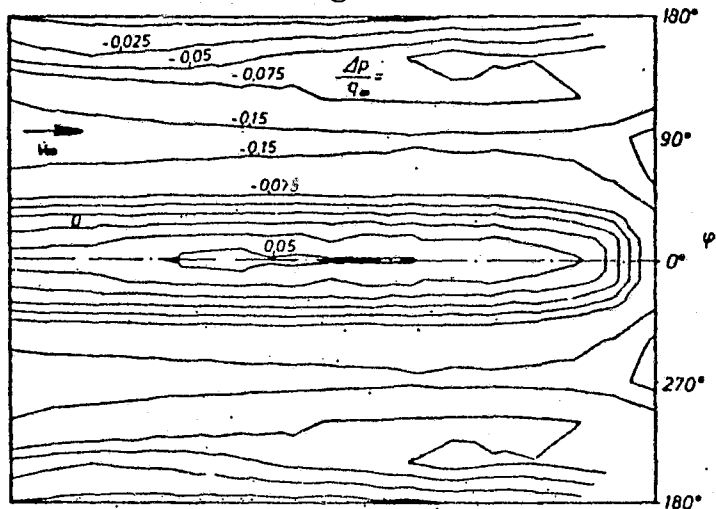
Pressure distribution on a fuselage with a lift jet in a cross flow  $\alpha = 6^\circ$   $\phi = 290$   $M_j = 1.$



Pressure distribution on a fuselage with a lift jet in a cross flow.  $\alpha = 15^\circ$   $\phi = 290$   $M_j = 1.$

Figure 50

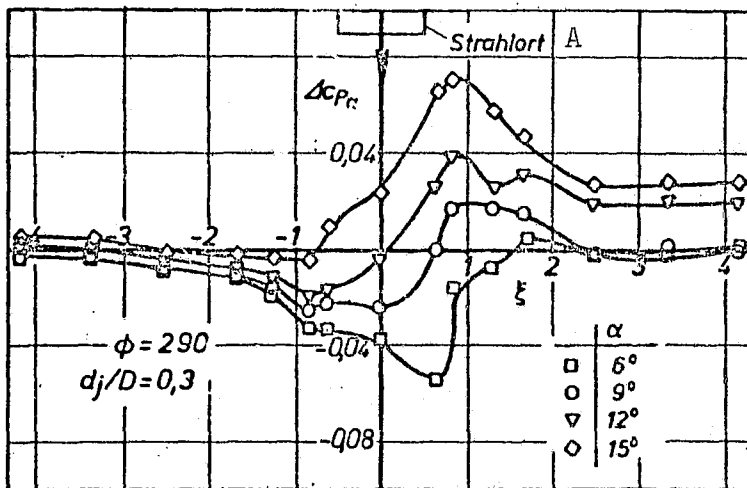
/91



Pressure distribution on a fuselage held obliquely to the oncoming flow. Angle of attack  $\alpha = 15^\circ$ .

Figure 51

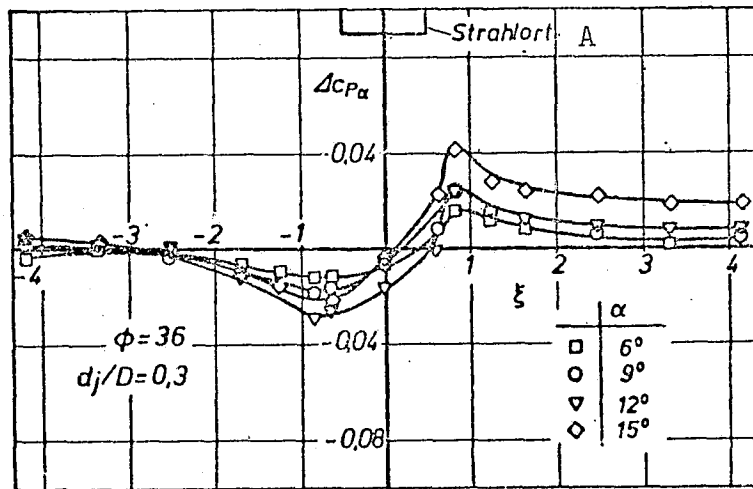
/92



Graph of changes in perpendicular force along a fuselage as a result of varying the angle of attack relative to the graph of perpendicular force at  $\alpha = 0^\circ$ .

Key: A) Jet locus

Figure 52

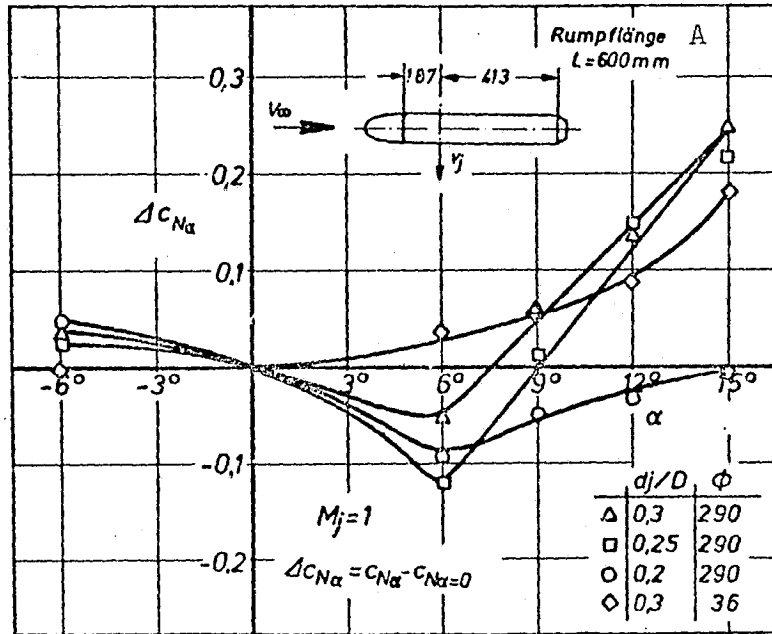


Graph of changes in perpendicular force along a fuselage as a result of varying the angle of attack relative to the graph of perpendicular force at  $\alpha = 0^\circ$ .

Key: A) Jet locus



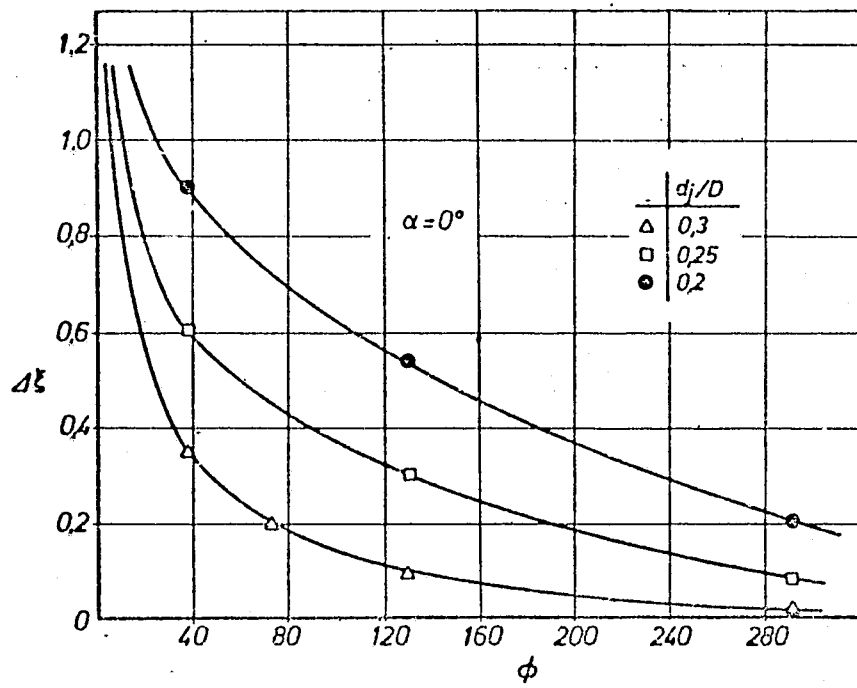
Figure 53



Change in the perpendicular force coefficient with respect to  $\alpha = 0^\circ$  as a result of changing the angle of attack.

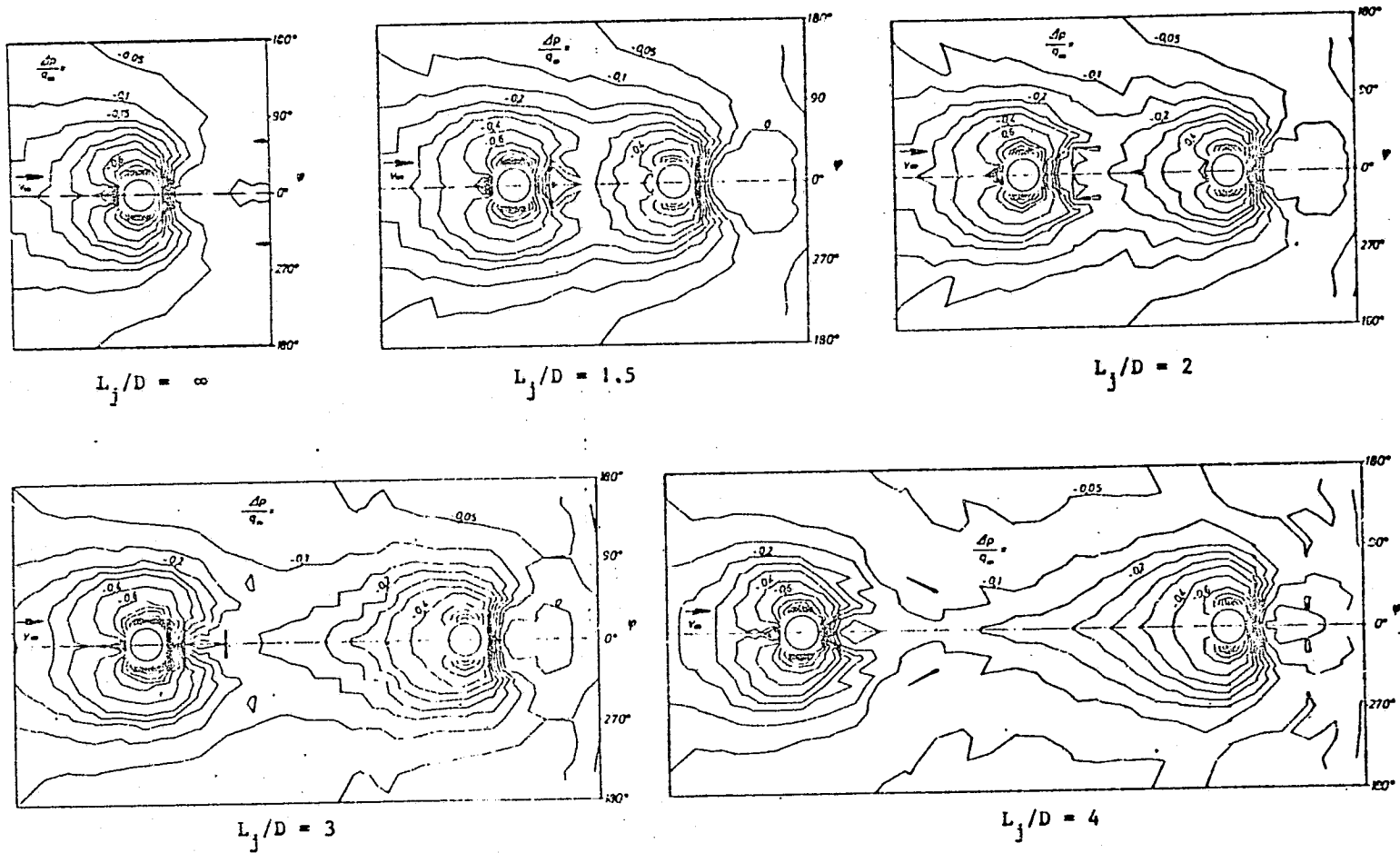
Key: A) Fuselage length

Figure 54



Coordinate shift in the jet wake

Figure 55



Pressure distribution on a fuselage with two tandem lift jets in a cross flow. Variation of the distance between the jets.

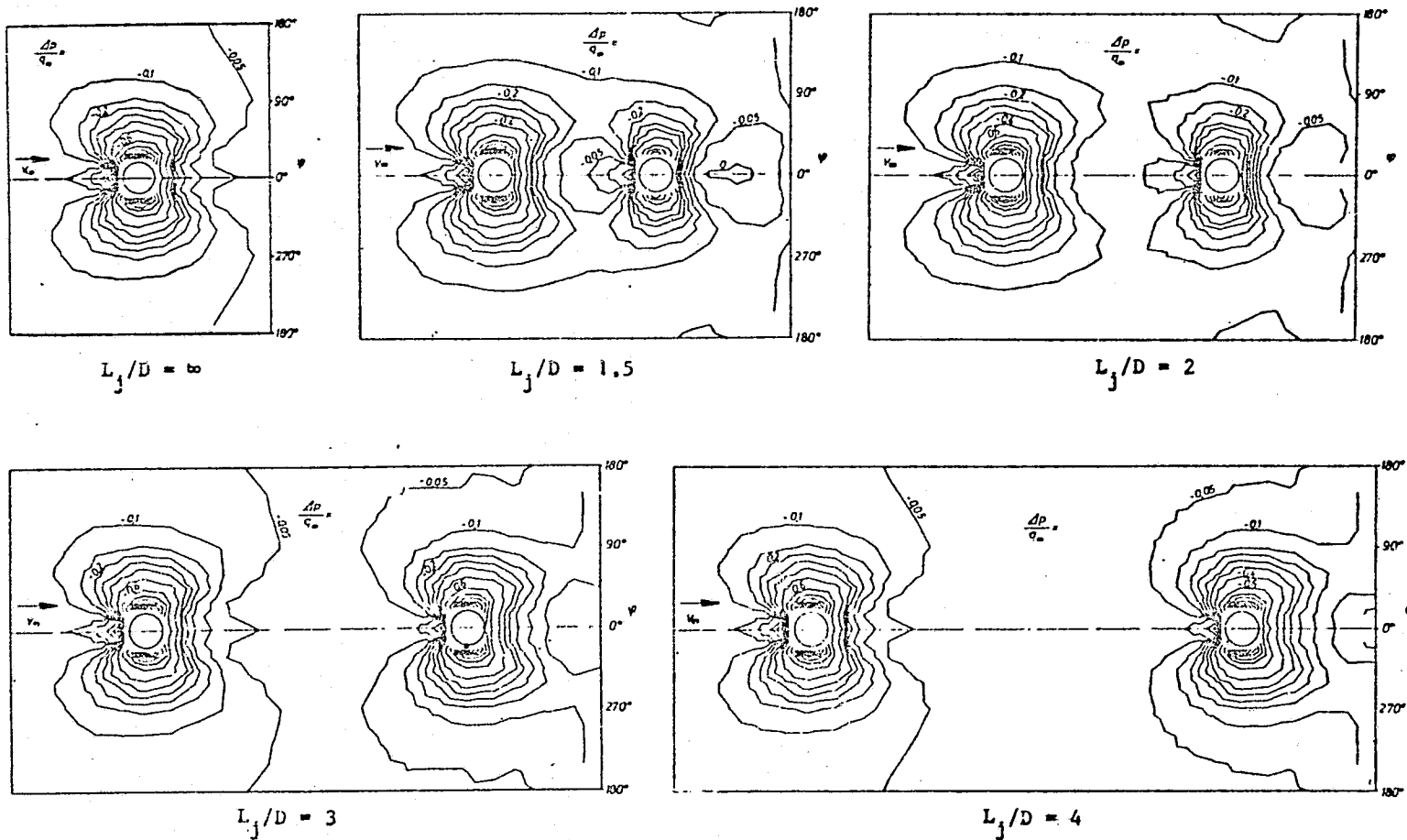
$$\alpha = 0^\circ$$

$$M_j = 1$$

$$\Phi = 290$$

$$d_j/D = 0.3.$$

Figure 5b



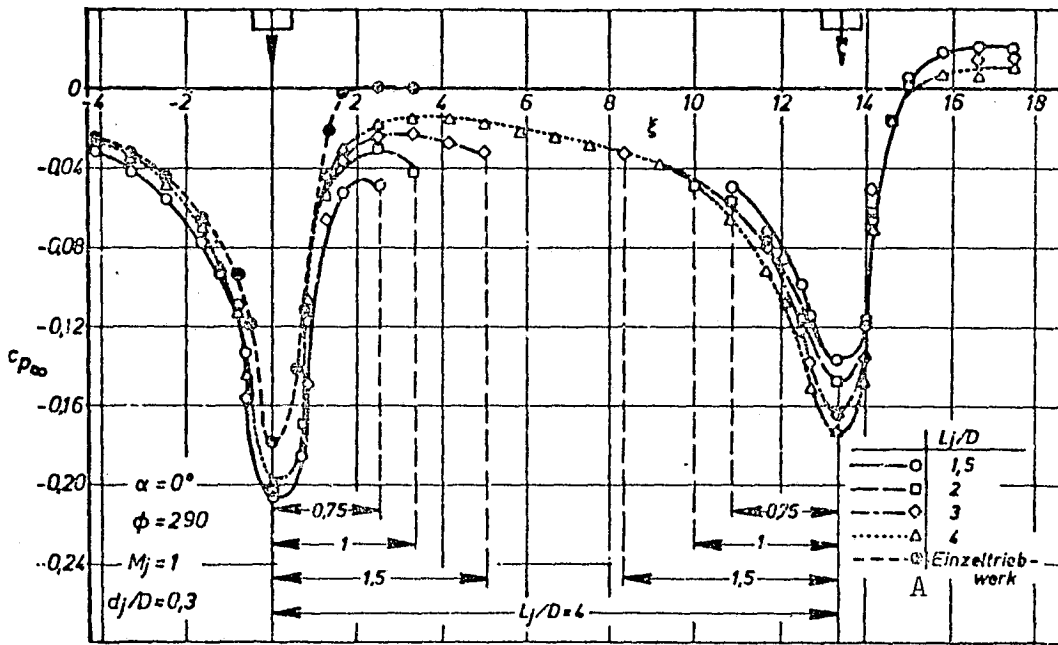
Pressure distribution on a fuselage with two tandem lift jets in a cross flow. Variation of the distance between the jets.

$$\alpha = 0^\circ$$

$$M_j = 1$$

$$\phi = 36$$

$$d_j/D = 0.3.$$



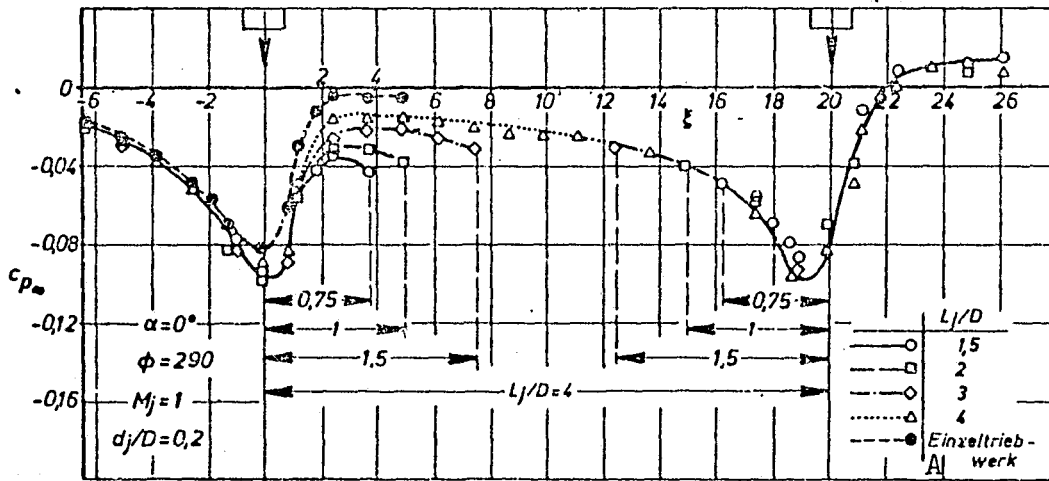
Changes in perpendicular force on the fuselage for different distances between the jets.

$\phi = 290$

$d_j/D = 0,3$

Key: A) Single jet

Figure 58



Changes in perpendicular force on the fuselage for different distances between the jets.

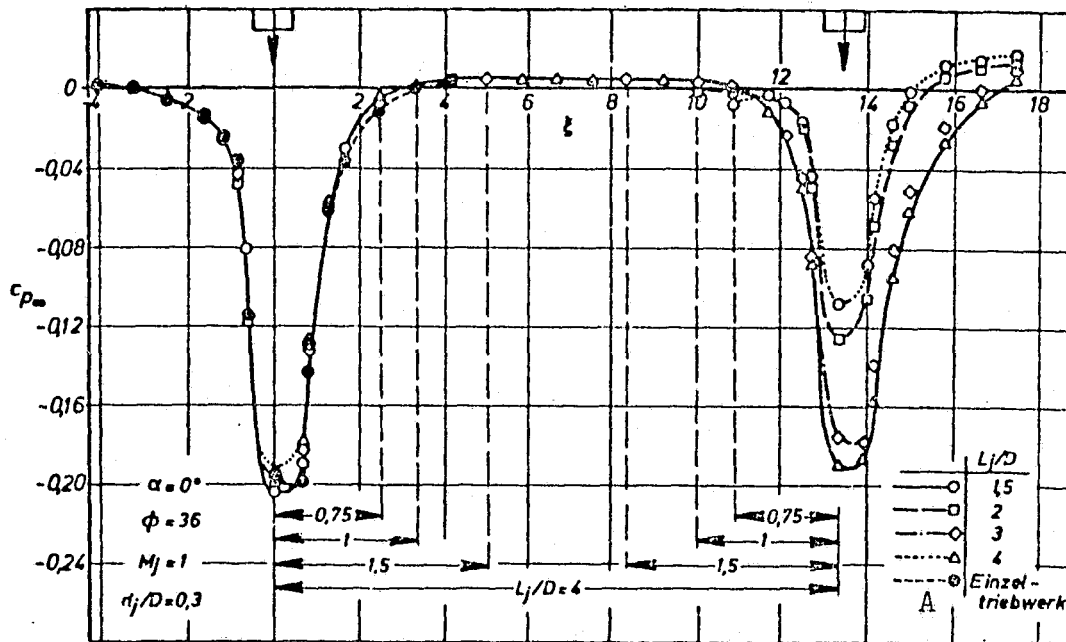
$\phi = 290$

$d_j/D = 0.2$

Key: A) Single jet

Figure 59

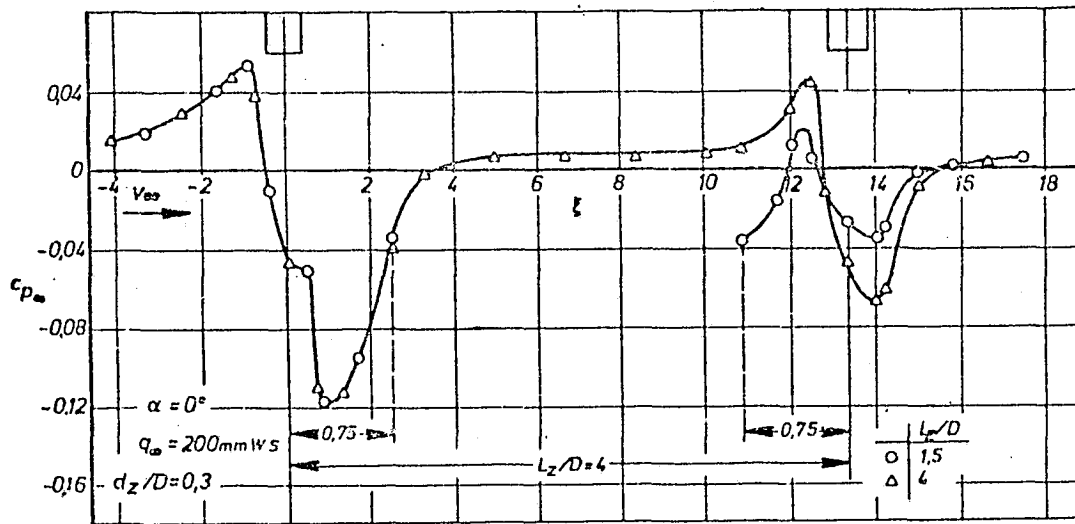
197



Changes in perpendicular force on the fuselage for different distances between the jets.  $\phi = 36$   $d_j/D = 0.3$ .

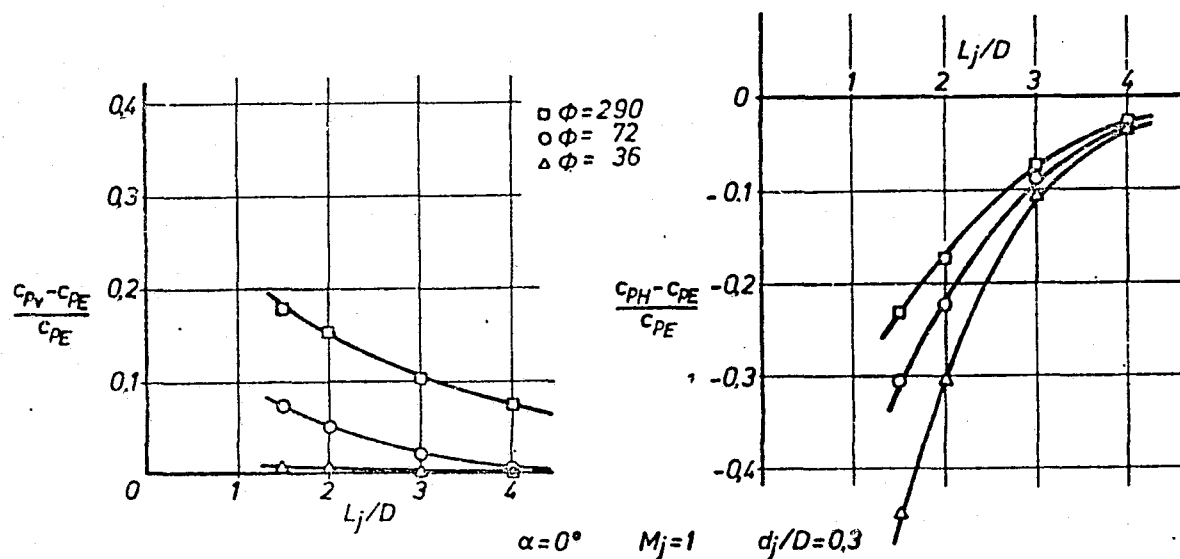
Key: A) Single jet

Figure 60



Fuselage with cylinders in place of jets. Changes in perpendicular force for different distances between the cylinders (shadow effect).

Figure 61



Interference effect of the rear jet on the forward jet due to the injector effect.

Interference effect of the forward jet on the rear jet due to shadowing.

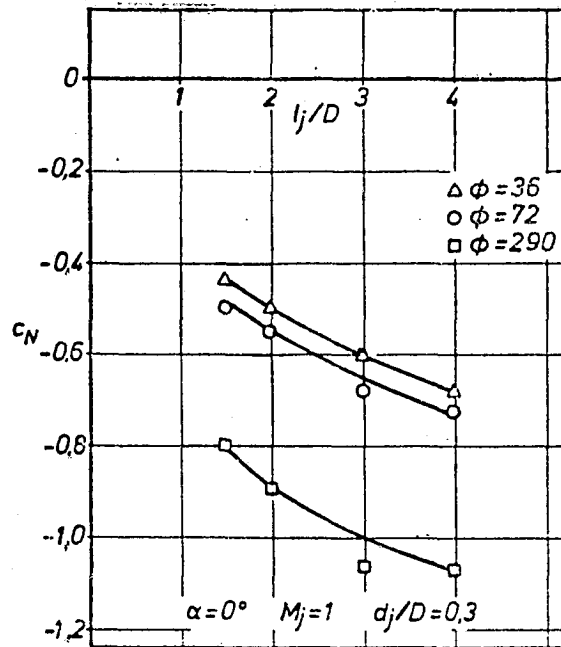
Interaction of the two jets:

- $c_{pE}$  - minimum pressure coefficient for the single jet
- $c_{pV}$  - minimum pressure coefficient for the forward jet
- $c_{pH}$  - minimum pressure coefficient for the rear jet



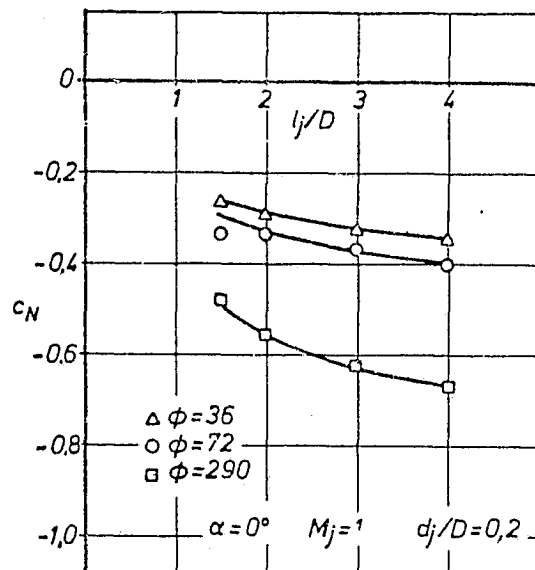
Figure 62

/99



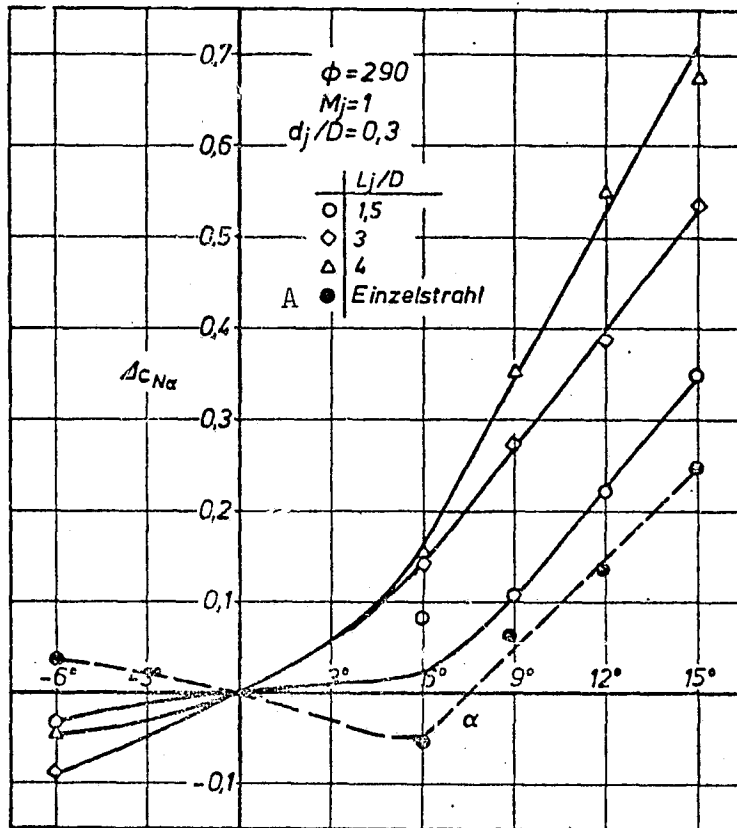
Perpendicular force coefficients of a fuselage with a double jet as a function of the distance between the jets. Curve parameter is the relative jet intensity  $\phi$ .

Figure 63



Perpendicular force coefficients of a fuselage with a double jet as a function of the distance between the jets. Curve parameter is the relative jet intensity  $\phi$ .

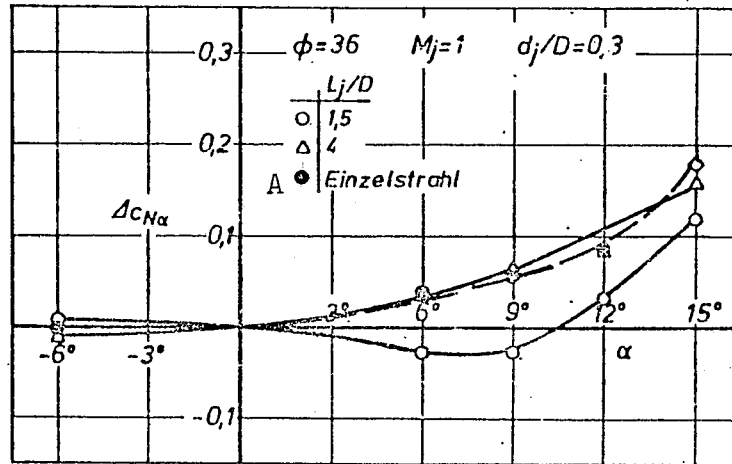
Figure 64



Changes in the perpendicular force coefficient with respect to  $\alpha = 0^\circ$  due to the angle of attack setting for different distances between the jets.

Key: A) Single jet

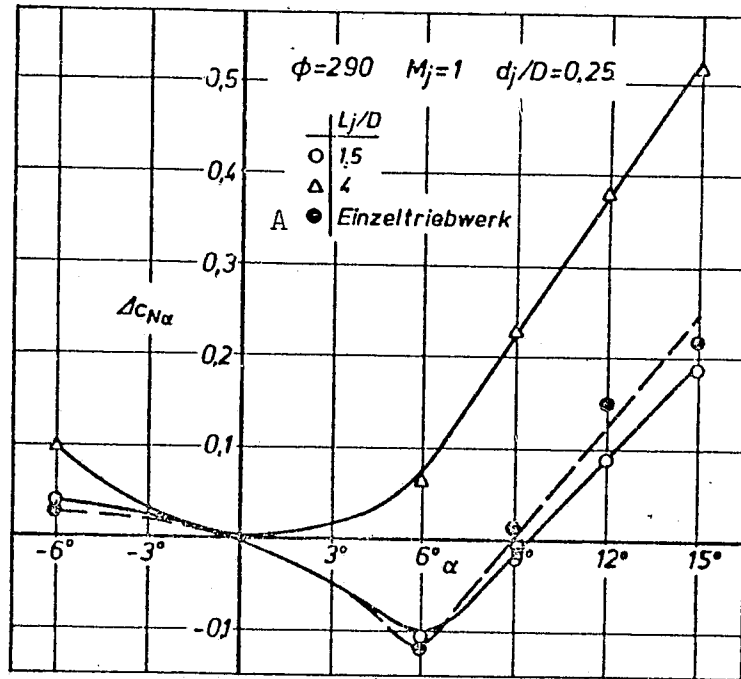
Figure 65



Changes in the perpendicular force coefficient with respect to  $\alpha = 0^\circ$  due to the angle of attack setting for different distances between the jets.

Key: A) Single jet

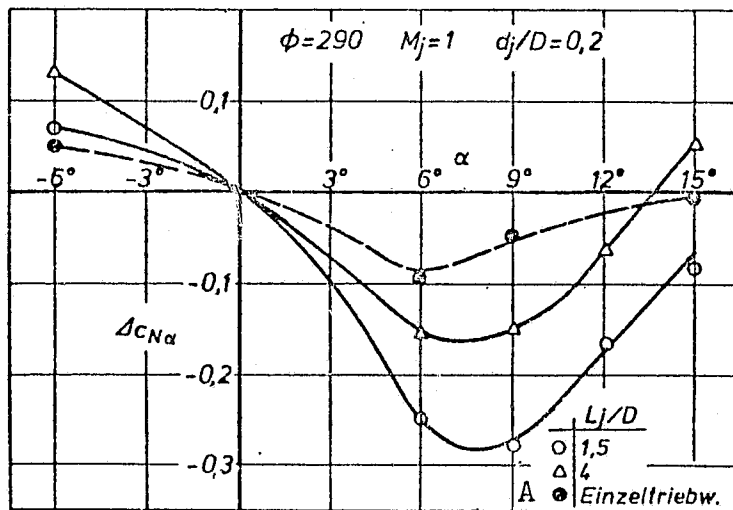
Figure 66



Changes in the perpendicular force coefficient with respect to  $\alpha = 0^\circ$  due to the angle of attack setting for different distances between the jets.

Key: A) Single jet

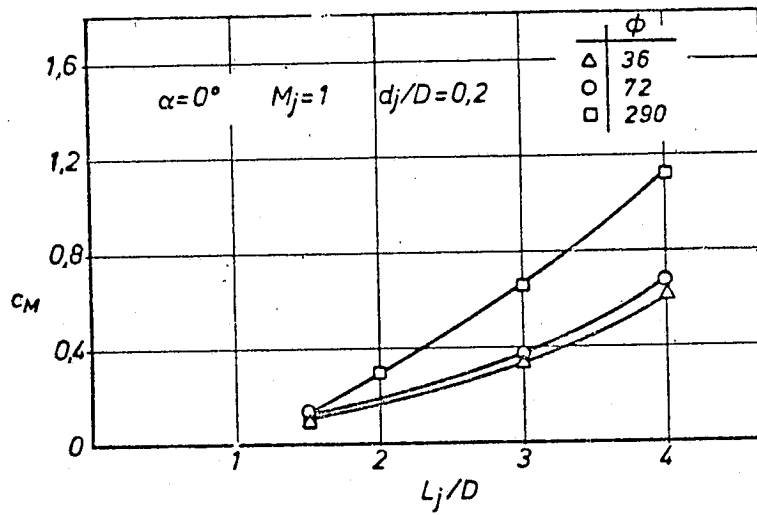
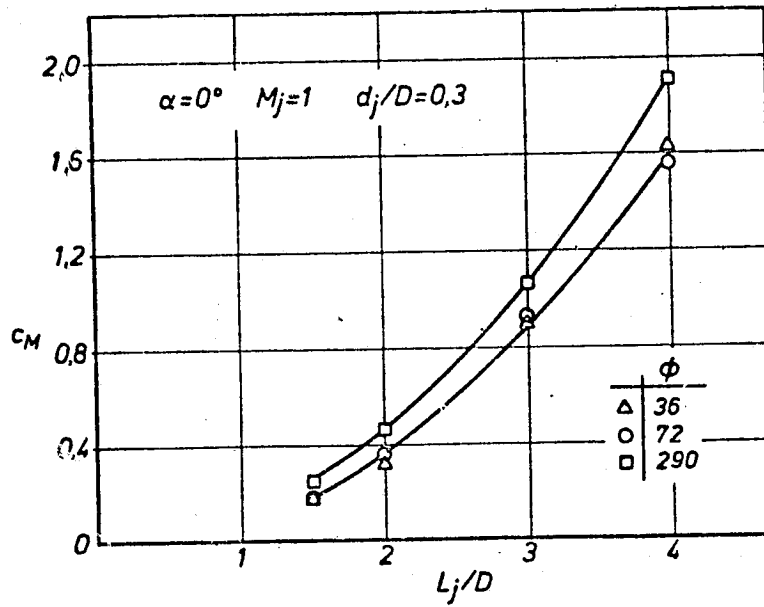
Figure 67



Changes in the perpendicular force coefficient with respect to  $\alpha = 0^\circ$  due to the angle of attack setting for different distances between the jets.

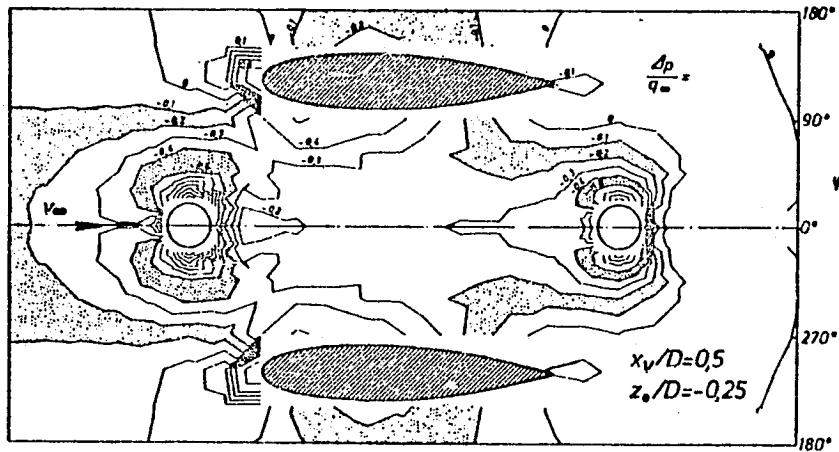
Key: A) Single jet

Figure 68

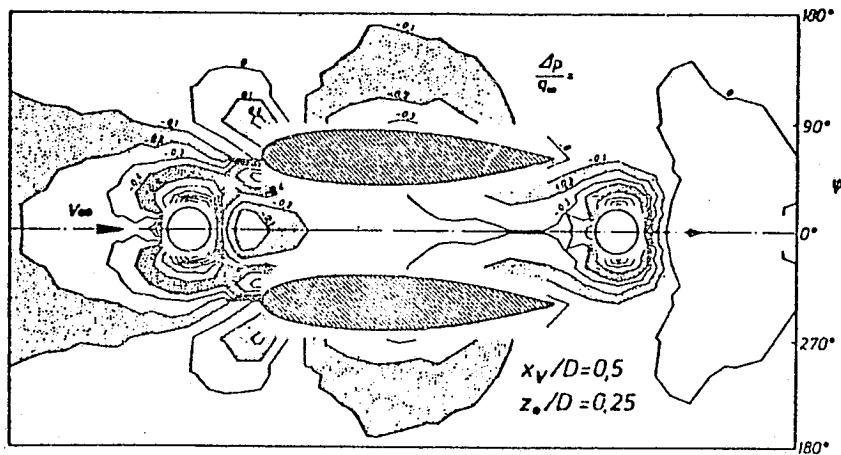


Pitching moment coefficients of a fuselage with a double jet as a function of the distance between the jets. Curve parameter is the relative jet intensity  $\phi$ .





A Azimutwinkel der Flügelsehne:  $\varphi = 120^\circ$  or  $\varphi = 240^\circ$

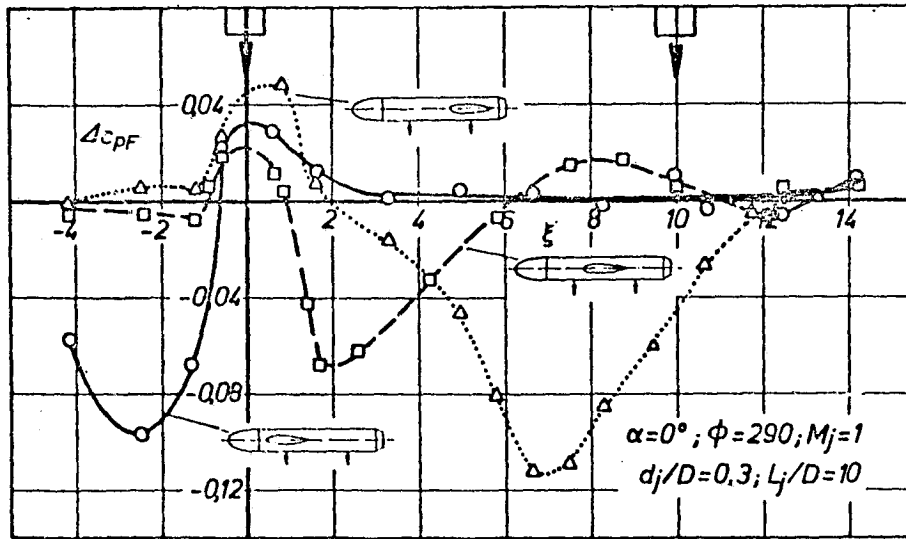


A Azimutwinkel der Flügelsehne:  $\varphi = 60^\circ$  or  $\varphi = 300^\circ$

Isobar field of the cylindrical portion of the fuselage for different wing positions.

$\alpha = 0^\circ$  ;  $M_j = 1$  ;  $\phi = 290$  ;  $L_j/D = 3$  ;  $d_j/D = 0.3$ .

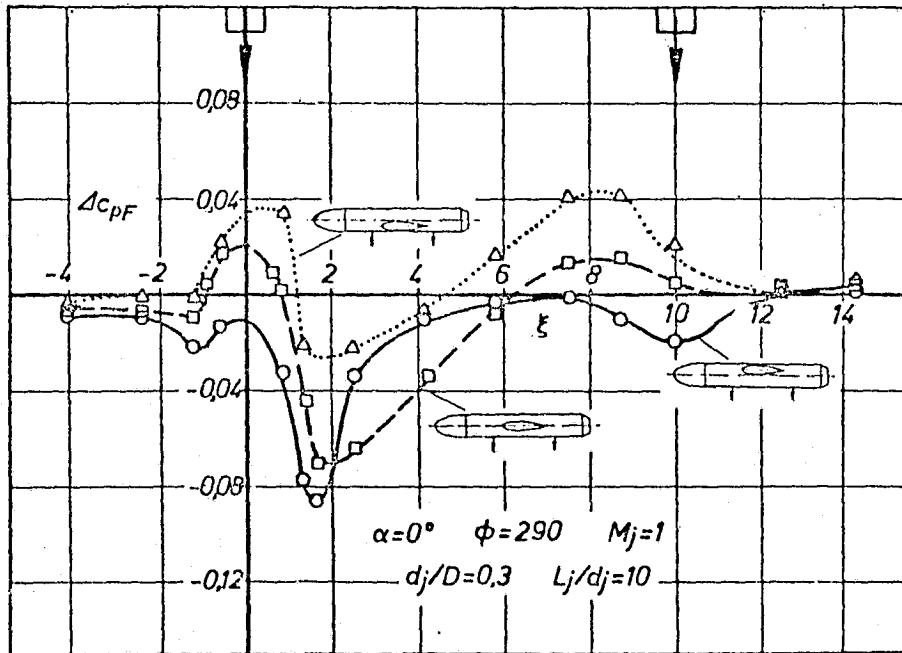
Key: A) Azimuth angle of the wing chord



Influence of the wing position on the changes in perpendicular force along the fuselage.

$$\Delta c_{pF} = c_{pF} \text{ (with wing)} - c_p \text{ (without wing)}$$

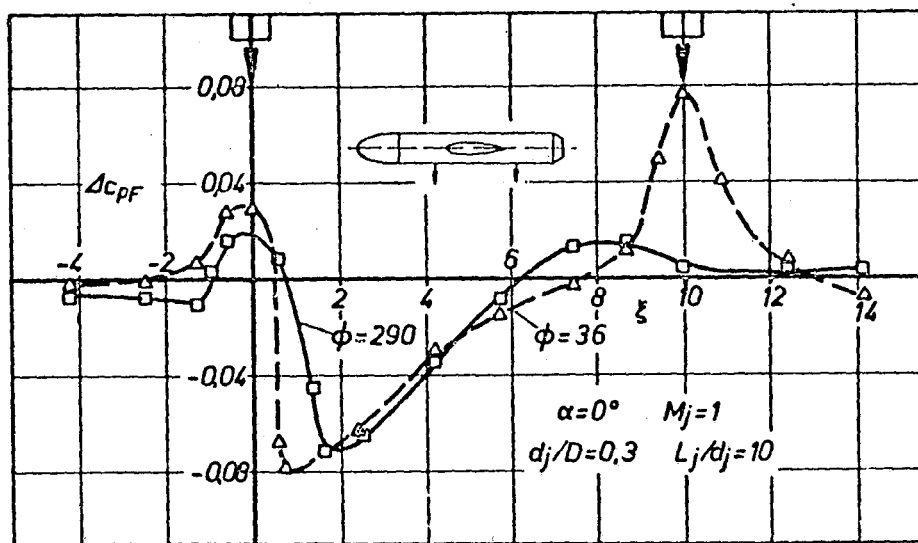
Figure 72



Influence of the wing position on the changes in perpendicular force along the fuselage.

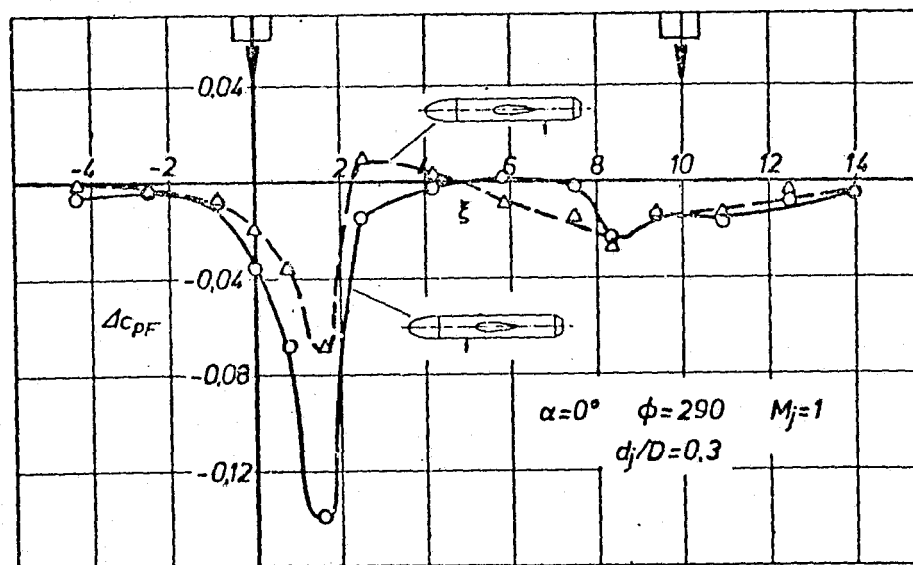


Figure 73

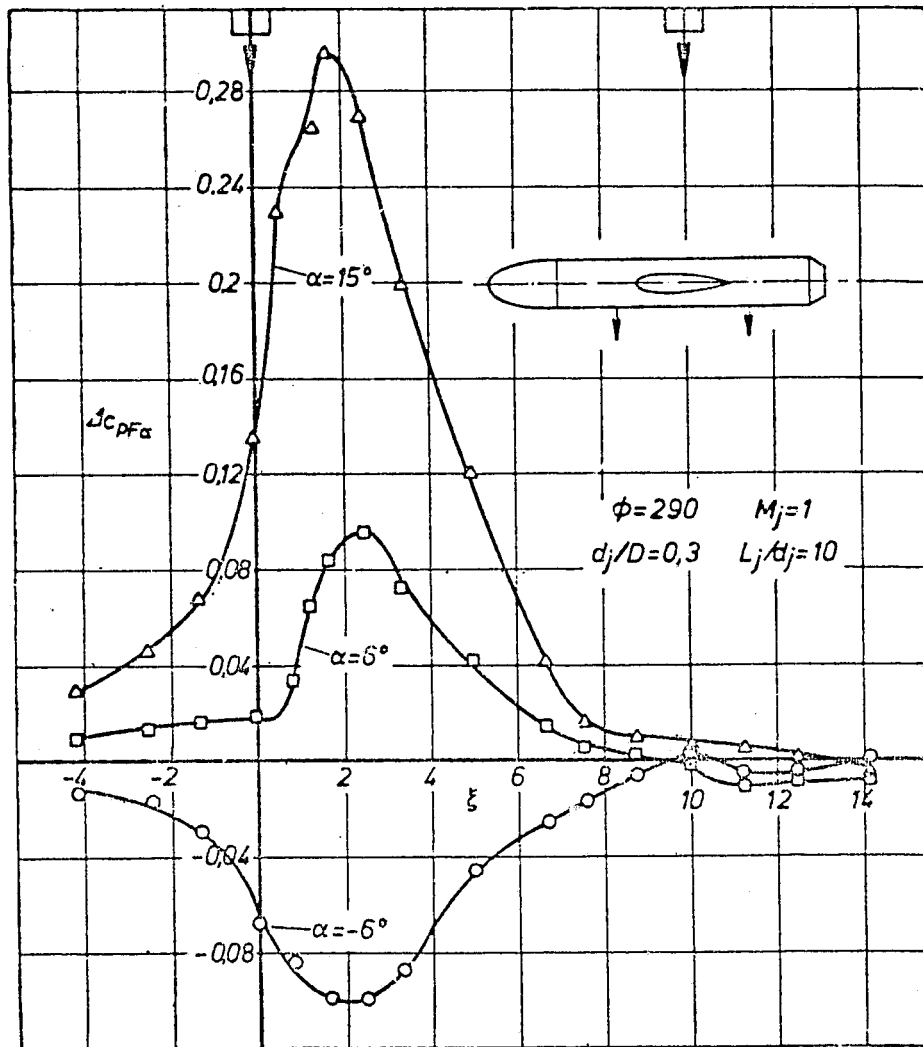


Influence of the relative jet intensity on the changes in perpendicular force along the fuselage with the wing located in the central position.

Figure 74

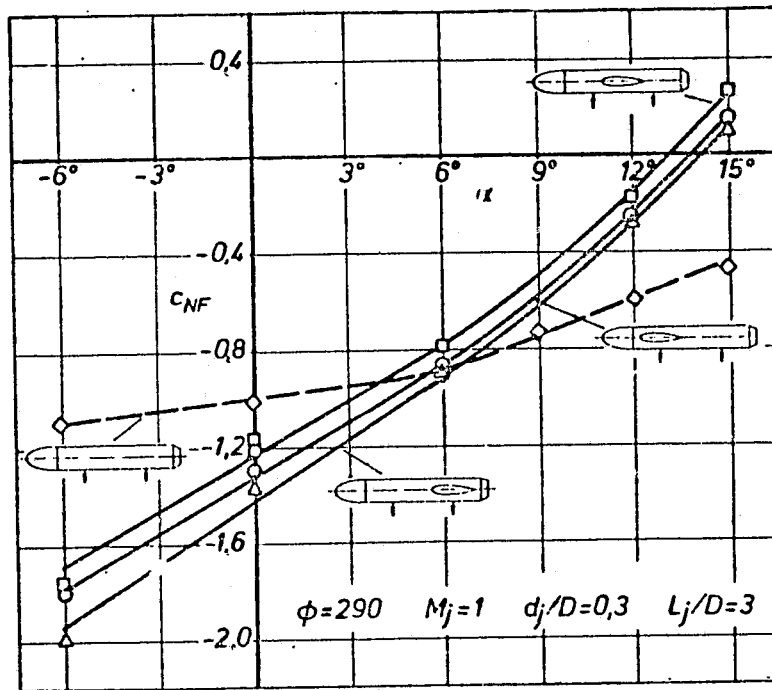


Influence of the wing position on changes in perpendicular force along a fuselage with 1 jet.



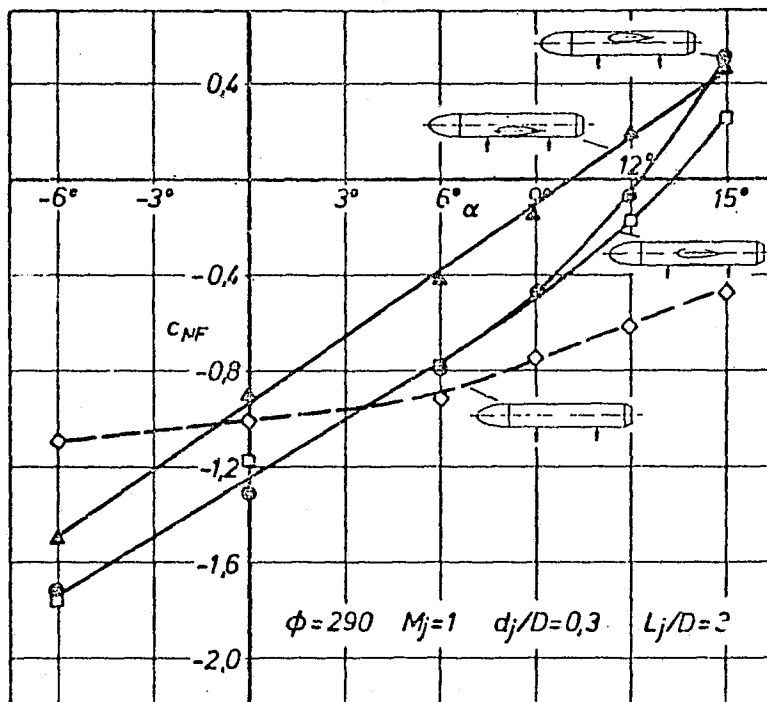
Influence of the angle of attack on changes in perpendicular force along a fuselage with a wing.

$$\Delta c_{pF\alpha} = c_{pF\alpha \neq 0} - c_{pF\alpha = 0}.$$

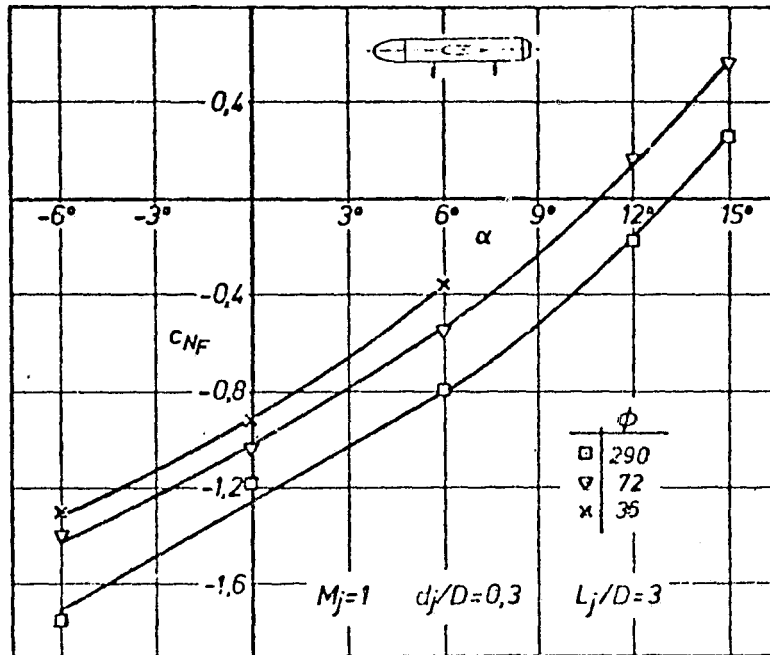


Changes in perpendicular force over the angle of attack for different wing positions.

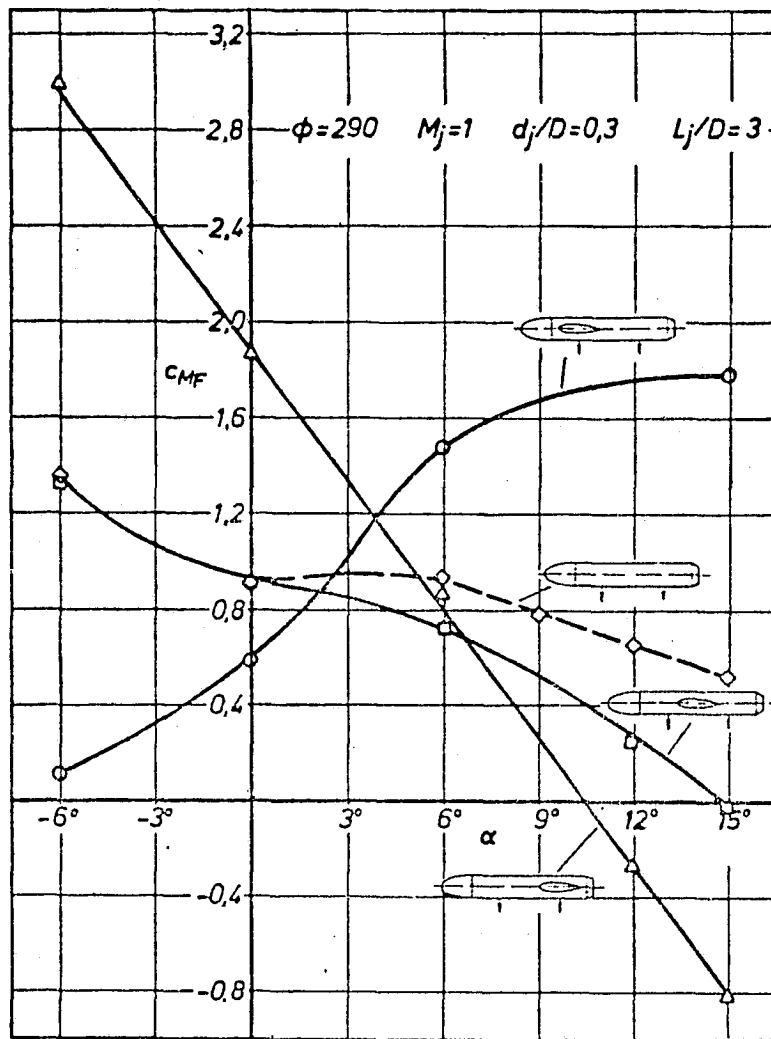
Figure 77



Changes in perpendicular force over the angle of attack for different wing positions.

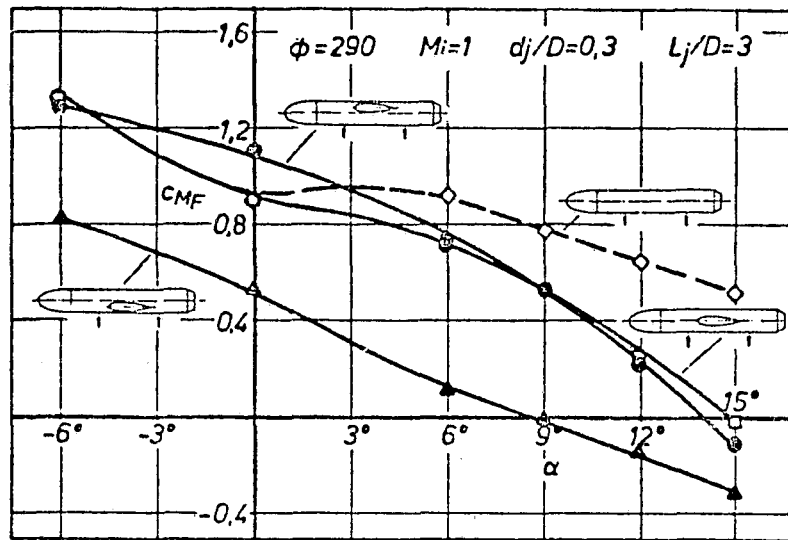


Changes in perpendicular force over the angle of attack with the central wing position for different relative jet intensities.



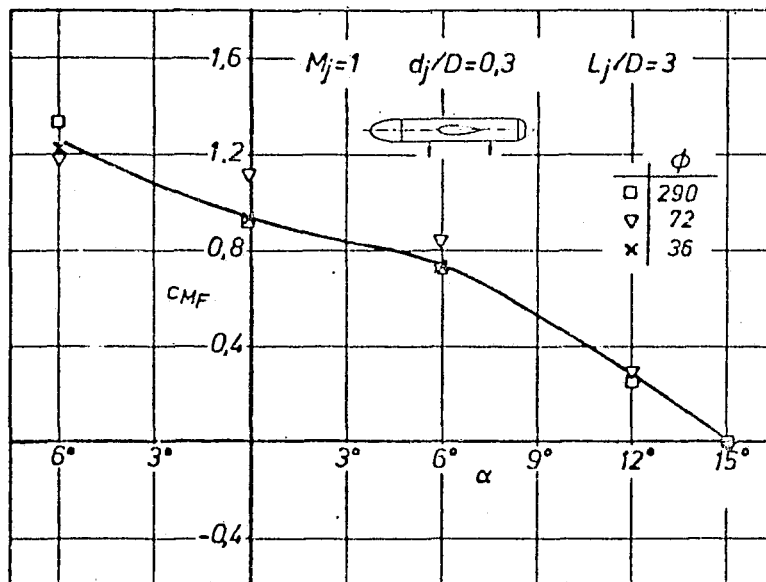
Changes in the pitching moment over the angle of attack for different wing positions.

Figure 80



Changes in the pitching moment over the angle of attack for different wing positions.

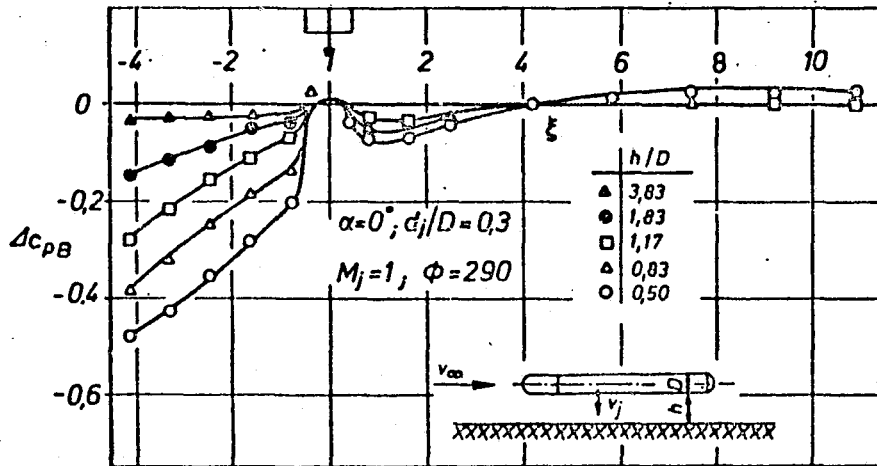
Figure 81



Changes in the pitching moment over the angle of attack with the central wing position for different relative jet intensities.

Figure 82

/112

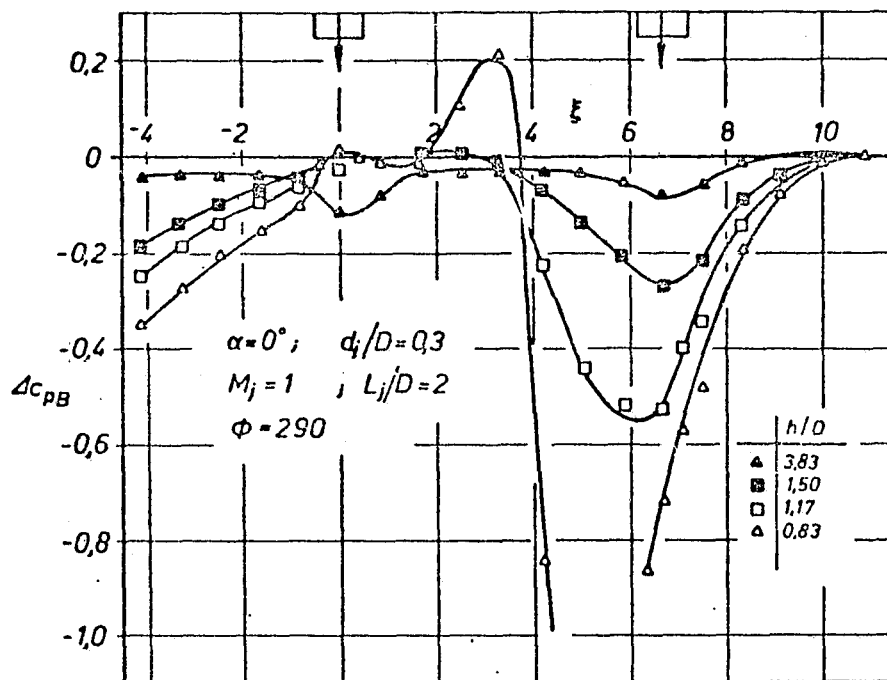


Influence of the distance above the ground on changes in perpendicular force along a fuselage with a single jet.

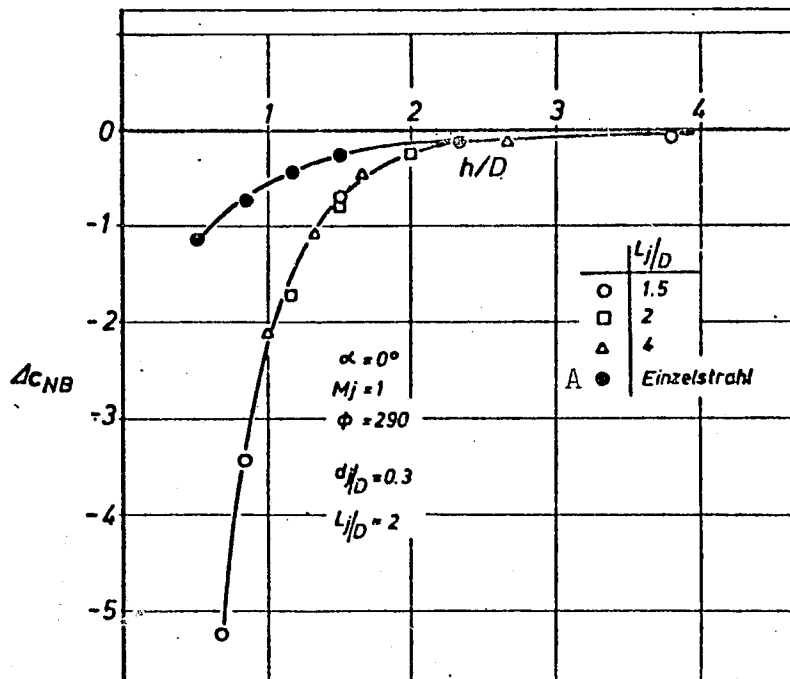
$$\Delta c_{pB} = c_{pB} \text{ (with ground effect)} - c_p \text{ (without ground effect)}$$



Figure 83



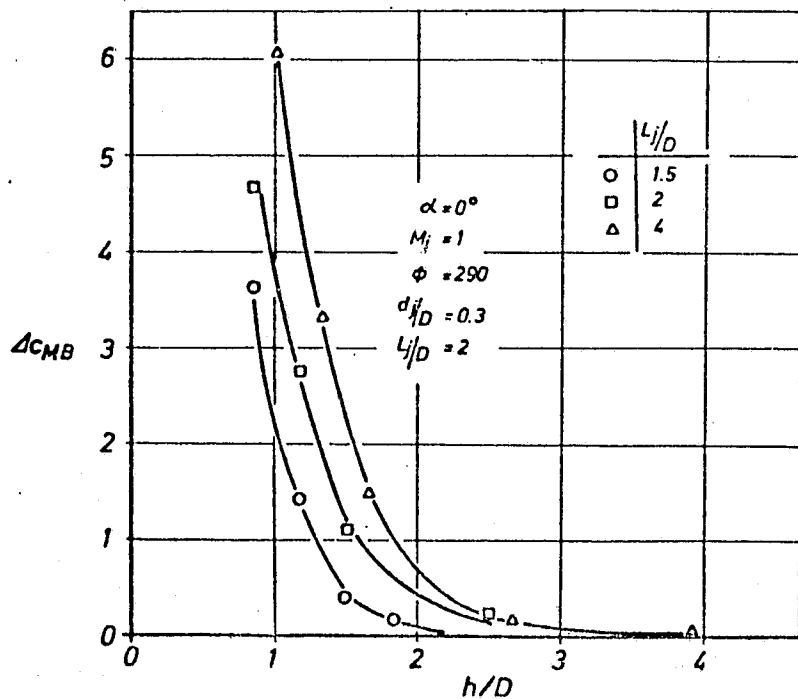
Influence of the distance above the ground on changes in perpendicular force along a fuselage with a double jet.



Change in the perpendicular force coefficient due to the effect of the ground.

Key: A) Single jet

Figure 85



Change in the pitching moment coefficient due to the effect of the ground.